This is to certify that the

thesis entitled

INVESTIGATION OF THE NEW FAMILY OF CUBIC
CHALCOGENIDE COMPOUNDS
$A_mB_nM_mQ_{2m+n}$ FOR THERMOELECTRIC
APPLICATIONS

presented by

Stephan De Nardi

has been accepted towards fulfillment
of the requirements for

M.S. degree in Chemistry

Major professor

Date 5/4/2000

O-7639

INVESTIGATION OF THE NEW FAMILY OF CUBIC CHALCOGENIDE COMPOUNDS $A_mB_nM_mQ_{2m+n}$ FOR THERMOELECTRIC APPLICATIONS

By

Stephan De Nardi

A THESIS

Submitted to
Michigan State University
in partial fulfillment of the requirements
for the degree of

MASTER OF SCIENCE

Department of Chemistry

2000

ABSTRACT

INVESTIGATION OF THE NEW FAMILY OF CUBIC CHALCOGENIDE COMPOUNDS $A_mB_nM_mQ_{2m+n}$ FOR THERMOELECTRIC APPLICATIONS

By

Stephan De Nardi

A growing concern for environmentally friendly devices as well as a need for more efficient materials, has revitalized recently the field of thermoelectricity. Several research groups are investigating new compounds that could replace the established materials Bi_2Te_3 and PbTe which have been used for several decades for thermoelectric applications.

A new family of quartenary chalcogenides semiconducting compounds of general formulae $A_mB_nM_mQ_{2m+n}$ (where A is K or Ag, B is Pb or Sn, M is Bi or Sb and Q is S, Se, or Te) was synthesized and characterized. Preliminary measurements show that these narrow band gap semiconductors possess promising transport properties for thermoelectric applications. A wide range of values have been observed for the parameters of interest (the Seebeck coefficient, and the electrical and thermal conductivity) depending on the elements chosen and the values of n and m. Among all the systems investigated, $KPb_{10}BiTe_{12}$ was chosen for further optimization. The thermal conductivity of this compound can be decreased significantly by increasing the mass fluctuation in the structure via solid solutions. The introduction of Sn as chemical dopant agent increased the figure of merit ZT. Significant differences between measurements of the Seebeck coefficient on cold pressed pellets and ingots were observed and investigated.

TABLE OF CONTENTS

LIST OF TABLES

LIST OF FIGURES

Chapter 1

Introduction and Thermoelectric Concepts

It would be too long here to list the numerous applications that thermoelectric materials (TE) can produce. From inertial guidance systems in aerospace industry, to wine coolers, military night vision equipments, laser diode coolers, hypothermia blankets, blood analyzers, or whipped cream dispensers in restaurants[1], the impact of this technology in our lives is important. The necessity of developing better thermoelectric materials lies not only in technological needs but also in the growing concern on global warming and the increasing demand on environmentally friendly devices. Today, more people than ever are concerned about pollution and warming effects. As an example, during the third World Conference on global warming, one of the major points of attraction was thermoelectric materials that can generate power from waste heat [2].

Thermoelectric materials can also be used for refrigeration purposes. A new class of isostructural conductive compounds of formula $A_mB_nM_mQ_{2m+n}$ where A is an alkali metal or silver, B lead or tin, M bismuth or antimony, and Q a chalcogenide was studied is this Thesis and showed particularly promising thermoelectric properties. They are narrow band gap semiconductors and possess different physical properties, depending not only on the elements chosen but also on the value of m and n.

The aim of this research was to explore this wide family of compounds and to optimize selected members in order to enhanced the figure of merit ZT that is defined as:

$$ZT = (S\,\sigma^2\,T)/\kappa \qquad \text{Eq. (1-1)}$$

Where S is the Seebeck coefficient, σ and κ the electrical and thermal conductivity respectively, and T is the absolute temperature.

1-1. Brief History of Thermoelectricity

The history of thermoelectricity began more than 150 years ago when Thomas Seebeck [3] (1822) and Jean Peltier [4] (1834) discovered the thermoelectric phenomenon. During this time period numerous investigations on the interaction between an electric current and a magnetic field, that was first discovered by the Danish physicist Oersted, were carried on by numerous scientists like Laplace and Ampere, just to cite a few. Around the same time period that Faraday found electromagnetic induction, Seebeck noticed that a small flow of electrical current was generated when a difference of temperature was applied to the junctions of two dissimilar conductors (see Figure 1-1a), referred later in this work as the thermoelements. This phenomenon is known as the Seebeck effect, the first of three fundamental effects in thermoelectricity, and it is mainly used today in spacecraft power generation [5](such as Voyager I and II).

Based on Seebeck's discovery, a French watchmaker, J. C. Peltier, found that heat was liberated or absorbed at a rate Q, depending on the direction of a current passing through two different conductors (see Figure 1-1b). He showed that this effect was reversible, proportional to the intensity of the current applied as well as independent on the size of the thermoelements, making it different form the well-known effect named after Joule. This constitutes the basic effect used in refrigeration and it can be expressed according to Eq. (1-2)[6]:

$$Q = \Pi J \qquad \text{Eq. (1-2)}$$

Where J is a flow of current and Π is the Peltier coefficient.

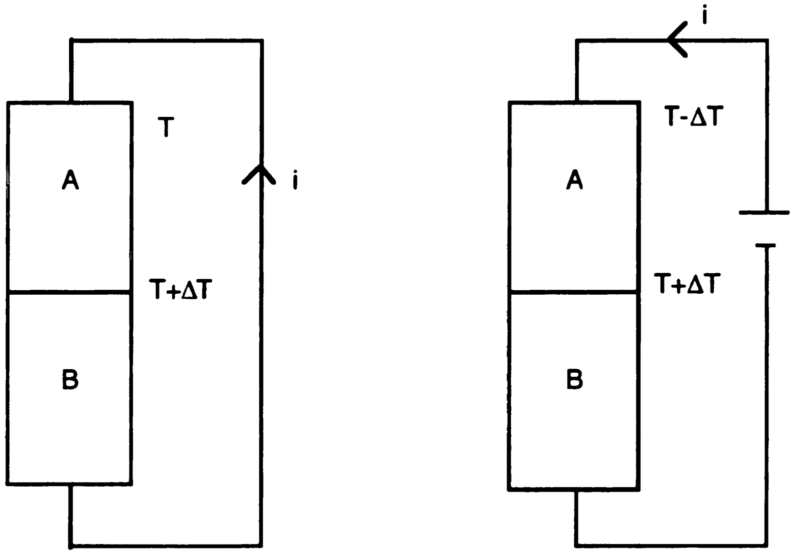

(a) (b)

Figure 1-1: The two principal effects in thermoelectricity: (a) Seebeck effect used in power generation and (b) Peltier effect used in refrigeration technology.

The explanation of this phenomenon was not demonstrated until Lenz, in 1838, froze a drop of water placed at a junction of bismuth and antimony rods after changing the direction of the current.

Finally, the third important effect of thermoelectricity was formulated by W. Thompson (Lord Kelvin) who demonstrated, in 1854, some 30 years after Seebeck's reports, that reversible heating and cooling was also created through a single conductor when a current flow was applied to it. He was able to establish the relationship between the Peltier coefficient and the thermoelectric power α as [6]:

$$Q = \alpha T J = \Pi J \qquad \text{Eq. (1-3)}$$

In fact, the association of the Thompson and the Peltier effects give rise to the Seebeck effect [7].

A century elapsed before research in this field really started. The initiator of the rebirth of interest toward thermoelectric phenomena was Ioffe [8] (1957) when he observed that doped semiconductors were the best TE materials. Until then, the compounds investigated were mostly metals, but because of their poor Seebeck coefficient and their large thermal conductivity, the interest in thermoelectric applications was limited. Ioffe's find led to numerous measurements on several compounds, and to the discovery of the best thermoelectric materials used to date: bismuth and lead telluride, as well as their antimony alloys [9, 10].

After a period of disinterest, due to the impossibility of further optimization of the compounds found, and the failure to discover better ones, funding revitalized research programs at the beginning of the 80's, mainly because of technological and scientific advances in other fields and because of the need to improve the efficiency of materials used in cooling devices; thermoelectric cooler efficiency being only 10% of Carnot cycle, but thermodynamic laws applied on thermoelectric phenomena show that achieving 100% is possible [11].

Nevertheless, even with only 30 % of the efficiency of Freon-based refrigerators TE devices created niches markets due to their reliability. For example in I.R. detector technology, where the expected lifetime of a detector is 10 years, the small size of TE devices allows their integration into compact optical systems [12]. Because TE materials can also be used as power sources (due to the Seebeck effect), research to find new materials such as $(GeTe)_{1-x}(AgSbTe_2)_x$ [13] (commonly called TAGS) were extensively carried on. Unfortunately, diffusion of Ag in the samples under the action of heat, created instability and short lifetime of the devices based on these materials. Applications included power generation for remote installations used in space exploration and petroleum industry. Once again, for such application the first requirement of the devices is reliability over efficiency.

Today, different optimized compounds are used depending on the working temperature range needed for the device. Figure 1-2 gives a summary of these thermoelectric materials according to their range of use. As we can see from this figure,

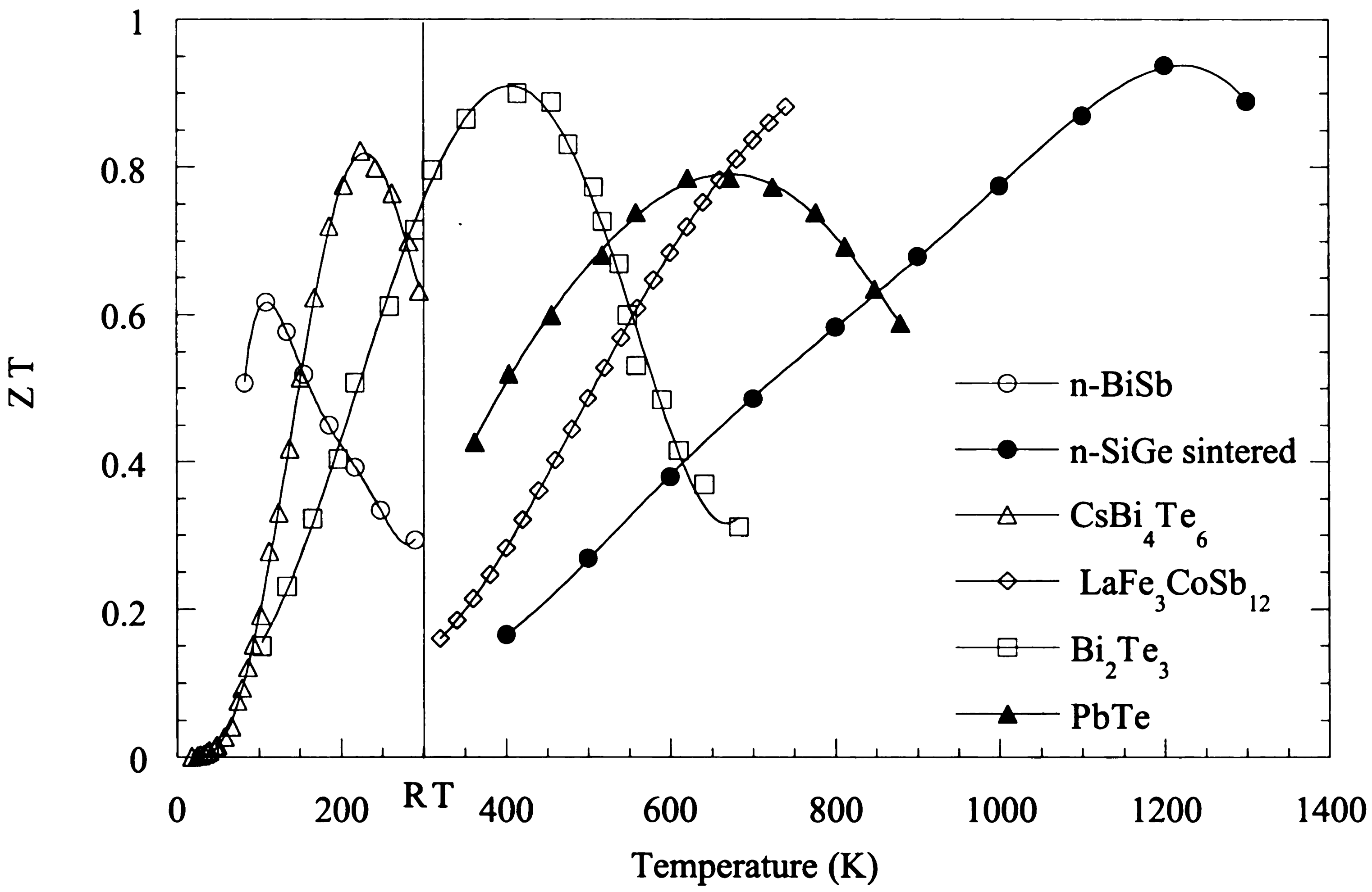

Figure 1-2: Figure of merit for the best thermoelectric materials: n-BiSb[14], Bi_2Te_3[14], PbTe[14], $LaFe_3CoSb_{12}$[15], n-SiGe[16], and $CsBi_4Te_6$[17].

there is a need for new compounds possessing good properties below and around room temperature. It is important to note that any material with a figure of merit superior to 1 will have possible industrial applications.

The interest in thermoelectricity is not recent but the need for new materials is increasing. There is great effort for developing new compounds that could surpass the properties of bismuth telluride that leads the market for the last 30 years. Taking into account the difficulty of "finding" the right compound, and optimizing it, long term planning is necessary and collaboration between physicists and engineers is the key to success. Such collaborations have been the paradigm in which the approach in this work has been developed.

1-2. Focus of this Research

Toward the need for developing new TE materials, investigations on different systems have been carried out by several research groups. TAGS (tellurium-antimony-germanium-silver) [13], skutterudites [15], half-Heusler alloys [18], clathrates [19], and quantum wells [20] are some systems that have been actively investigated. Metallic compounds typically have a small thermopower and a large thermal conductivity as already mentioned, therefore the use of semiconductors, as shown by Ioffe [8] constitute a better choice.

Our research group has been involved for several years in research on ternary and quartenary bismuth chalcogenide systems. Several promising compounds have been discovered. Such new materials include for example $BaBiTe_3$ [21] and $CsBi_4Te_6$ [17]. The latter one possesses a value of ZT equal to 0.8 at room temperature making it as good as the best $Bi_{2-x}Sb_xTe_{3-y}Se_y$ alloys. Promising quartenary compounds have also been synthesis such as $K_{1-x}Sn_{5-x}Bi_{11-x}Se_{22}$ [22] and $A_{1+x}M'_{4-2x}Bi_{7+x}Se_{15}$ [23] (with A=K, Rb; M'=Sn, Pb).

In addition, materials having complex composition and structure may possess complex electronic structure and may have a high thermoelectric power as well as low thermal conductivity. Therefore we investigated the system of isostructural semiconductive compounds having for general formula: $A_mB_nM_mQ_{2m+n}$, where A is an alkali metal or silver, B is lead or tin, M is Bismuth or Antimony, and Q is S, Se, or Te. This system crystallizes in the cubic face centered NaCl structure type with $Fm\bar{3}m$ for space group. Crystals of $KPbBiTe_3$ were first discovered using a flux method [24] by Dr. D.-Y. Chung. The structure was solved and as shown on Figure 1-3, the chalcogenides occupy the anionic positions, while the cations are disordered in the Na^+ sites.

The reasons our attention was attracted on this family of quartenary compounds can be summarized as follows:

- As mentioned, complex structures might give rise to complex electronic band structures that could be easily “tunable” in order to obtain enhanced properties.
- By choosing heavy elements such as Bi, Te, and Pb, we expect low phonon frequencies and therefore low thermal conductivity [25] .

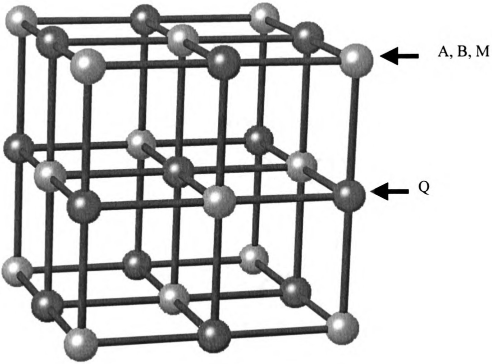

Figure 1-3: NaCl crystal structure type of $A_mB_nM_mQ_{2m+n}$ compounds with A, B, M on the Cl^- atomic sites and Q on the Na^+ sites.

- One system highly investigated is M_2Q_3 (with M=Sb, Bi ; Q=S, Se, Te) [26]. These optimized compounds are good TE materials, and since M and Q can be integrated in the general formula of our compounds, we expect good thermoelectrical properties as well .
- As previously mentioned, our research group has investigated many ternary and quartenary compounds such as $BaBiTe_3$ [21], $CsBi_4Te_6$ [17], $K\,Bi_{6.33}S_{10}$ [27], $K_2Bi_8S_{13}$ [27], α-β-$K_2Bi_8Se_{13}$ [28], $K_{2.5}Bi_{8.5}Se_{14}$ [28], $Ba_4Bi_6Se_{13}$ [29], $Eu_2Pb_2Bi_6Se_{13}$ [29], and $A_{1+x}Pb_{4-2x}Sb_{7+x}Se_{15}$ (A=K, Rb) [29]. The ternary system K/Bi/Se [30] has also been investigated and all these compounds showed promising properties. Since only bismuth-antimony telluride and bismuth antimony alloys are widely used today tend to confirm that Bi plays a decisive role in the enhancement of thermoelectric properties. It is important to note that its contribution is not well understood at the present time.
- A quartenary compound should have very low thermal conductivity especially if it exhibits mass fluctuation in the lattice.
- Due to their high polarizabilities, the use of heavy elements such as Pb, Bi, Sn, Sb, Se, and Te should give rise to compounds with large dielectric constants that would create a strong screening of the impurities and therefore increase the mobility of the carriers.

Because of these considerations, the investigation of this new family of compounds is justified. The starting goal of this work was to obtain new TE compounds that could be used around room temperature, with the hope of being able to "tune" the band gap and to maximize the dimensionless figure of merit ZT, by varying the composition of the compounds.

The material of reference in any TE research is Bi_2Te_3 and its alloys. Our goal is to surpass some or all of its transport properties summarized in Table 1-1 and to achieve a ZT greater to 1.

Table 1-1. Thermoelectric properties of n-type PbTe and Bi_2Te_3 at optimum temperature (T_{max}).

Compound	T_{max} (K)	σ (S/cm)	S(μV/K)	κ(W/m·K)	ZT	M_p (°C)	Ref.
Bi_2Te_3	400	800-1000	±210	1.4-1.6	0.8-1.1	585	*
PbTe	650	360	-180	1.1	0.70	1197	31

*data provided by Marlow Industries Inc.

1-3. Concepts and Important Physical Properties

In order to understand how to optimize materials for applications, let us take a closer look at the different variables that constitute the figure of merit ZT (see Eq. 1-1):

the electrical conductivity, the thermal conductivity, and the Seebeck coefficient. These important parameters are affected by energy gap, carrier concentration, and effective mass.

Performance of a Material

Because we need a tool to compare different thermoelectric materials, the figure of merit Z was introduced; often the dimensionless figure of merit ZT is used instead, where T is the absolute temperature. This dimensionless variable is proportional (see Eq. 1-1) to the square of the Seebeck coefficient S (μV/K), to the electrical conductivity σ (S/cm), and to the inverse of the thermal conductivity κ (W/m·K). It is important to note that these three parameters are not independent and their values are determined by the details of their electronic structure, and by the scattering and number of charge carriers. Therefore, by modifying one property, one can affect the other in the wrong direction. Usually when increasing the electrical conductivity the Seebeck coefficient decreases, and vice versa. Therefore, a subtle equilibrium must be found in order to achieve optimization. As we can see from Eq. 1-1, in order to increase the figure of merit ZT, we must decrease the thermal conductivity, while increasing or keeping constant the two other parameters. This can be achieved by doping, and/or by preparing solid solutions.

Electrical Conductivity σ

A semiconductor normally exhibits thermally activated electrical conductivity that increases with rising temperature. There are two types of electronic semiconductors, intrinsic and extrinsic, depending on the presence of impurity levels in the forbidden energy gap. The dependence of the conductivity as a function of the temperature for different types of materials is shown in Figure 1-4.

Metals (curve a) have very high conductivity, typically above 2000 S/cm that decreases as the temperature increases. Instead, semiconductors (curve b) exhibit a conductivity that rises with temperature but the magnitude is much lower than for a metal, and typically in the range of 10^{-5} to 2000 S/cm depending on the band gap. Insulators have conductivity inferior to 10^{-7} S/cm.

(a) Intrinsic Electronic Semiconductor.

If a semiconductor does not have impurities, its energy diagram can be represented as Figure 1-5a. As the temperature increases, electrons from the valence band where they were engaged in bonding orbitals, are excited to the conduction band where they can move freely. As they leave the valence band, holes are created and left behind. Under the action of an electric field, the holes move in the opposite direction of the electrons present in the conduction band.

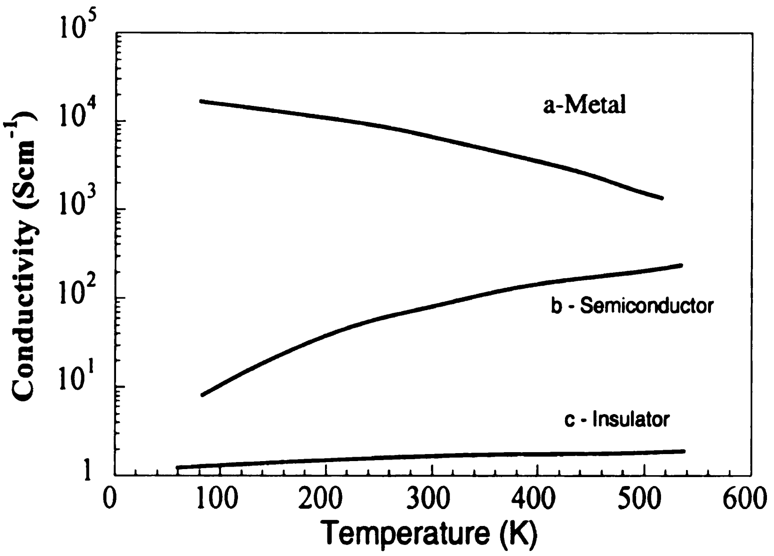

Figure 1-4: Variation of the conductivity as a function of temperature for different materials.

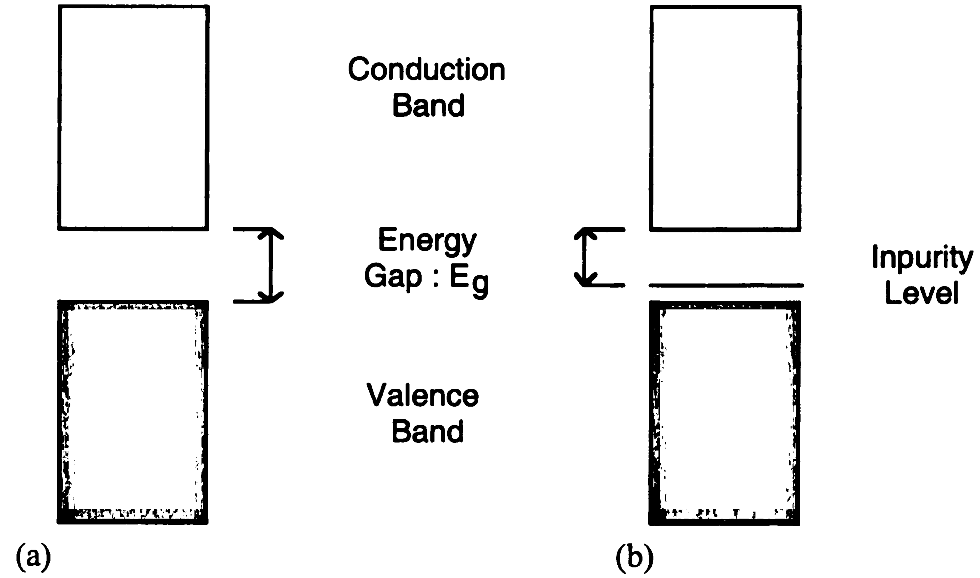

Figure 1-5: (a) Intrinsic and (b) extrinsic semiconductor.

This creates an electrical conduction that is expressed in Siemens per centimeters (S/cm) and can be written as [32]:

$$\sigma = \sigma_0 \exp\left(\frac{-E_g}{2k_B T}\right) \qquad \text{Eq. (1-4)}$$

where σ_0 is the limit of the conductivity at high temperature, E_g is the energy gap, k_B the Boltzmann constant, and T the absolute temperature. It is important to note that for industrial applications, extrinsic semiconductors are used because their conductivity can be precisely controlled through doping. In practice, all semiconducting materials are "extrinsic" since they are either adventitiously or intentionally doped.

(b) Extrinsic Electronic Semiconductor

The values of the conductivity can be greatly increased by the addition of small controlled amount of impurities in the pure semiconductor. The band diagram can be represented as Figure 1-5b. Impurity levels have been created in the forbidden energy gap by addition of these dopants. Two cases are then possible.

- If the impurity added has one electron less than the element in the system that it replaces, the later will provide the missing electron for the partial covalent bond (Figure 1-6a) leaving a moving hole behind. We therefore obtain a p-type doped material and the conductivity is equal to $\sigma = \sigma_0$ exp. $(-E_p/k_B T)$ where σ_0 is the limit of the conductivity at high temperature, and E_p the energy level of the impurity added.

- In the case where the element added has one electron in excess, this electron will move freely in the crystal since it cannot be integrated in covalent bonding (Figure 1-6b). The system is then said to be n-type, and $\sigma = \sigma_0 \exp.(-E_n/k_BT)$ where E_n is the energy level of the impurity having one electron in excess.

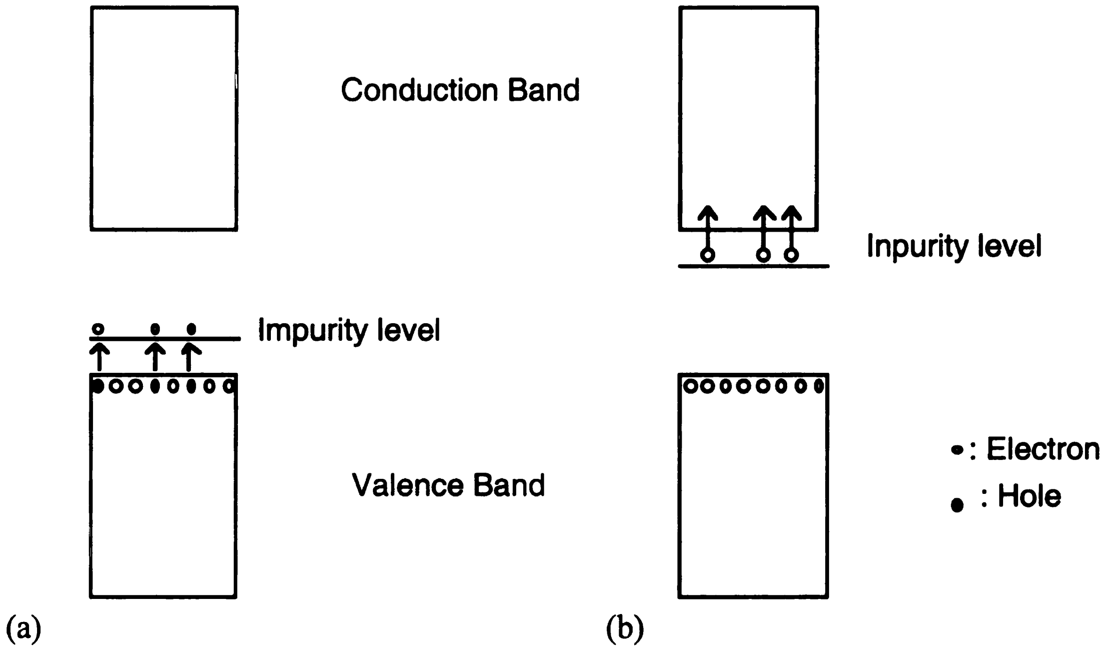

Figure 1-6: (a) p-type doped and (b) n-type doped semiconductor.

The electrical conduction can also be expressed as a function of the mobility (see Eq. 1-5) which is a proportional coefficient between the average drift velocity v_d of the charge distribution and the applied field E[32].

$$\sigma = Ne\mu_n + Pe\mu_p \qquad \text{Eq. (1-5)}$$

where N and P are respectively the number of electrons and holes moving in the system expressed in number per cm^{-3}, and μ_n and μ_p the mobility of the negative and positive charge carriers expressed in $cm^2/V \cdot sec$.

Thermal Conductivity (κ)

The value of the thermal conductivity of a compound plays a decisive role in its possible use as a thermoelectric material. Because the value of ZT is inversely proportional to the thermal conductivity, a low value is necessary (see Table 1-2). From these data, we can see that metals possess the highest thermal conductivity values while the lowest are found for insulators. Semiconductors lie between.

The thermal conductivity of a material is mainly the sum of two components: the lattice (phonons) κ_l, and the electronic part κ_e[33(b)].

$$\kappa = \kappa_e + \kappa_l \qquad \text{Eq. (1-6)}$$

In this equation, we have neglected the bipolar contribution that is due to the simultaneous movement of electrons and related holes, only important in the intrinsic region of the semiconductor.

For an intrinsic undoped semiconductor, the thermal conduction will be mainly due to the lattice contribution. As electrons (or holes) are added to the system, the electronic contribution rises since the electrons (or holes) act as carriers of heat.

Table 1-2. Thermal conductivity at room temperature for different type of materials[33(a)].

Compound	κ_{RT} (W/m·K)	Compound	κ_{RT} (W/m·K)
Metals		Semiconductor	
copper	400	Bi_2Se_3	2.4
Ag	430	Se	2
		Te	3
Semimetals		PbSe	1.7
Bi	8.5	PbTe	2.3
Sb	18	PbS	3.0
		GeTe	1-3
Other		CdS	20
Glass	0.8		
Concrete	0.9		

Nevertheless, they also serve as scattering centers for the phonons (quanta of lattice waves) that will diminish the mean free path λ of the heat carriers, and as a consequence diminish the lattice thermal conductivity. It is understandable that predictions on the evolution of the thermal conductivity are therefore challenging since the addition of a dopant has a double effect on κ.

(a) Electronic Thermal Conductivity

This contribution, due to electrons (or holes) that carry heat in the system, is insignificant at very low doping level but become more important as the number of charge carrier increase. The electronic participation of the thermal conductivity is given by the Wiedemann-Franz law as a function of the electrical conductivity σ, the absolute temperature T, and the Lorenz factor L_0 in the approximation where only one band contributes to the transport properties [33(c)].

$$\kappa_e = \left(\frac{k_B}{e}\right)^2 L_0 \sigma T \qquad \text{Eq. (1-7)}$$

The Lorenz factor is dependent upon the scattering mechanisms that occur in the system, and upon the level of doping. It has a wide range of variation: from a value of 2 in the case where an acoustic scattering mechanism is dominant, to a value of 4 for a ionized impurity scattering mechanism (see Figure 1-7) [33(d)].

The reduced Fermi level ξ is introduced as: $\xi = E_F / k_B T$with E_F being the energy measured at the band edge. The problem is then reduced to determining the appropriate value of L_0 for the system studied. Nevertheless, values converge to $\pi^2/3$ for high carrier concentration, in other words, for high doping level. This value is the one usually used in calculations.

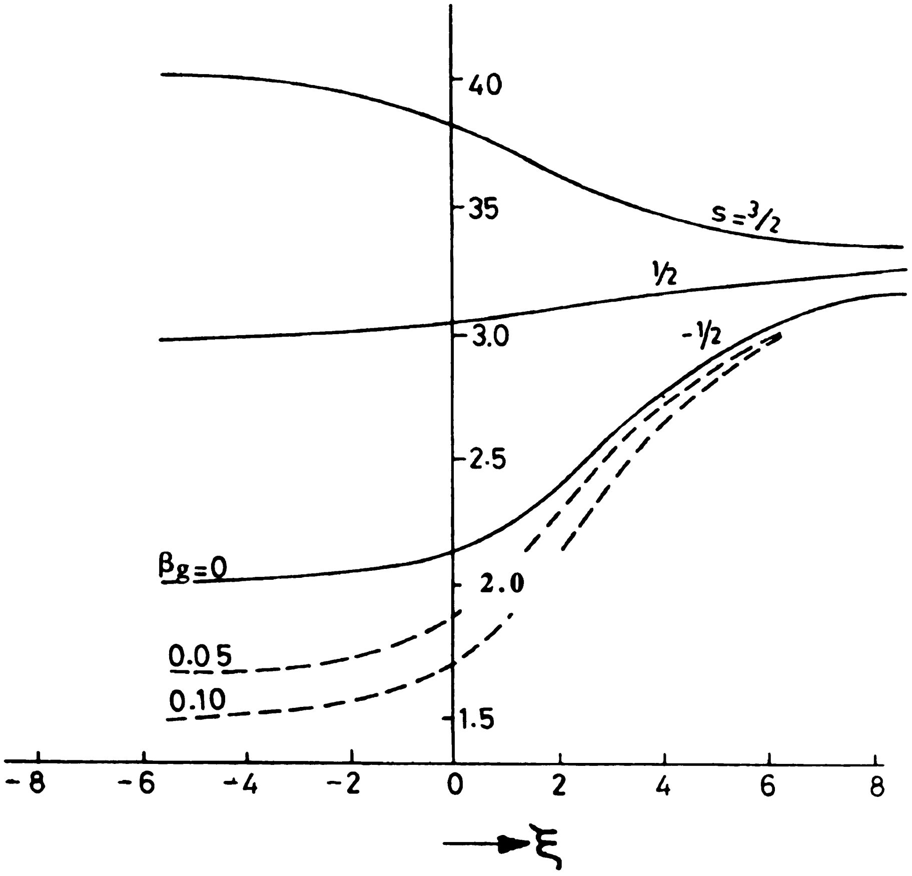

Figure 1-7: Lorentz factor L_0 as a function of the reduced Fermi level and different scattering process (s).

(b) Lattice Thermal Conductivity

In a crystal, atoms can vibrate around their positions and give rise to standing or traveling vibrational waves through the lattice. These normal modes of vibration have characteristic frequencies. Phonons are defined as the quanta of excitation of these normal modes of lattice vibration that are created. As impurities are introduced, the normal modes of vibration are altered or new ones are created. If a temperature gradient is built, the phonon distribution deviate from the equilibrium and a flow of heat is generated.

The lattice thermal conductivity follows a T^3 law at very low temperatures, and a T^{-1} law [33(e)] (see Figure 1-8) at temperature higher than the Debye temperature. These dependencies can be explained by an Umklapp three-phonon scattering, and boundary scattering mechanism [34]. A three phonon interaction is created by the anharmonic nature of the crystal potential and can be simply described in Figure 1-9a [34], where two longitudinal phonons, represented by the wave vectors $\mathbf{q}_1$ and $\mathbf{q}_2$ interact to produce a third one ($\mathbf{q}_3$). In terms of conservation of energy, this is described as : $\omega_3 = \omega_1+\omega_2$. The conservation of the momentum give us $\mathbf{q}_1+ \mathbf{q}_2 = \mathbf{q}_3$ (normal process). In fact, the phonon momentum can be changed in some cases and we have the new expression:

$$\mathbf{q}_1 + \mathbf{q}_2 = \mathbf{q}_3 + \mathbf{G}$$

(where **G** is the reciprocal lattice vector) as shown in Figure 1-9b.

Therefore depending on the value of G, two cases have to be considered:

- If $G = 0$, the total phonon momentum is conserved. The flow of phonon will continue independently of the temperature. Since the mean free path λ stays unchanged, no thermal resistance is created.
- In the case of $G \neq 0$, the mean free path is altered and a thermal resistance is created. This generates a maximum in the thermal conductivity at the boundary between the T^3 and the $1/T$ dependence (see Figure 1-8).

Leibfreid and Schlomann (1954) [35] derived the following equations that can account for the behavior of the lattice thermal conductivity as a function of the temperature, if we assume that an Umklapp process takes place:

$$\kappa_l = \kappa_0 \, f(\Theta_D / T) \qquad \text{Eq. (1-8a)}$$

At high temperature, $T > \Theta_D$ $\quad f(\Theta_D / T) = \Theta_D / T$ $\qquad$ Eq. (1-8b)

While, when $T < \Theta_D$ $\quad f(\Theta_D / T) = \left(\frac{T}{\Theta_D}\right)^3 \exp\left(\frac{\Theta_D}{bT}\right)$ $\qquad$ Eq. (1-8c)

To this effect, we have to add the boundaries scattering, at low temperature, and the exponential rise of the lattice thermal conductivity (in Eq. 1-8c) is changed to a T^3 law. The prediction given by the $1/T$ law at high temperature (from Eq. 1-8b) is in good agreement with the experimental values if the volume and the pressure are kept constants.

Using these equations, we can justify the T^3 rise of the thermal conductivity by considering Eq. (1-8b) and the $1/T$ at higher temperature from the Eq. (1-8c).

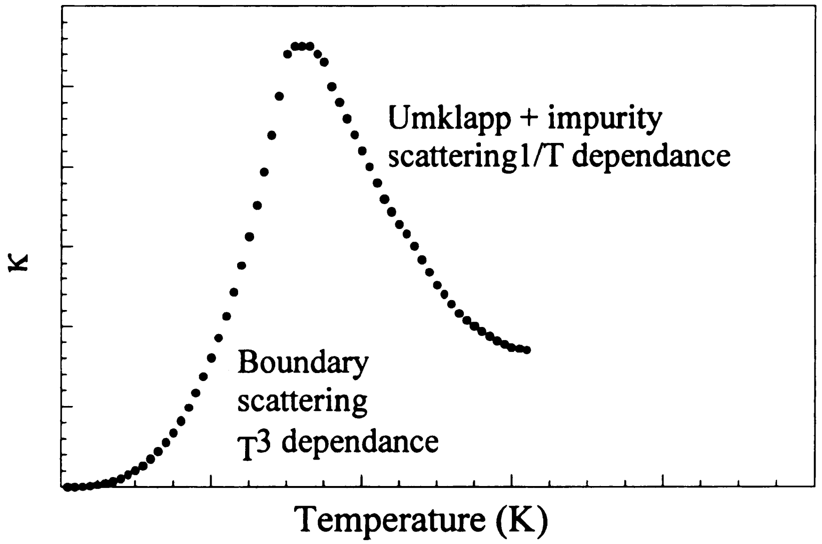

Figure 1-8: Thermal conductivity and the different scattering processes involved.

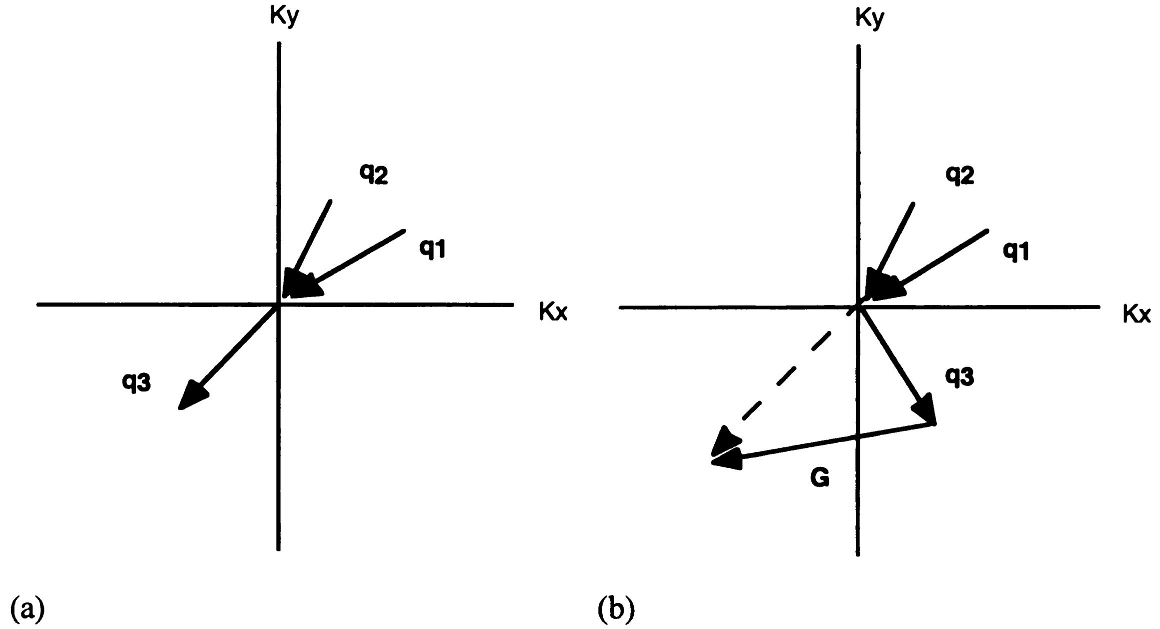

(a) (b)

Figure 1-9: Three phonons interaction. (a) Normal process and (b) Umklapp process.

(c) Radiative Losses

This important phenomenon is common to all materials. Photons passing through a material will give rise to thermal radiations. The contribution due to this effect was formalized by Genzel[36]:

$$\kappa_{\text{photons}} = \left(\frac{16}{3}\right)\sigma_0 n^2 T^3 \alpha^{-1} \qquad \text{Eq. (1-9)}$$

where σ_0 is the Stefan-Boltzmann constant, n the refractive index of the material and α the absorption coefficient. The radiative losses follow a T^3 law as seen in Eq. (1-9).

Bhandari and Rowe pointed out that this contribution is appreciable for tellurium, selenium, and the lead chalcogenides. Therefore, we can expect to find this part in the measurement of the materials presented in this dissertation.

During the analysis of the thermal conductivity data, the photon contribution need to be subtracted since the value of κ_{photons} depends on the shape of the samples measured and is not an intrinsic property of the material. In order to obtain κ of a certain sample without the photon contribution, the following methodology is adopted:

1 - The electronic contribution is calculated using the Wiedemann-Franz law and subtracted from the experimentally measured thermal conductivity. Let us call κ' the remaining thermal conductivity contribution.

2 - At high temperature, typically superior to 150 K, a 1/T fit is applied to the appropriate part of the κ' plot (see Figure 1- 8). The difference between the fit and κ' give the radiative contribution $\kappa_{photons}$.

3 - κ_l is then obtained by keeping the values of κ' at low temperature and by using the value given by the fit at higher temperature.

4 - The total thermal conductivity without the contribution from radiative losses is then obtained by adding the lattice and the electronic contribution.

5 - In order to verify that the rise in the original plot of the thermal conductivity at high temperature is due to radiative losses, $\kappa_{photons}$ is plotted against T^3. A good linear fit act as proof of the hypothesis developed, since the contribution from radiative losses should vary linearly with T^3, see Eq. (1.9).

In the following work, the photon contribution was subtracted as indicated above. Therefore, plots of the thermal conductivity before and after corrections will be presented for each measurement made if radiative losses are presents.

Seebeck Coefficient (S)

As soon as a new compound is synthesized, the first property measured is the Seebeck coefficient since it is squared in the equation for ZT. It is a relatively simple measurement that can be done on semiconductors and, in addition to the value of S at different temperatures, the measurement of this property gives also other valuable information on the material such as its class (metal, insulator, semiconductor), its doping state (n-type, p-type), and sometimes its energy gap.

The Seebeck coefficient can be in a simple way be viewed as being the measure of the "heat" per carrier over the temperature.

$$S = \frac{\text{"heat" per carrier}}{\text{Charge per carrier times T}}$$

Boltzmann transport theory lead to understanding of the Mott equation:

$$S = \left(\frac{\pi^2}{3}\right)\left(\frac{k_B^2 T}{e}\right)\left(\frac{d \ln \sigma(E)}{dE}\right)_{E=E_F} \qquad \text{Eq. (1-10)}$$

where σ(E) is the electrical conductivity depending on the band filling (the Fermi energy E_F). If we consider the electronic conductivity being independent of the energy, σ(E) is then proportional to the density of state at E and S is a measure of the difference of the electrical conductivity above and below the Fermi surface. It is important to note that the Seebeck coefficient is inversely dependent upon the carrier concentration [37] of the dopant since it is dependent on the reduced Fermi level ξ by:

$$S = \left(\frac{k_B}{e}\right)\left(\frac{5}{2} + s - \xi\right) \text{ and } \xi \text{ is related to n by } n = 2\left(\frac{2\pi m^* k_B T}{h^2}\right)^{3/2} \exp(\xi).$$

However, because the carrier concentration affects only slightly the thermal conductivity, it is possible to enhance the figure of merit by optimizing S and σ through changes in the carrier concentration. Nevertheless, if σ became too large Wiedemann-Franz law predicts that the thermal conductivity will rise considerably. As a rule of thumb κ increases of about 0.7 W/m·K with an increases of σ of 1000 S/cm.

(a) Trend of S

The plots of Figure 1-10 show the behavior of S for different type of materials as a function of the temperature. Therefore, by looking at the value and the shape of the curve, one can tell if the measured sample is a metal, an insulator, or a semiconductor.

For a metal, S decreases as the temperature decrease in accordance to the relation between S and T[38]:

$$S \sim \left(\frac{k_B^2 T}{e E_F} \right) \qquad \text{Eq. (1-11)}$$

where e is the charge of the carrier and ε_F the Fermi level. The value of k_B/e being approximately 87 μV/K, S must be much inferior to it, since for a metal the transport take place within k_BT. On the contrary, for a semiconductor, the absolute value of S increases as the temperature decreases based on Eq. (1-12). In the case where only one type of carrier is present, a value superior to 87 μV/K is expected[38].

$$S \sim \frac{\left(\frac{E_g}{2}\right)}{(eT)} \approx \left(\frac{k_B}{e}\right)\left(\frac{E_g}{(2k_BT)}\right) \qquad \text{Eq. (1-12)}$$

Finally, among other possible behaviors, some narrow band gap semiconductors can exhibit a combination of metallic and semiconductors behavior. The thermopower in this case may be reminiscent of either a metal or a semiconductor, or may even be nearly temperature independent depending on the size of the bang gap and the degree of doping.

(b) Sign

The sign of S is a simple and safe way to find what kind of carrier is predominant in a compound in a given range of temperature. The Seebeck coefficient can be written as a function of a difference of potential over a difference of temperature as in Eq. (1-13).

$$S = \Delta V / \Delta T \qquad \text{Eq. (1-13)}$$

A negative Seebeck coefficient indicates that the compound is n-type, meaning that the majority of the carriers are electrons. When measuring the Seebeck coefficient, a temperature gradient is applied to a material and a cold (T_c) and hot (T_h) sides are generated. The electrons move from T_h to T_c because electrons on T_h have higher kinetic energy than those on the cold side (i.e. kinetic theory of gases). As a consequence, a flow is established from T_h to T_c creating a negative charge build up on T_c, and a current is generated form T_c to T_h in order to avoid more charging on T_c. This creates charge separation between T_h and T_c and the generation of a voltage difference ΔV. If the material is n-doped the created voltage is negative and because of Eq. (1-13), S is also negative. In the case of the compound has a majority of hole carriers (p-type), a similar flow is generated with holes moving from T_c to T_h. Nevertheless, the potential created will be in opposite direction of the one created by electrons and the sign of S will be positive. Seebeck measurement is an effective, fast and easy way to determine the type of the majority carriers.

(c) Energy Band Gap

Often, the behavior of semiconductors is slightly different from what described in (a). Because of the existence of two different regions (extrinsic and intrinsic), $|S|$ does not vary linearly. As the temperature rises, extrinsic carriers are exited from impurity states. This allows the gap between the Fermi level and the appropriate band to increase , which enhanced the absolute value of the Seebeck coefficient. As soon as the temperature is large enough, carriers coming from impurities reach a saturation level and electrons-holes pairs across the band gap are excited (intrinsic region), creating opposite carriers and therefore $|S|$ decreases, because S is the sum of the contribution due to the electrons and the contribution due to the holes (see Eq. 1-14).

$$S = \frac{\sigma_e S_e + \sigma_h S_h}{\sigma_e + \sigma_h} \qquad \text{Eq. (1-14)}$$

If we plot S as a function of the temperature, Figure 1-11, the Seebeck coefficient pass through a maximum. The energy gap of the semiconductor can then be estimated based on Eq. (1-15)[39]:

$$E_g \approx 2eS_{max}T_{max} \qquad \text{Eq. (1-15)}$$

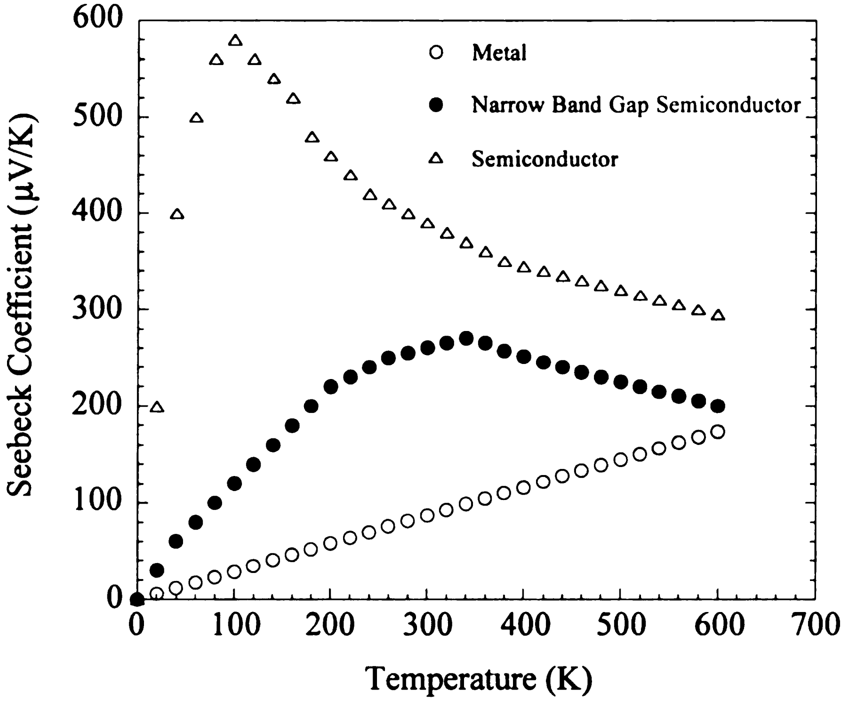

Figure 1-10: Seebeck coefficient behavior for different types of materials

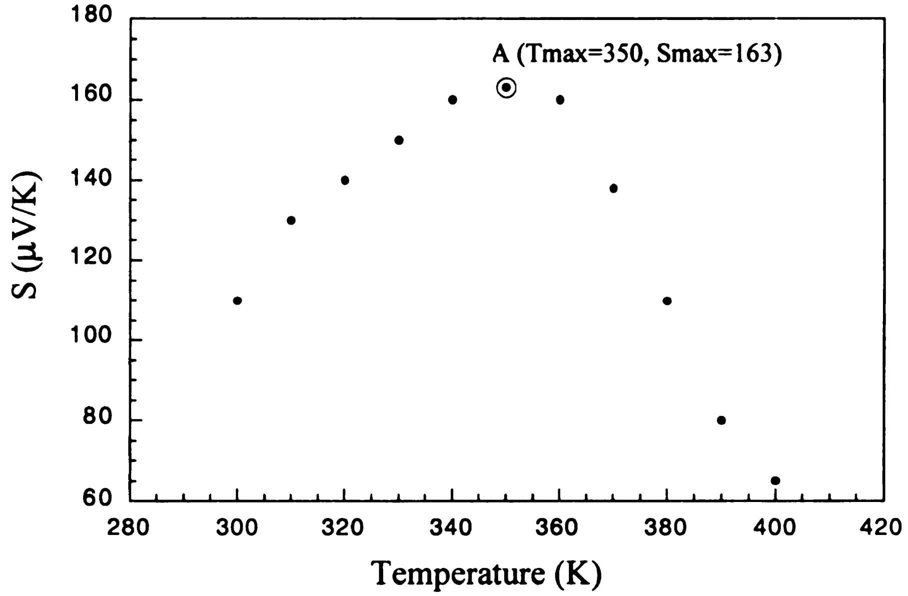

Figure 1-11: Seebeck measurement showing a maximum at the point A

Because for wide band gap materials, T_{max} is superior to 150 °C, this way of calculating E_g only works for narrow band gap semiconductors.

In conclusion, the measurement of the Seebeck coefficient should be the first measurement made. The interpretation of the data can give valuable information about the properties of the material such as its type, the type of the charge carriers involved in the electrical conduction and even in some cases its band gap. Multiple measurements should be made for the same material to insure reproducibility.

Other Important Properties and Notions

(a) Energy gap

As described above, the band gap of a semiconductor can be measured from the analysis of Seebeck experiments if $|S|$ passes through a maximum. It can also be obtained from conductivity measurements using Eq. (1-4), but the most reliable way to obtain it is optically. Analysis of the spectrum recorded can give us the value of the band gap as well as its nature i.e. direct or indirect.

After data are collected using an infrared or solid state UV/Vis spectrometer (see chapter 2 for more details), the absorption (α/S) is calculated from the reflectance data using the Kubelka-Munk function[40]: $\alpha/S = (1-R)^2 / 2R$, where R is the reflectance at a given wavenumber, α the absorption coefficient, and S is the scattering coefficient. The value of the band gap is then given by the intersection point between energy axis at the absorption offset and the line extrapolated from the linear portion of the absorption edge as shown in Figure 1-12.

In a direct band gap, the energy (hv) and momentum (q) of the photon are enough to excite an electron from a lower to a higher energy state (see Figure 1-13a). For such transition, the spectrum shows an abrupt change in the absorption edge (Figure 1-13-b). A linear variation of the square of the absorption coefficient as a function of the energy is characteristic of a direct band gap (see Eq. 1-16)[41].

$$\alpha(h\nu) = A(h\nu - E_g)^{1/2} \qquad \text{Eq. (1-16)}$$

with A is a constant proportional to the effective mass of electrons and holes.

In an indirect band gap the momentum of the photon is not enough to allow the transition and a third particle is involved: a phonon (Figure 1-14a). The threshold in an indirect transition, as seen in Figure 1-14b, is less abrupt than in a direct transition since the probability of the transition occurrence is decreased by the necessity of having involved a third component. Because a phonon can be absorbed or emitted, the equation similar to Eq. 1-16 is more complicated.

$$\alpha\,(h\nu) = \alpha_a\,(h\nu) + \alpha_e\,(h\nu) \qquad \text{Eq. (1-17)}$$

where $\alpha_a(h\nu)$ is the absorption when a phonon is absorbed and $\alpha_e(h\nu)$ when a phonon is emitted; A is a constant [41].

$$\alpha_a(h\nu) = A'\frac{\left(h\nu - E_g + E_P\right)^2}{\exp\left(E_p/(k_B T)\right) - 1} \qquad \text{Eq. (1-18)}$$

$$\alpha_e(h\nu) = A'\frac{\left(h\nu - E_g - E_P\right)^2}{1-\exp\left(-E_p/(k_BT)\right)} \qquad \text{Eq. (1-19)}$$

Therefore the use of a plot of $\alpha(h\nu)$ at a certain power versus the energy $h\nu$ in this scenario is not possible.

A last case to consider is the case of a heavily doped indirect semiconductor. Here the momentum is conserved through electron-electron scattering and a plot of the square of the absorption coefficient versus the energy should give a linear fit according to Eq. (1-20).

$$\alpha(h\nu) = C(h\nu - E_g - D)^2 \qquad \text{Eq. (1-20)}$$

C and D being two constants[41].

Lovett[42] defines a narrow band gap semiconductor when the value of its band gap is less than ten times k_BT (0.26 eV). Table 1-3 give a list of some materials with their corresponding band gaps. It is important to note that for thermoelectric materials the band gap should be high enough to avoid the creation of minority carriers that would decrease the thermopower S.

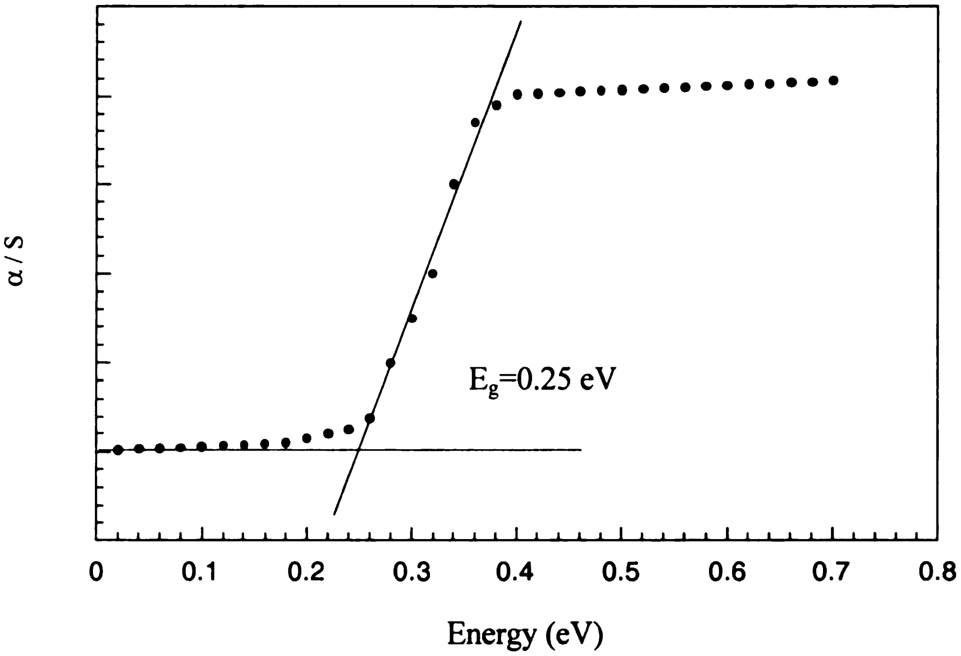

Figure 1-12: Calculation of an energy gap using absorption spectroscopic data.

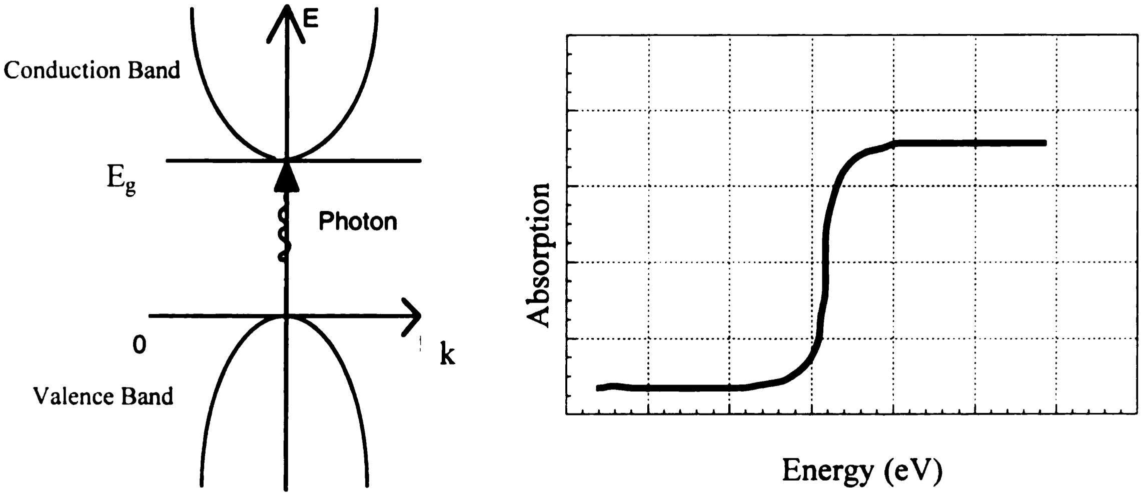

(a) (b)

Figure 1-13: (a) Direct transition process and (b) absorption coefficient showing a abrupt absorption edge with an energy increase.

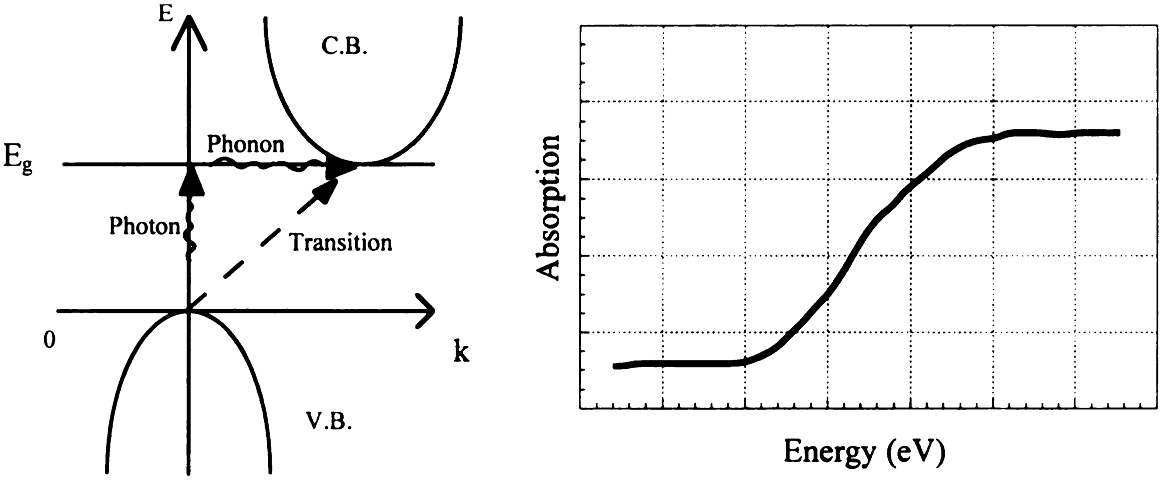

(a) (b)

Figure 1-14: (a) Indirect transition involving a phonon and (b) absorption coefficient showing a slower increase with energy.

Table 1-3. Energy gap (eV) for some semiconductors. The nature of the band gap is also reported (i.e. direct (i) or indirect (d))[43].

Semiconductor	Energy Gap			Semiconductor	Energy Gap		
	0 K	300 K			0 K	300 K	
AgCl		3.2	i	InSb	0.24	0.18	d
AlAs	2.3	2.16	i	HgTe	-0.3		d
Bi_2Te_3	0.16		i	PbS	0.29	0.35	d
C (diam)	5.4		i	Sn	0	0	
CuBr		2.94		SnTe	0.3	0.18	d
CdSe	1.84	1.74	d	PbTe	0.19	0.3	d
InAs	0.43	0.34	d	PbSe	0.17	0.27	d

(b) Charge Carrier Concentration

The carrier concentration is defined as the number of charge carriers of a certain type per unit volume. This concentration shows different properties for different materials. For metals, n is independent of the temperature which explain the decrease of the conductivity that follows the behavior of the mobility due to the increase in the scattering probability. For semiconductors n is a function of the temperature and increases exponentially as T increases.

A typical plot of the carrier concentration as a function of temperature is shown in Figure 1-15. Three distinct regions are present. At low temperature (high T^{-1}), only few carrier are exited to the conduction bands. As the temperature increases thermal excitation allows more transitions until a saturation plateau is reached (called exhaustion). When the temperature is increased further, the intrinsic carriers are excited and we observe a large increase of n. As West[44] noted, it is important to try to obtain the larger temperature range possible for the exhaustion part, making the device performance stable over large temperature range.

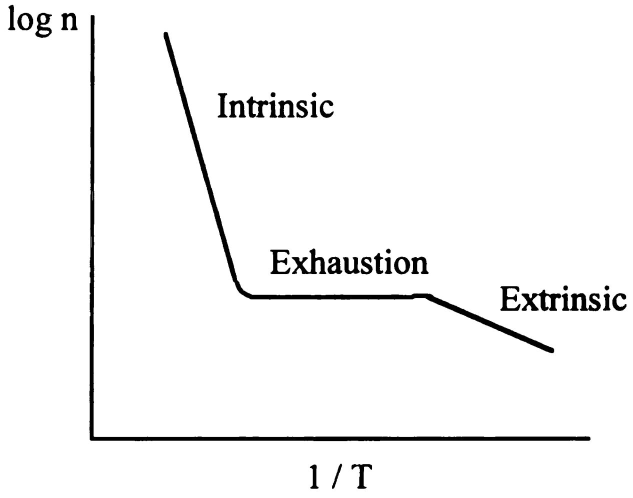

Figure 1-15: Carrier concentration behavior for a semiconductor as a function of temperature.

The figure of merit ZT is a function of the Fermi energy. The Fermi energy is in turn a function of the carrier concentration, carrier effective mass and the temperature. Nevertheless, the thermal conductivity depends little on n, at least until a certain level. The Seebeck coefficient is a function of 1/ln(n). Therefore, it is the conductivity that can be optimized by controlling the carrier concentration introduced as impurities, and through it the figure of merit.

It has been demonstrated that for an intrinsic semiconductor the product NP (see Eq. 1-20) is a constant (N and P being the concentration of electrons and holes respectively). Therefore when introducing one type of charge carrier in the system, the concentration of the other type is adjusted to keep the product constant[45].

$$NP = 4\left(\frac{k_B T}{2\pi h^2}\right)^3 \left(m_e m_h{}^{3/2} \exp\left(\frac{E_g}{k_B T}\right)\right) \qquad \text{Eq. (1-21)}$$

For extrinsic semiconductors, optimization of the transport properties is reached for a certain number of charge carriers; if more charge carriers are added, the properties of the materials deteriorate. For small band gap semiconductors, n should be in the range[46] of $10^{18}\,cm^{-3}$ and $10^{20}\,cm^{-3}$. If the charge carrier concentration is too high then the electronic part of the thermal conductivity would increase considerably which is undesirable for TE applications.

The role of carriers and their concentration is not fully understood but some basis exists and the "goal of the game" is therefore to introduce the right amount of dopant (the right carrier concentration) in order to optimize ZT.

(c) Effective Mass (m^*_e, m^*_h)

An electron in a vacuum when submitted to an electromagnetic field will have a thermal velocity depending on its mass m_0. If the electron is moving in a crystal, it will feel the periodic electric field due to the presence of the atoms in the crystal. If the electric field is E and v the velocity of the electron, then:

$$-e\,E = m\,v \qquad \text{Eq. (1-22)}$$

(Newton's law Force = mass * acceleration)

with $$v = (3\,k_B\,T / m)^{1/2} \qquad \text{Eq. (1-23)}$$

In the case of a free electron, m is equal to m_0 ($9.1\ 10^{-31}$ kg) in the equation of the velocity. The effective mass m* is defined as the mass that the electron possesses when moving in the crystal under E, and is equal to [47]:

$$m^* = h^2\left(\frac{d^2\varepsilon}{dk^2}\right)^{-1} \qquad \text{Eq.(1-24)}$$

The denominator term is the "curvature" of the electronic structure band considered. Therefore if m* is large i.e. if the carriers are heavy, the band will be less disperse than for light carriers (see Figure 1-16)

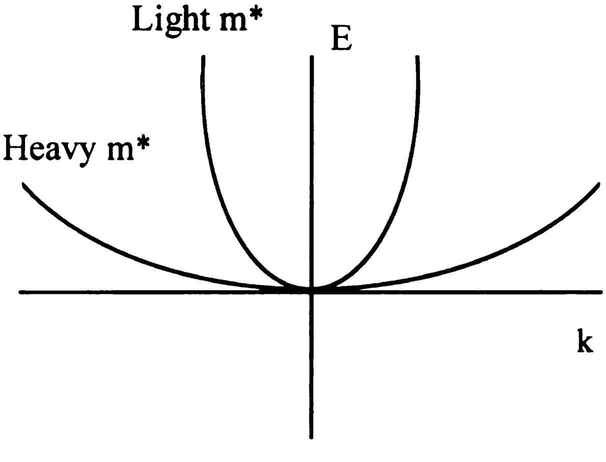

Figure 1-16: Effect of the effective mass on the electronic band.

Electrons and holes have different effective masses when present in different materials since they are submitted to different atomic parameters and lattice potentials. Table 1-4 shows different values of m^*_h and m^*_e. As we can see, these values vary notably from material to material, which will give different velocities and create different electronic band curvatures.

The role of the effective mass of electrons and holes in the enhancement of the figure of merit ZT is not fully understood. Bhandari and Rowe[37] suggest that a high m^*_e and m^*_h / m^*_e might increase ZT .

Table 1-4:. Different effective mass ratio for several different type of semiconductors.

Semiconductor type		m_e^* / m_0	m_h^* / m_0	Semiconductor type		m_e^* / m_0	m_h^* / m_0
(IV)	Si	0.23	0.12	IV-Vi	PbS	0.25	0.25
	SiC	0.60	1.20		PbSe	0.33	0.34
III-V	AlSb	0.30	0.40		PbTe	0.22	0.29
	InSb	0.01	0.18	II-IV	Mg_2Si	....	0.46
II-VI	CdTe	0.14	0.37	II-V	CdSb	0.16	0.10

Data from page 234 of reference 7

In summary, it has been shown that many physical properties have to be considered in order to fully understand the mechanism by which the figure of merit ZT can be optimized. Great attention is given to the measurement of the Seebeck coefficient due to its importance in the formulation of ZT. Nevertheless, each term of this equation is important and often large value of the thermal conductivity counterbalances large S. However, as it has been demonstrated for Bi_2Te_3, κ can be decreased by preparing appropriate solid solutions, and the electrical conductivity increased by introducing the right amount of charge carriers through doping, leading to optimum ZT for this material. We hope to accomplish the same goal for the materials described in this dissertation.

References

1. Kryotherm, "Areas of thermoelectric modules application", [Online] Available http://www.kryotherm.spb.ru/cooling2.html., February 23, **2000**
2. M. Rowe, *Thermoelectric News*, **1998**, 12
3. T.J. Seebeck, *ABH. Preuss. Akad. Wiss.*, **1822-1823**, 265
4. J.C. Peltier, *Ann. Chim. Phys.*, 56, **1934**, 371
5. G.L. Bennett, "Space Applications", in CRC Handbook of Thermoelectrics, Ed. by D.M. Rowe, **1994**, 515
6. A.F. Ioffe "Physics of Semiconductor", Ed. Academic Press Inc. New York, **1960**
7. D.D. Pollock, "Thermoelectricity Theory, Thermometry, Tool", Philadelphia, ASTM, **1985,** 111
8. A.F. Ioffe, "Semiconductor, Thermoelements and Thermoelectric Cooling", Infosearch Ltd., London, **1958**
9. H. Sherrer, S. Sherrer, "Bismuth Telluride, Antimony Telluride, and Their Solid Solution", in CRC Handbook of Thermoelectrics, Ed. by D.M. Rowe, **1994**, 211
10. V. Fano, "Lead Telluride and Its Alloys", in CRC Handbook of Thermoelectrics, Ed. by D.M. Rowe, **1994**, 257
11. M.G. Kanatzidis, F.J. Disalvo, *Naval Research Reviews*, 4, **1996**,14
12. A.W. Allen, Supplement to *Laser Focus World.* March **1997**
13. E.A. Skrabeck, D.S. Trimmer, "Properties of the General TAGS System", in CRC Handbook of Thermoelectrics, Ed. by D.M. Rowe, **1994**, 267
14. T.M. Tritt Science, 272, **1996,** 1276
15. B.C. Sales, D. Mandrus, R.K. Williams, *Science*, 272, **1996**, 1325
16. C.B. Vining, "Silicon Germanium", in CRC Handbook of Thermoelectrics, Ed. by D.M. Rowe, **1994**, 257
17. D.Y. Chung, T. Hogan, P. Brazis, M. Rocci-lane, C. Kannewurf, M. Bastea, C. Uher. M.G. Kanatzidis, *Science*, 287, **2000**, 1024
18. K. Mastronardi, D. Young, C.C. Wang, P. Klalifah, R.J. Cava, *Appl. Phys. Lett.*, 74, 10, **1999**, 1415
19. C. Uher, J. Yang, S. Hu, *Mat. Res. Soc. Proc.* 545, **1999**, 247
20. H. Scherrer, Z. Dashevsky, V. Kanster, A. Casian, I. Sur, A. Sandu, *Mat. Res. Soc. Proc.* 545, **1999**, 99
21. D.Y. Chung, S. Jobic, T. Hogan, C.R. Kannewurf, R. Brec, R. Rouxel, M.G. Kanatzidis, *J. Am. Chem. Soc.*, 119, **1997**, 2505-2515
22. A. Mroztek, D.Y. Chung, T. Hogan, M.G. Kanatzidis, submitted for publication
23. K.S. Choi, D.Y. Chung, A. Mroztek, W. Brazis, C.R. Kannewurf, M.G. Kanatzidis, submitted for publication
24. A.C. Sutorik, M.G. Kanatzidis, *Prog. Inorg. Chem.*, 43, **1996**, 151
25. G.D. Mahan, *Solid State Phys.*, 51, **1998,** 81
26. (a) M.J. Smith, R.J. Knight, C.W. Spencer, *J. Appl. Phys.* 23, **1962**, 2186-2190
    (b) L.R. Testardi, J.N. Bierly, F.J. Donahoe, *J.Phys. Chem. Solids.* 23, **1962**, 1209
    (c) C.H. Champness, P.T. Chiand, P. Parekh, *Can. J. Phys.* 43, **1965**, 653
    (d) Y.M. Yim, E.V. Fitzke, *J. Electrochem. Soc.*, 115, **1968**, 556

27. (a) M.G. Kanatzidis, T.J. McCarthy, T.A. Tanzer, L.H. Chen, L. Iordanidis, T. Hogan, C.R. Kannerwurf, C.R. Uher, B. Chen, *Chem. Mater.*, 8, **1996**, 1465
(b) B. Chen, C. Uher, L. Iordanidis, M.G. Kanatzidis, *Chem. Mater.*, 9, **1997**, 1655
28. (a) D.Y. Chung, K.S. Choi, L. Iordanidis, M.G. Kanatzidis, J.L. Schindler, W. Brazis, C.R. Kannewurf, B. Chen, S. Hu, *Chem. Mater.*, 9, **1997**, 3060
(b) T.J. McCarthy,S.P. Ngeyi, J.H. Liao, D. DeGroot, T. Hogan, C.R. Kannewurf, M.G. Kanatzidis, *Chem. Mater.*, 5, **1993**, 331
29. D.Y. Chung, L. Iordanidis, K.S. Choi, M.G. Kanatzidis, *B. Kor. Chem. Soc.*, 19 (2), **1998**, 1283
30. B. Aurivillus, *Acta Chem. Scand.*, A37, **1983**, 399
31. T.C. Harman, J.M. Honig, "Thermoelectric and Thermomagnetic Effect and Applications", Ed. McGraw-Hill, **1967**, 290
32. J.P. Suchet, "Electrical Conduction in Solid Materials", Ed. Pergamon Press LTD., **1975**, 23
33. C.M. Bhandari, D.M. Rowe, "Thermal Conduction in Semiconductor", Ed. Wiley Eastern Ltd., India, **1988** (a) p3, (b) p1, (c) p186, (d) p62, (e) p114
34. C. Kittel, "Introduction to Solid State Physics, Third Ed., J. Wiley & Sons, Inc., **1966**, 190
35. G. Leibfreid, E. Schlomann, Nach. Akad. Wiss. Gottingen, *Mat. Phys. Klasse,* 4, **1954**, 71
36. L. Genzel, *Z. Physik*, 135, **1953**, 177
37. C.M. Bhandari, D.M. Rowe, "Optimizaton of Carrier Concentration" in CRC Handbook of Thermoelectrics, Ed. by D.M. Rowe, **1994**, 43
38. P.M. Chaikin, "Organic Superconductivity", Ed. by V.Z. Kresin and W.A. Little, Plenum Press, New York, **1990**, 101
39. H.J. Goldsmid, J.W. Sharp, *J. Electron. Mater.*, 28, 7, **1999**, 869
40. W.W. Wendlandt, H.G. Hecht, "Reflectance Spectroscopy", Interscience Publishers, New York, **1966**
41. T.S. Moss, G.J. Burrell, B. Ellis, "Semiconductor Opto-Electronics", Ed. Wiley & Sons, New York, **1973, 48-94**
42. D.R. Lovett, "Semimetals & Narrow Band Gap Semiconductors", Ed. Pion Ltd. **1977**, 1
43. M.L. Cohen, J.R. Chelikowsky, "Electronic Structure and Optical Properties of Semiconductors", Springer Series in Solid State Science, 75, **1964**, 45
44. A.R. West, "Solid State Chemistry and its Applications", Ed. John Wiley & Sons Ltd., **1984**, 514
45. See for example H.P. Meyers, "Introduction to Solid State Physics" Sec. Ed., **1997**, 275
46. H.M. Rosenberg, "The Solid State", Oxford University Press, Sec. Ed., **1983**, 145

Chapter 2

Investigation of the Thermoelectric Properties of the Family of Cubic Semiconducting Quartenary Chalcogenides:

$A_mB_nM_mQ_{2m+n}$

2-1. Introduction

In the search for better thermoelectric materials, a new family of quartenary chalcogenides compounds exhibiting promising thermolelectric properties has been synthesized and characterized. A wide range of values for the different transport properties have been measured indicating that we might be able to enhanced the by acting on the composition of the materials.

The first compound discovered belonging to this wide family of compounds of general formula $A_mB_nM_mQ_{2m+n}$ (where A is K or Ag, B is Pb or Sn, M is Bi or Sb, and Q is Te, Se, or S) was $KPbBiTe_3$ using a flux method by Dr. Chung. These materials crystallize in the space group $Fm\bar{3}m$ and possess the NaCl crystal structure type with A, B and M disordered on the Na^+ cationic sites and Q on the Cl^- anionic positions. Such disorder is particularly attractive for TE materials because mass fluctuation in the crystal will decrease the mean free path of the phonon and therefore, the thermal conductivity.

In the general formula $A_mB_nM_mQ_{2m+n}$, m and n can theoretically have any values allowing a continuous range of stoichiometry. This is true as long as the elements that are used for A, B, M, or Q have a valence charge of +1, +2, +3 and -2 respectively, verifying the following charge neutrality equation:

$$m(\text{charge of A}) + n(\text{charge of B}) + m(\text{charge of M}) + (2m+n)(\text{charge of Q}) = 0$$

Any deviation from this rule will lead to compounds with different structure types and different properties. The number of parameters present in the general formula of the compounds, i.e. m, n, A, B, M and Q, should allow us to tailor their physicochemical and transport properties, and hopefully to discover materials with high figure of merit ZT.

The flux method used to discover $KPbBiTe_3$ does not allow the synthesis of substantial amount of material needed for transport measurements. Therefore, we explored new synthesis methods in order to obtain large quantities of pure materials having controlled stoechiometries. Preliminary physicochemical characterization and measurements were made using our equipment and, depending on the results, promising samples were sent to other laboratories for additional measurements. The methodology used during this work is summarized in Figure 2-1.

Several members of the family of compounds studied in this research ($A_mB_nM_mQ_{2m+n}$) have already been reported in the literature[1-8]. Others can be included in the general formula if we extend the scope of the elements that can be used for A to Cu and Tl.

Guseinov and al.[1] studied and reported transports properties for the systems $AgPbBiQ_3$ as well as $TlPbBiQ_3$. These reported compounds are n-type semiconductors

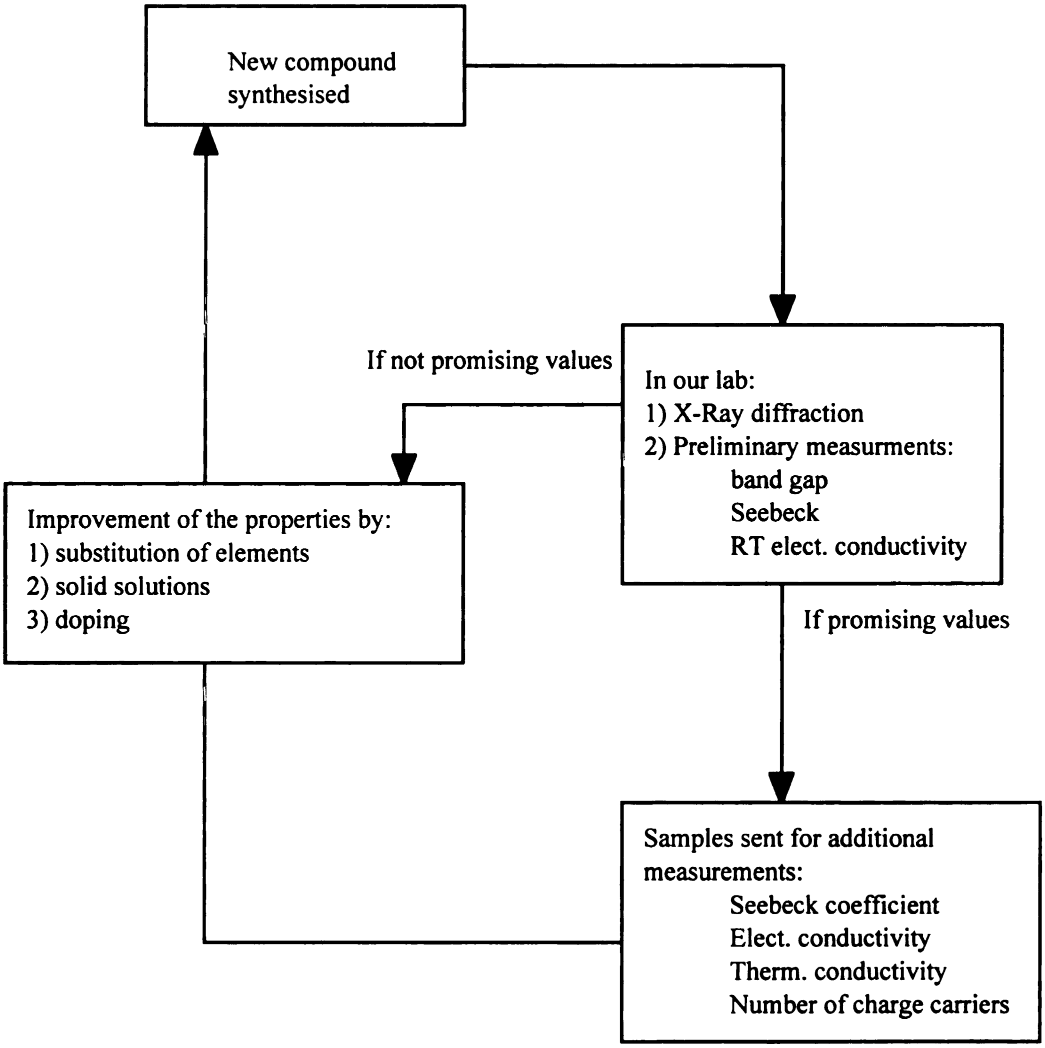

Figure 2-1: Research methodology.

indicating that the majority carriers are electrons. A wide range of electrical conductivity (from 2142 S/cm for $TlPbBiTe_3$ to 115 S/cm for $AgPbBiSe_3$) have been measured. This supports the idea that the transport properties of these materials can be tuned by changing the stoichiometry and the elements used. Seebeck coefficient of 100 μV/K for members of the thallium system and a high value of 345 μV/K for $AgPbBiS_3$ have been reported. Thallium based compounds were not investigated in this work.

Table 2-1. Known members of the system $A'_mB_nM_mQ_{2m+n}$

(With A'= Ag, Cu, Tl; B = Pb, Ge; M = Bi, Sb; and Q = S, Se, Te).

Compound	a (Å)	Reference	Compound	a (Å)	Reference
$AgGeBiTe_3$	6.105	2	$AgPbBiSe_3$		6
$AgPbBiS_3$	5.752	3	$AgPbSbTe_3$	6.260	7
$Ag_4PbBi_4S_9$	5.874	4	$CuBiPbSe_3$	6.046	1
$AgPbBiTe_3$	6.300	1	$TlPbBiTe_3$	6.488	1
$AgPbSbS_3$	5.785	5	TAGS (1)		8

(1) TAGS: Te/Ag/Ge/Sb system of formula $(AgSbTe_2)_{1-x}(GeTe)_x$

TAGS are well known for their thermoelectric properties, and can also be seen as members of the broad family $A_mB_nM_mQ_{2m+n}$ by writing them as $Ag_{1-x}Ge_xSb_{1-x}Te_{2(1-x)+x}$ and replacing 1-x by m and x by n. We then obtain the general formula $Ag_mGe_nSb_mTe_{2m+n}$, which is identical to the one studied in this Thesis. Compounds belonging to this system were used for power generation. They show a transition from rhombohedral to cubic

NaCl structure type at room temperature for a ratio of m/n superior to 3, which was regarded as an instability problem. For members having a m/n ratio inferior to 3, measurements show a value of ZT superior to 1 for temperature above 500 K.

The few data available in the literature on the compounds belonging to the system $A_mB_nM_mQ_{2m+n}$ support our choice of further investigation. Our goal in this work was to prepare new members of this large family and study their thermoelectric properties.

2-2. Experimental Section

Reagents

High purity reagents were used as obtained: Potassium metal 99% purity, Aldrich Chemical Co., Inc., Milwaukee, WI; Silver, Lead metal 99.999%, 200 mesh, cerac, Milwaukee, WI; Tin metal 99.999%, 200 mesh, Cerac, Milwaukee, WI; Antimony 200 mesh, Cerac, Milwaukee, WI, Bismuth 99.999%, Noranda Advanced Materials, Quebec, Canada; Tellurium 99.999%, Noranda Advanced Materials, Quebec, Canada; Selenium >99.5 %, 100 mesh, Aldrish Chemical Co., Milwaukee, WI or 99.999%, Noranda Advanced Materials, Quebec, Canada and Sulfur (>99.999%) were used in this work. Binary starting materials were prepared as follow:

K_2Te: This material was prepared by mixing 12.7g (0.1 mole) of Te with 7.82g (0.2 moles) of K into a 250 ml round bottom flask. A 150-ml volume of NH_3 was condensed into the round bottom flask and cooled down to -78 °C in a bath of dry ice and acetone under nitrogen atmosphere. The solution was stirred overnight and evaporation of liquid ammonia, after condensation by slow warming to room temperature, produced the desired materials under the form of yellow fine powder. Great care must be taken to avoid explosion and exposure of the product to air. **K_2Se** and **K_2S** were prepared under similar conditions.

Bi_2Te_3: Mixtures of 24 mmole of Bi (5 g) and 36 mmole of Te (4.59g) were loaded into 13 mm Silica tubes, sealed under vacuum ($<10^{-4}$ Torr) using a diffusion pump and heated up to 800 °C in 7 hours. An isotherm at 800 °C for 15 hours followed. The tubes were then quenched into an ice bath in order to prevent large grain growth and facilitate the grounding of the materials into fine powders. **Bi_2Se_3** and **Bi_2S_3** were prepared under the same conditions.

PbTe: Mixtures of 48 mmoles of Pb (10 g) and 48 mmoles of Te (6.125g) were loaded into 13 mm Silica tubes, sealed under vacuum ($<10^{-4}$ Torr) using a high diffusion pump and heated up to 680 °C using the following heating profile:

$$50 \xrightarrow{12} 650 \xrightarrow{72} 650 \xrightarrow{10} 100 \xrightarrow{1} 50 \qquad \begin{matrix}\text{hours}\\ \text{T (°C)}\end{matrix}$$

PbSe and **PbS** were prepared using the same experimental conditions.

The materials were then ground into fine powders using a mortar and pestle and checked for purity by powder X-ray diffraction.

Synthesis of $A_mB_nM_mQ_{2m+n}$ Compounds

Method I: Binary compounds were prepared according to the reaction below.

$$nPbQ + (m/2)Bi_2Q_3 + (m/2)K_2Q \rightarrow K_mPb_nBi_mQ_{2m+n} \qquad \text{Eq. (2-1)}$$

Stoichiometric amounts of K_2Q, Bi_2Q_3 and PbQ were mixed under nitrogen atmosphere in a vacuum Atmosphere Dry-Lab glovebox. For example, $KPb_{10}BiTe_{12}$ was prepared by mixing 0.026 g of K_2Te (0.12 mmole) with 0.836 g of PbTe (2.5 mmole) and 0.100 g of Bi_2Te_3 (0.125 mmole). The mixture was loaded into graphite tubes, which were then placed into 13-mm carbon coated Silica tubes. Graphite tubes and carbon coating were used to limit the extend of glass attack due to the reaction with K_2Q (and in particular K_2Te). The tubes were sealed under vacuum ($<10^{-4}$ Torr) and heated using one of the following heating profiles and isolated as explained later. In the case of $KPb_{10}BiTe_{12}$, the heating profile used was H-2. The mixture was heated to 700 °C in 18 hours and let at this temperature for 120 hours. This was followed by a temperature increase to 750 °C in two hours and by an isotherm at this temperature for 1 day. A decrease to 50 °C in 24 hours concluded the synthesis.

$$\text{H-1:}\quad 50 \xrightarrow{18} 700 \xrightarrow{96} 700 \xrightarrow{18} 50 \qquad \begin{array}{l}\text{hours}\\ \text{T (°C)}\end{array}$$

$$\text{H-2:}\quad 50 \xrightarrow{18} 700 \xrightarrow{120} 700 \xrightarrow{2} 750 \xrightarrow{24} 750 \xrightarrow{24} 50 \qquad \begin{array}{l}\text{hours}\\ \text{T (°C)}\end{array}$$

$$\text{H-3:}\quad 50 \xrightarrow{12} 500 \xrightarrow{18} 700 \xrightarrow{140} 700 \xrightarrow{24} 750 \xrightarrow{24} 750 \xrightarrow{24} 50 \qquad \begin{array}{l}\text{hours}\\ \text{T (°C)}\end{array}$$

The compounds were then purified by eliminating any alkali polychalcogenides that had not reacted during the synthesis. Under nitrogen atmosphere, the reaction products were washed with dimethylformamide (DMF). If traces of polychalcogenides were present, a brown coloration appeared; DMF was changed until no coloration was visible. Products were then rinsed with water, methanol, and ether, and left under nitrogen atmosphere to dry. The compounds obtained were re-melted into 3 or 9 mm silica tubes in order to be sent for measurements by other laboratories. The use of a 9 mm tubes instead of a 3 mm silica tubes were found later to constituted a better choice to minimize glass attack.

Method II: "Flame Reaction". The prep was performed according to the reaction:

$$mA + nB + mM + (2m + n)Q \rightarrow A_mB_nM_mQ_{2m+n} \qquad \text{Eq. (2-2)}$$

Stoichiometric amounts of A, B, M, and Q were mixed under nitrogen atmosphere in a vacuum Atmosphere Dry-Lab glovebox. For example $KPb_{10}BiTe_{12}$ was synthesized by mixing 0.039 g of K (1 mmole) with 2.071 g of Pb (10 mmole), 0.209 g of Bi (1 mmole), and 1.531 g of Te (12 mmole). The mixture was loaded into 13-mm carbon coated silica tubes. The tubes were sealed under vacuum ($<10^{-4}$ Torr) and heated to 150 °C in 1 hour. This was followed by an isotherm at the same temperature for 1 hour and a decrease to room temperature in 1 hour. The tubes were then opened and the products loaded into 13-mm Silica tubes, sealed under vacuum and heated using a high temperature torch flame until melting of content. If the first heating step to 150 ° C was omitted, it was more difficult to recover the potassium metal and PbQ that were projected on the inner side of the tube during the flame reaction. Therefore, the first heating was intended to ensure proper reaction of potassium and to keep the entire material at the bottom of the tube.

Method III: "Flame Reaction". This method is identical to Method II with the exception that the mixture were mixed under nitrogen atmosphere and loaded into non-carbon coated tubes. The tubes were sealed heated as previously mentioned, and flamed without being opened.

Physical and Transport Property Measurements

(a) X-ray powder diffraction: Purity of the products was determined by X-ray powder diffraction using:

- a CPS 120 INEL X-ray powder diffractometer using monochromatized radiation Cu K-L_{III} (λ = 1.54059A). The standard used for calibration in the position sensitive detector is silicon powder (Standard Reference Material 640b).
- or/and a Rigaku Rotaflex powder X-ray diffractometer with Ni-filtered Cu Kα radiation operating at 45 kV and 100 mA.

Accurate d-spacings were determined from the experimental powder pattern data with the program PROLIX[9] using a second-degree polynomial Pearson VII function. The cell parameters were refined using the program U-Fit[10].

(b) Solid State Infrared and UV/Vis Spectroscopy

Samples were ground and analyzed at room temperature in the near infrared region (6000 - 400 cm^{-1}) using a Nicolet MAGNA-IR 750 spectrometer equipped with a Collector Diffuse Reflectance of Spectra-Tech. Inc. The diffuse reflectance spectrum was used to determine the value of the band gap as explained in Chapter 1 using the Kubelka-Munk function. Spectra in the 200-2500 nm region were recorded with a Shimadzu UV-3101 PC double beam, double monochromator spectrometer having barium sulfate ($BaSO_4$) as a reference.

(c) Scanning Electron Microscopy (SEM)

Qualitative microprobe analysis of the products were performed using a Scanning Electron Microscope JEOL JSM-35C equipped with a Tracor Northern Dispersive Spectroscopy Detector. Because of overlapping of lines (exited energy levels) between heavy elements such as Pb and Bi, accurate quantification could not be done. Since incorrect estimations of Pb and Bi affect the quantification of other elements present, and because the samples were mainly synthesized as powders, the use of this technique for quantitative purposes was not possible. Nevertheless, EDS was used to check the presence of elements in a qualitative way.

(d) Differential Thermal Analysis (DTA)

DTA was done on a Shimadzu DTA-50 thermal analyzer. Samples were loaded into carbon coated silica ampoules, sealed under vacuum (with a residual pressure <10^{-4} Torr) and heated to 1000 °C at a rate of 10 °C/min followed by a cooling at the same rate. Equal amount of alumina sealed in similar silica container was used as reference.

(e) Room temperature four-probe conductivity

Room temperature conductivity was measured using a four-probe home made measurement system. The system was calibrated using a Bi_2Te_3 block as a reference with its conductivity given by the literature. Because this measurement is strongly dependent on the shape of the sample, some discrepancies are expected between values measured with this type of equipment and values measured with different techniques by our collaborating groups.

(f) Seebeck measurements

Measurements of the Seebeck coefficient as a function of the temperature were done using a programmable Seebeck controller SB100 from MMR Technologies, Inc. The reference chosen was a 0.002" constantan wire, and all mounting of the sample and the reference on the stage were made using silver paste. Several runs were performed on each sample in order to verify the reproducibility, accuracy and variation of each measurement. The measurements ranged from 80 K to 700 K.

(g) Measurements performed in other laboratories

Promising samples were sent to different research groups in order to verify the accuracy of the preliminary measurements and to perform variable measurements not possible in our facilities. These research groups are those of:

- Professor C. Uher, Department of Physics, University of Michigan, Ann Arbor, Michigan[11]. This group performed most of the thermal conductivity studies reported here.
- Professor C. R. Kannewurtf, Department of Electrical Engineering and Computer Science, Northwestern University, Evanston, Illinois[12].
- Professor T. Hogan, Department of Electrical and Computer Engineering & Material Science and Mechanics, Michigan State University, Michigan State University, Michigan[13].

2-3. Results and Discussion

Synthesis and Crystallographic Data

(1) K/Pb/Bi/Te system

$K_mPb_nBi_mTe_{2m+n}$ compounds were synthesized using Method I, and obtained in a "lava" like form. A brown coloration was observed in the DMF solution during the isolation process indicating that amount of K_2Te had been left unreacted. Lead-rich members such as KPb_8BiTe_{10} and $KPb_{10}BiTe_{12}$ were obtained using the heating profile

H-2, while members having lower Pb content were synthesized using the heating profile H-3.

X-ray powder diffraction patterns of the compounds KPb_8BiTe_{10} and $KPb_{10}BiTe_{12}$ (See Figure 2-2a and 2-2d) were in excellent agreement with the NaCl structure type without any detectable impurities. The lattice parameters were calculated using the program U-Fit and are equal to 6.459 (1) and 6.471 (2) Å for KPb_8BiTe_{10} and $KPb_{10}BiTe_{12}$ respectively (see Table 2-2). In the case of the low lead content members such as $KPbBiTe_3$, the NaCl cubic phase was present (see Figure 2-2b) but poor crystallinity of the samples prevented the determination of accurate lattice parameters.

The use of flame reactions (Method II and III) was introduced in order to decrease the time necessary to the synthesis of the compounds allowing faster decisions in the research orientation, as well as obtaining more crystalline low lead content compounds that could not be synthesized using Method I. The crystallinity of those members such as for example KPb_2BiTe_4 improved (see Figure 2-2c), but no relation was observed between the lattice parameters and the amount of lead and tellurium present in the system (see Table 2-2). Furthermore, discrepancies appeared between identical compounds made with identical experimental conditions. For example, Method IIa was identical to method IIb and identical to Method II with the exception that no carbon coated was used to prevent glass attack. Most certainly, vaporization and deposition of some elements (notably Pb) to the colder parts of the tubes as well as loss of K_2Te during glass attack can account for the differences in the values of the lattice parameters. Re-alignment of the

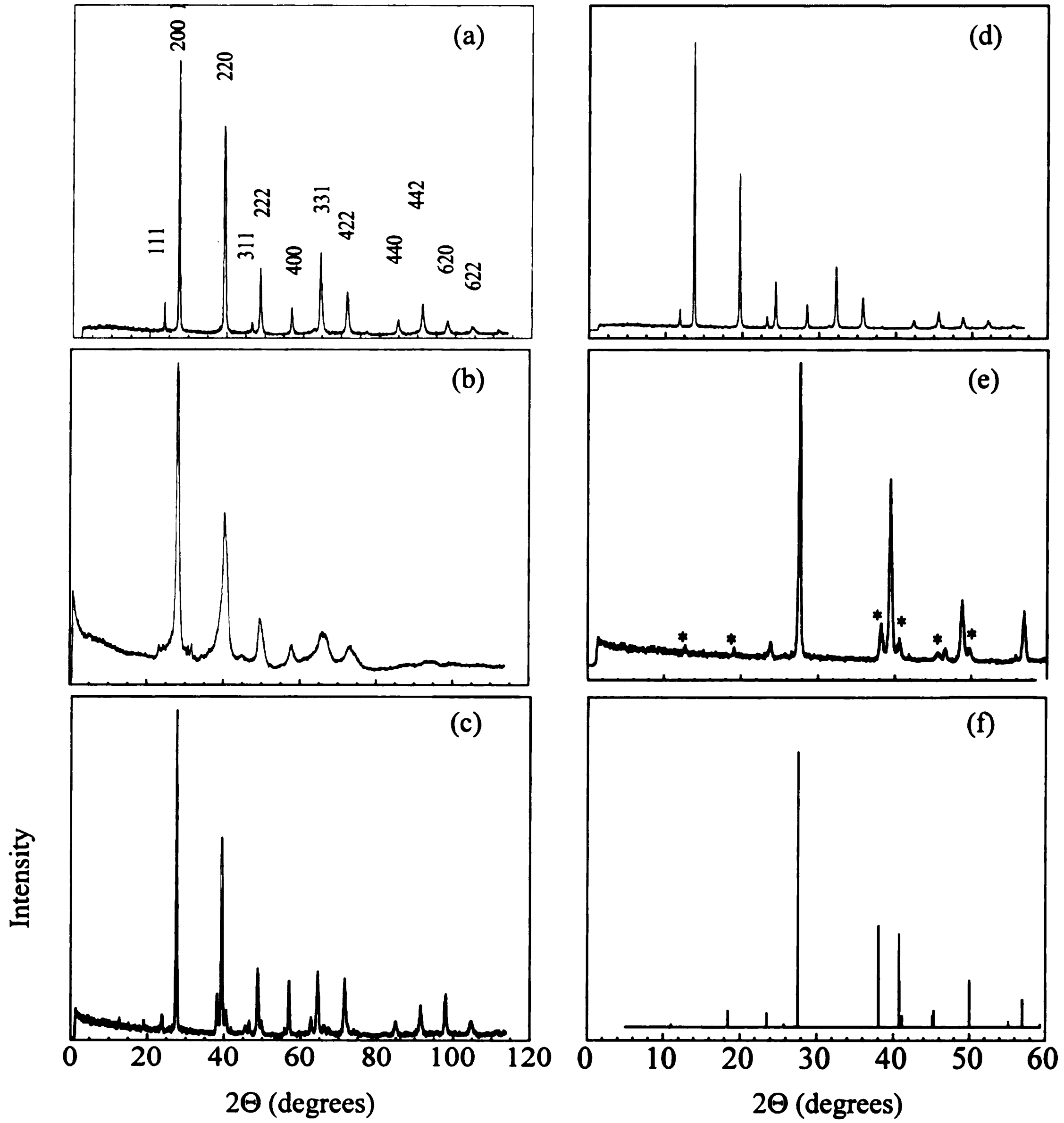

Figure 2-2: X-ray powder diffraction patterns of (a) KPb_8BiTe_{10}, (b) $KPbBiTe_3$, (c) KPb_2BiTe_4 (using flame reaction), (d) $KPb_{10}BiTe_{12}$ (e) impurity phase in KPb_2BiTe_4, and (f) calculated BiTe.

X-ray beam that occurred between the measurements can also account for a shift of the peaks and therefore a difference in the values of the cell parameters.

In addition, as the amount of lead is decreased (i.e. smaller n values), an impurity phase became dominant (see Figure 2-2e). Comparison between BiTe, Bi_2Te_3, $Pb_2Bi_2Te_5$, $PbBi_4Te_7$, and $PbBi_2Te_4$ showed that these compounds have similar X-ray powder patterns as noted by Zhukova and Zaslavskii[14]. A closer look at the low angle peaks indicates that the impurity phase formed is most probably BiTe (see Figure 2-2f). Annealing of the compounds at 750 °C for 1 day removed the impurity phase.

All methods used to synthesized members of this system showed drawbacks. Method I involving a slow homogenous heating left unreacted small amounts of K_2Te, while the flame Methods II and III allow loss of some elements by condensation on colder parts of the tubes and prevent good homogeneity. In both of these methods, reactivity of K_2Te toward silica caused the loss of some potassium and tellurium. This problem was minimized in Method I by using graphite tubes, but not eliminated. The decision to use flame Method II and III for further work has been made because no particular method appeared to be better. Therefore, we choose the fastest ones.

Table 2-2. Cell parameter of KPb_nBiTe_{n+2} members for different experimental conditions.

Composition	Method I	Method II	Method IIa	Method IIb	Method III a
KPb_2BiTe_4			6.475 (1) [1]		
KPb_4BiTe_6		6.455 (1)		6.456 (3)	6.471 (1)
KPb_6BiTe_8		6.451 (1) [1]	6.466 (1) [1]	6.444 (1)	
KPb_8BiTe_{10}	6.459 (1)	6.451 (1) [1]	6.527 (9) [1]	6.441 (2)	6.471 (1)
$KPb_{10}BiTe_{12}$	6.471 (1)	6.453 (1) [1]		6.452 (1)	

[1]: Presence of an impurity phase in the powder pattern.

(2) K/Pb/Bi/Se systems

Compounds of the general formula KPb_nBiSe_{n+2} (with n = 1, 2, 3, 4, and 5) were obtained using the experimental conditions of Method I with the heating profile H-1, while members with n = 8 and 10 were synthesized using heating profile H-2. No coloration was observed in the DMF during isolation indicating that all K_2Se reacted.

Powder X-ray diffraction showed pure NaCl cubic phases (see Figure 2-3a). The cell parameters were calculated and are reported in Table 2-3. PbSe is given in reference (see Figure 2-3b). Contrary to the K/Pb/Bi/Te system, members with low lead content (n=1) were successfully synthesized.

It is useful to treat the K/Pb/Bi/Se system as solid solutions $(KBiSe_2)_{1-x}(PbSe)_x$. This approach is possible because both $KBiSe_2$ and PbSe crystallize with the same NaCl structure type. Any value of x between 0 and 1 should give a compound with a cell parameter between those of $KBiSe_2$[15], i.e. 5.92 (1) Å and PbSe[16], i.e. 6.1213 (8) Å. Surprisingly, the cell parameters of the KPb_nBiSe_{n+2} compounds are higher than these two

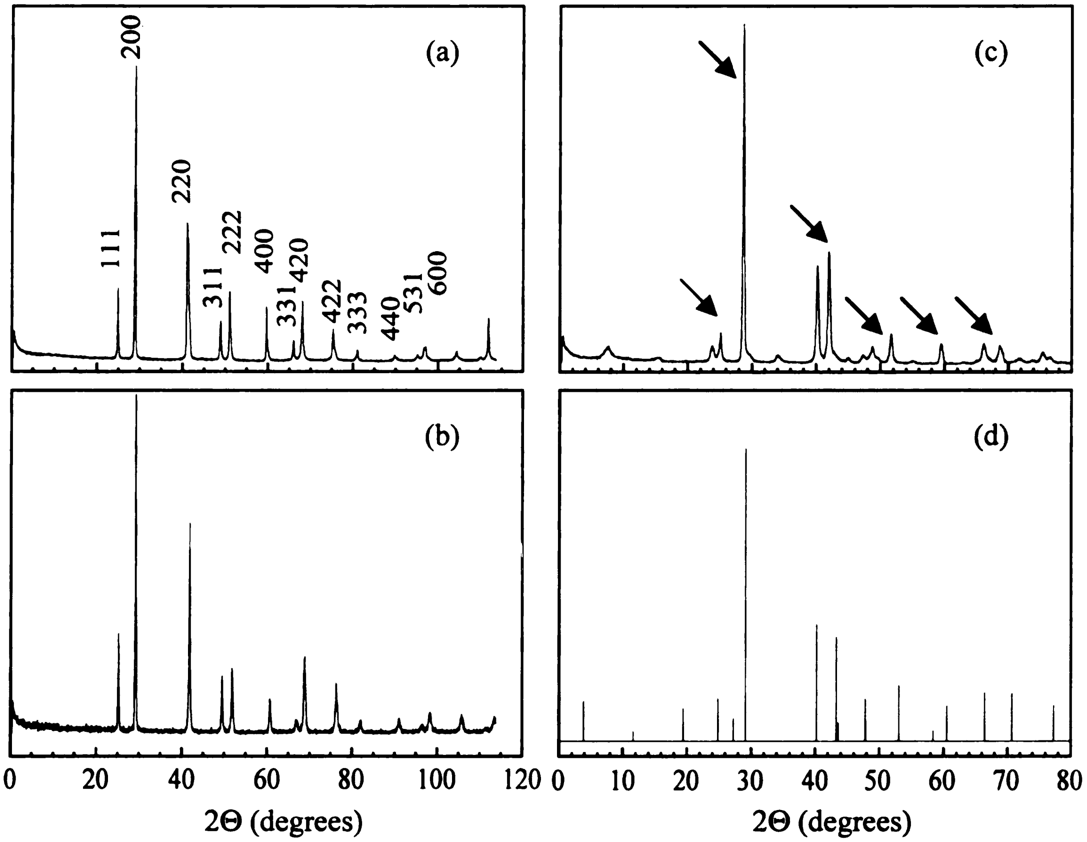

Figure 2-3: X-ray powder diffraction patterns of (a) KPb_3BiSe_5, (b) PbSe, (c) $K_2PbBi_2Se_5$, and (d) calculated BiSe. (The peaks corresponding to the correct cubic phase in (c) are marked by arrows).

values. The lattice parameter of PbSe was calculated on powder and showed a slightly lower value of 6.105 (2) Å. We did not synthesize $KBiSe_2$ in order to check the cell parameter but some doubts are raised toward the value of the cell parameter given in the literature. The cell parameters of the selenium compounds were plotted as a function of x (see Figure 2-4) and a value of 6.332 Å for $KBiSe_2$ can be extrapolated. As expected a linear trend exists as the cell parameter decreases when x increases. Vegard's Law[17] is well followed by this system indicating that the stoichiometry of the compounds are close to the expected ones. The possibility of small amount of PbSe formed as impurity can account for some slight shift in the cell parameters.

Figure 2-4: Cell parameter variation in the system $(KBiSe_2)_{1-x}(PbSe)_x$.

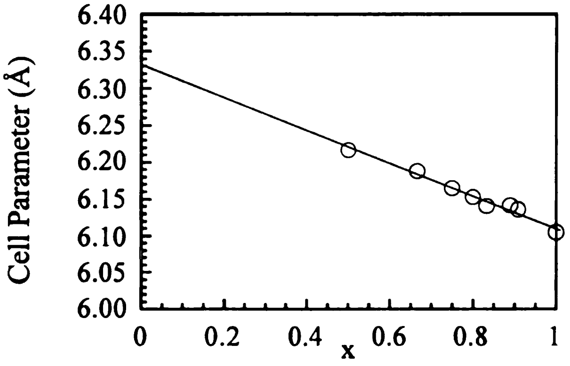

In a similar way than for the tellurium system, impurities are formed when x < 0.5 (see Figure 2-3c). Simulated powder patterns showed that one of them is probably BiSe, which is isostructural to BiTe (see Figure 2-3d).

Compounds synthesized using flame Method II show inconsistencies in the cell parameters as it was noticed for the K/Pb/Bi/Te system. (see Table 2-4). In this case, the loss of PbSe by deposition on colder part of the tube is responsible for these discrepancies.

Table 2-3. Cell parameters for selected members of the family KPb_nBiSe_{n+2} (with n = 1, 2, 3, 4, 5, 8, 10) and KPb_mBiS_{n+2} (with n=1, 4, 8).

Composition	Cell parameter (Å)	Composition	Cell parameter (Å)
$KPbBiSe_3$	6.217 (2)	$KPbBiS_3$	5.998 (1)
KPb_2BiSe_4	6.188 (4)	KPb_4BiS_6	5.949 (1)
KPb_3BiSe_5	6.165 (3)	KPb_8BiS_{10}	5.935 (1)
KPb_4BiSe_6	6.1528 (8)		
KPb_5BiSe_7	6.141 (3)		
KPb_8BiSe_{10}	6.1416 (8)		
$KPb_{10}BiSe_{12}$	6.136 (1)		

(3) K/Pb/Bi/S system

Comparable results to the ones obtained for the selenium system were observed for the sulfur compounds. $KPbBiS_3$, KPb_4BiS_6, and KPb_8BiS_{10} were synthesized using method I and the heating profile H-2. No coloration was noticed in the DMF solvent used to wash the products during isolation indicating that all the K_2S reacted.

Powder patterns obtained from X-ray diffraction showed pure cubic phases in perfect accordance with the NaCl cubic structure (see Figure 2-5a). PbS is given as reference in Figure 2-5b. As for the K/Pb/Bi/Se system, the sulfur system can be seen as a solid solution of $(KBiS_2)_{1-x}(PbS)_x$. The calculated cell parameters were plotted as a function of x with the cell parameter of $KBiS_2$[18] taken from the literature and being equal to 6.040 (1) Å, while the cell parameter of PbS was calculated on powder and equal to 5.9286 (4) Å. Figure 2-6 shows that the system follows Vegard's Law, and as a consequence indicates that the stoichiometry of the compounds synthesized are close to the expected ones.

As for the previous systems, Method II gave inconsistent results (see Table 2-4) due to the vaporization and deposition of PbS on the inner sides of the silica tubes.

Table 2-4. Cell parameters for members of the KPb_nBiSe_{2+n} and KPb_nBiS_{2+n} systems made by "flame" induced reaction.

Composition	Cell Parameter (Å)	Composition	Cell Parameter (Å)
$KPbBiS_3$	5.971 (1)	KPb_4BiSe_6	6.135 (1)
KPb_2BiS_4	5.949 (1)	KPb_8BiSe_{10}	6.141 (1)
KPb_4BiS_6	5.9354 (1)	$KPb_{10}BiSe_{12}$	6.130 (1)
KPb_8BiS_{10}	5.9382 (6)		
$KPb_{10}BiS_{12}$	5.9345 (7)		

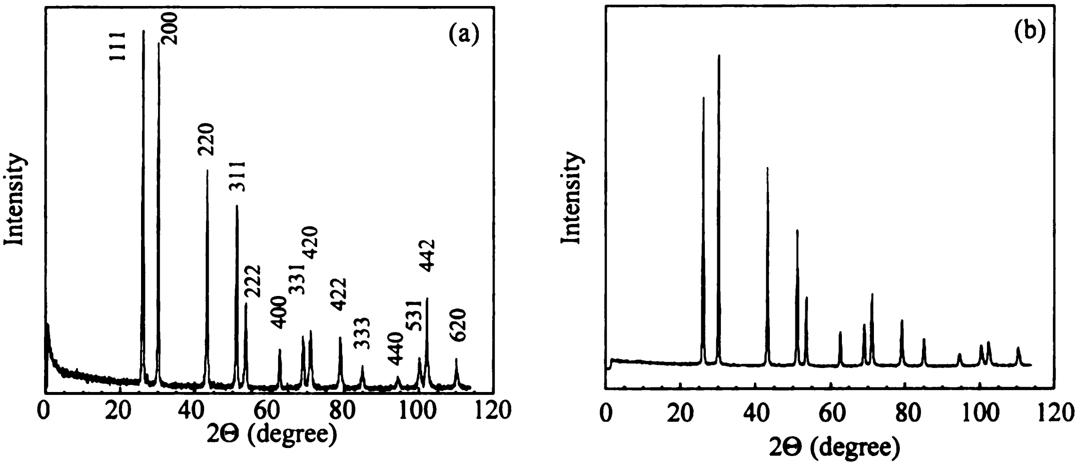

Figure 2-5: X-ray powder diffraction patterns of (a) KPb_8BiS_{10} and (b) PbS.

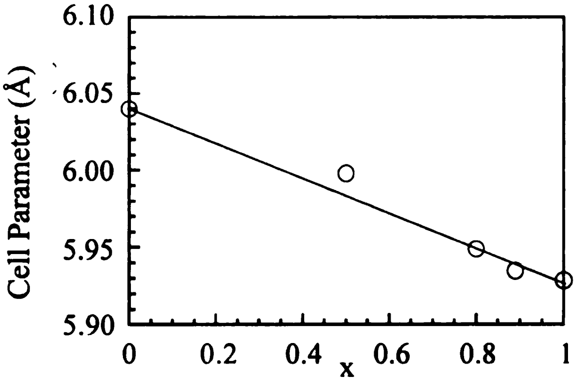

Figure 2-6: Cell parameter variation in the system $(KBiS_2)_{1-x}(PbS)_x$.

(4) Ag/Pb/Bi/Te System

Members of the system $Ag_mB_nM_mQ_{2m+n}$ were synthesized using experimental conditions described in Method III. The products obtained had the form of gray shiny ingots.

X-ray powder patterns of the compounds listed in Table 2-5 exhibit pure cubic phases similar to the one shown in Figure 2-7 and are in total agreement with the NaCl structure type. After rewriting the system Ag/Pb/Bi/Te as the solid solution $(AgBiTe_2)_{1-x}(PbTe)_{x,}$ a plot of the cell parameters as a function of x (Figure 2-8) shows that the system deviates from Vegard's Law for high value of x. Additional compounds need to be made in this region to see a more clear trend. Nevertheless, the stoichiometry of the compounds should be in relative agreement with the targeted compositions.

Table 2-5. Cell parameters for members of silver based systems.

Compound	Cell Parameter (Å)	Compound	Cell Parameter (Å)
$AgPb_{10}SbS_{12}$	5.905 (1)	$Ag_2PbBi_2Te_5$	6.239 (2)
$AgPb_{10}SbTe_{12}$	6.4415 (4)	$AgPb_3BiTe_5$	6.416 (2)
$AgSn_{10}BiS_{12}$	6.259 (2)	$AgPb_6BiTe_8$	6.429 (2)
$AgPb_{10}BiSe_{12}$	6.118 (1)	$AgSn_8BiSe_{10}$	5.927 (1)

In the case of the Ag/Sn/Bi/S system, plate crystals of SnS grow as an impurity phase when tin rich members such as $AgSn_8BiS_{10}$ were synthesized with flame reaction.

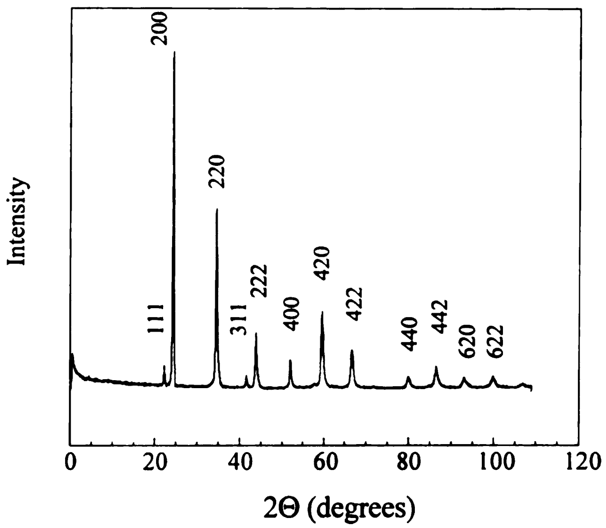

Figure 2-7: X-ray powder diffraction pattern of $AgPb_{10}BiTe_{12}$.

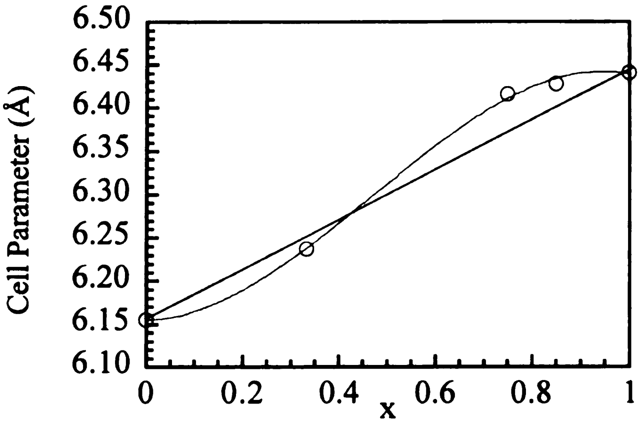

Figure 2-8: Cell parameter variation in the system $(AgBiTe_2)_{1-x}(PbTe)_x$.

(5) Other systems

Three more systems were briefly investigated using method II. They are those of K/Pb/Sb/Te, K/Sn/Bi/Te, and K/Sn/Sb/Te. Ingots were obtained from the flame reactions.

Members with high Pb content showed pure cubic phases in perfect agreement with the NaCl structure type. The lattice parameters were determined and reported in Table 2-6.

Table 2-6. Cell parameters of members of the K/B/M/Te system (where B is Pb or Sn and M is Bi or Sb).

Compound	Cell Parameter (Å)	Compound	Cell Parameter (Å)
$KPbSbTe_3$	*	$KSnBiTe_3$	*
KPb_5SbTe_7	6.448 (2)	KSn_5BiTe_7	*
$KPb_{10}SbTe_{12}$	6.460 (4)	$KSn_{10}BiTe_{12}$	6.2922 (1)
$KSnSbTe_3$	*		
KSn_5SbTe_7	6.278 (2)		
$KSn_{10}SbTe_{12}$	6.364 (4)		

* accurate cell parameters could not be calculated due to the presence of an impurity phase.

Based on the powder pattern of $KSnBiTe_3$ (see Figure 2-9) the impurity phase was attributed to BiTe but because low angle peaks are difficult to observe due to background noise, some doubts remain. Similarly, the impurity phase present for $KSnSbTe_3$ and $KPbSbTe_3$ is attributed to SbTe that is isostructural to BiSe.

Members of the K/Pb/BiSe and K/Pb/Bi/S systems were successfully synthesized using Method I. Due to the higher reactivity toward silica of K_2Te compared to K_2Se or K_2S, control of the stoichiometry in the K/B/M/Te systems is problematic using either of the methods presented.

Most of the systems investigated showed the presence of a stable impurity phase having the BiSe structure type (when values of n/m reach 1). In the case of the Ag/Sn/Bi/S system, the binary SnS formed along with the desired cubic phase.

The family of compounds $A_mB_nM_mQ_{2m+n}$ can be seen as the solid solution $(AMQ_2)_{1-x}(PbQ)_x$. In the case of the K/Te based systems this approach is not possible because $KBiTe_2$ and $KSbTe_2$ apparently do not have a NaCl structure type. Attempts of making these compounds with the NaCl structure type were unsuccessful. Concerning the K/Pb/Bi/Te system, the value reported in the literature for $KBiSe_2$ is questionable, being too low to be used for the solid solution system $(KBiSe_2)_{1-x}PbSe_x$.

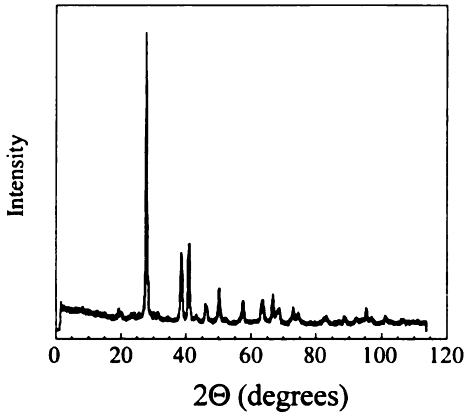

Figure 2-9: X-ray powder diffraction pattern of $KSnBiTe_3$.

Physical Properties

(1) K/Pb/Bi/Te system

Using diffuse reflectance infrared spectroscopy, band gaps were observed and values of 0.38 eV for both KPb_8BiTe_{10} and $KPb_{10}BiTe_{12}$ were determined (see Figure 2-10). This value classified these compounds as narrow band gap semiconductors. No well-defined bang gap was detected for $KPbBiTe_3$, KPb_2BiTe_4, and KPb_4BiTe_6 although one is expected. The shape of the absorption spectrum suggests that a self-doping effect takes place masking the true band gap.

Self-doping in these materials is derived from defects created during the synthesis. The rapid synthesis and fast crystallization may cause anti-site defects, vacancies and even non-stoichiometry. These factors create energy levels between the gap which absorb light thus masking the true band gap. It is possible that these defects may be repaired by proper annealing of the materials after synthesis.

Differential thermal analysis of these compounds do not show any endothermic peaks, indicating that the melting point of these compounds lay above 1000 °C (limit of our DTA analyzer). Remelting the compounds into silica tubes showed that the materials react with the silica, with accompanying glass attack. The amount of glass attack increases with increasing the content in potassium. Nevertheless, the compounds melt congruently. This is an important property since it allows the material to be used at high temperature without being decomposed.

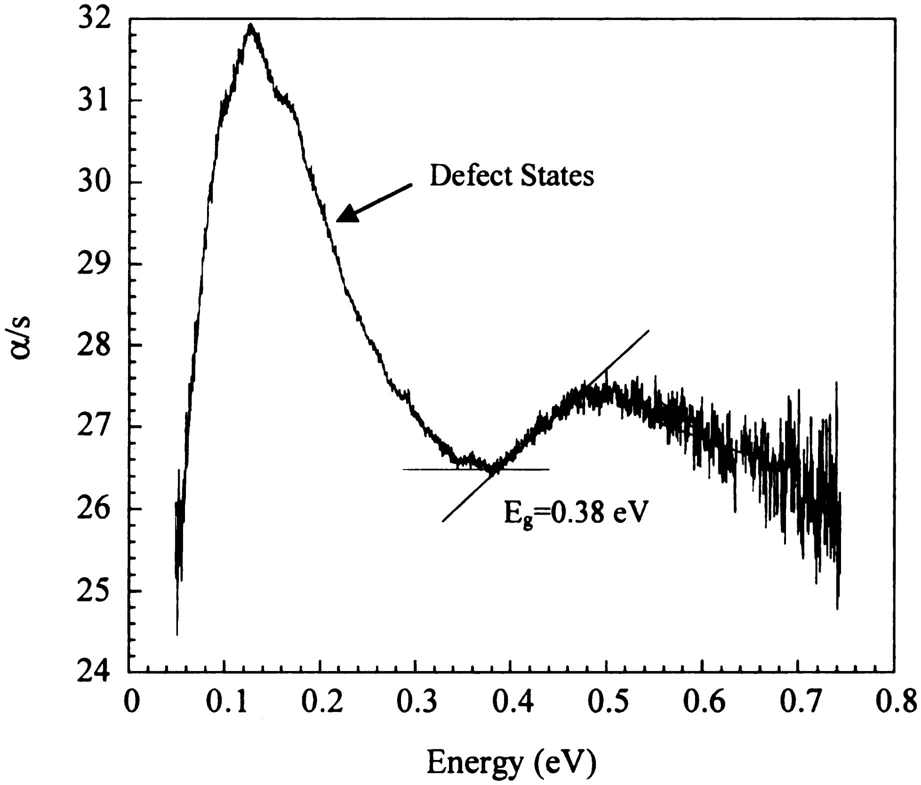

Figure 2-10: Optical absorption spectrum of $KPb_{10}BiTe_{12}$ showing the energy gap.

(2) K/Pb/Bi/Se system

Energy gaps for selenium compounds were calculated to vary from 0.46 eV to 0.675 eV for $KPb_{10}BiSe_{12}$ and $KPbBiSe_3$ respectively (see Table 2-7). Contrary to the previous system, the band gaps here were well defined.

As mentioned above, we can treat the system as a solid solution of $KBiSe_2$ and PbSe. The variation of the band gaps as a function of x is not a linear function as a plateau is reached for values of x inferior to 0.5 (see Figure 2-11). The value used for PbSe was taken from the literature as 0.26 eV. A typical example of an absorption spectrum for KPb_5BiSe_7 is shown in Figure 2-12.

Compounds obtained from flame reactions did not show well defined absorption spectra (see Figure 2-13), again probably because of self-doping effects caused by the rapid synthesis of these materials. Differential thermal analysis did not show any melting peaks below 1000 °C.

Table 2-7. Energy gap for members of the family of compounds KPb_nBiQ_{n+2}.

Composition	Energy Gap (eV)	Composition	Energy Gap (eV)
$KPbBiSe_3$	0.68	KPb_8BiTe_{10}	0.38
KPb_2BiSe_4	0.67	$KPb_{10}BiTe_{12}$	0.38
KPb_3BiSe_5	0.66	$KPbBiS_3$	0.87
KPb_4BiSe_6	0.64	KPb_4BiS_6	0.71
KPb_5BiSe_7	0.62	KPb_8BiS_{10}	0.61
KPb_8BiSe_{10}	0.50		
$KPb_{10}BiSe_{12}$	0.46		

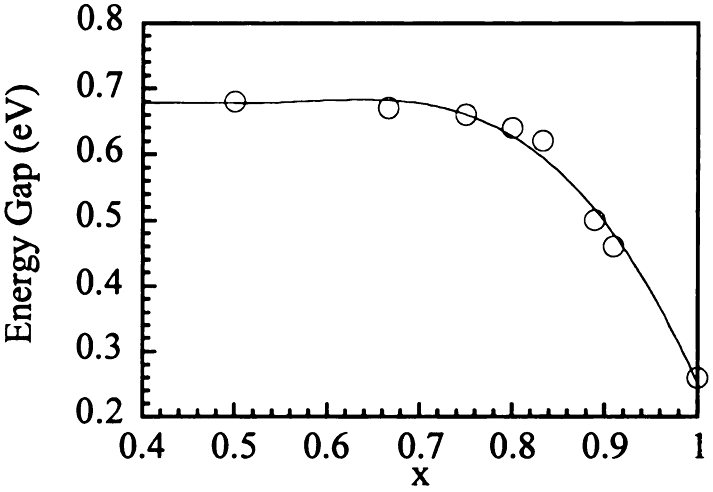

Figure 2-11: Variation of the energy gap as a function of x for the system $(KBiSe_2)_{1-x}(PbSe)_x$.

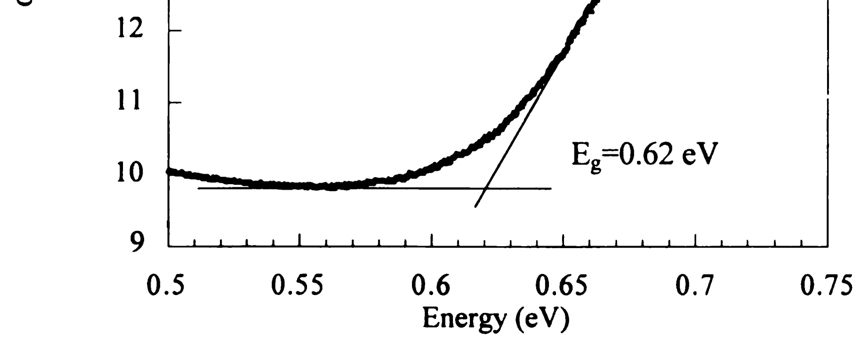

Figure 2-12: Optical absorption spectrum of KPb_5BiSe_7 showing the energy gap.

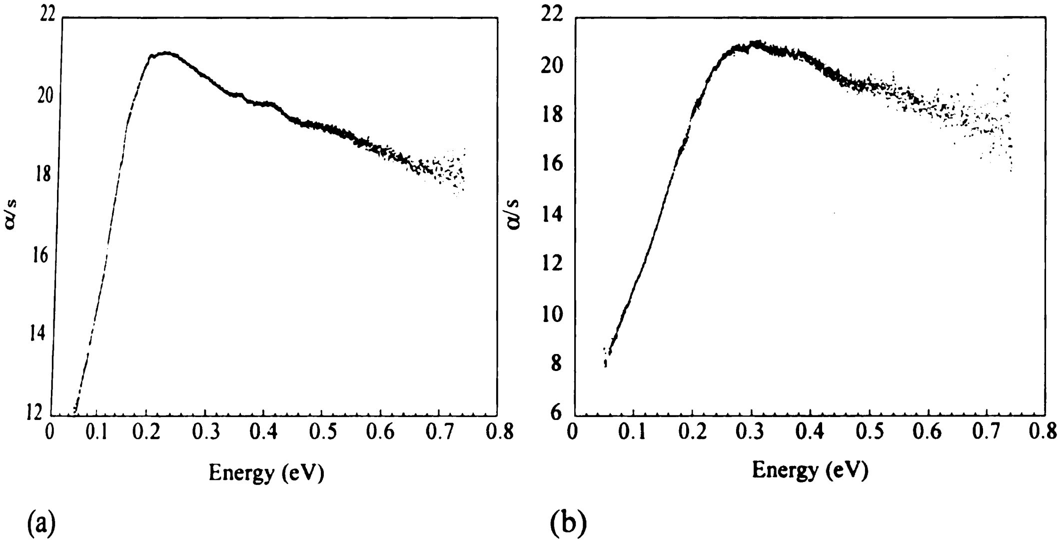

Figure 2-13: (a) Optical absorption spectrum of $KPb_{10}BiSe_{12}$. The band gap of the compound is masked by mid gap energy levels. (b) No band gap appears after annealing of the sample for 24 h at 400 °C.

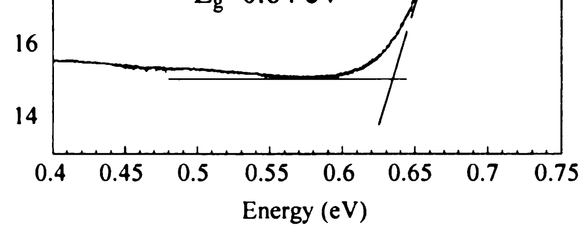

igure 2-14: Optical absorption spectrum of KPb_8BiS_{10} showing the energy gap.

(3) K/Pb/Bi/S system

Higher values of band gaps were observed for the corresponding sulfide members compared to those of Se and Te analogs. The values of the well-defined band gaps reported in Table 2-7 vary from 0.61 for KPb_8BiS_{10} to 0.87 eV for $KPbBiS_3$. An example of an absorption spectrum for KPb_8BiS_{10} is shown in Figure 2-14.

In the products obtained with the "flame reaction", no band gaps were observed due to self-doping effects as discussed above.

DTA did not show melting peaks below 1000 °C. Furthermore, experiments of melting sulfur compounds loaded into silica tubes showed that their melting point is higher than those of the tellurium and selenium systems, and at least as high as the melting point of the silica tubes.

(4) Other Systems

The absorption spectra of members of the silver systems did not show any clear band gap transitions. Their absorption spectrum has similar characteristics to the ones showing a self-doping effect, nevertheless, in the case of $AgPb_{10}BiTe_{12}$ the band gap was observed and estimated at 0.28 eV.

No band gaps were visible for $KSn_{10}BiTe_{12}$ and other members of the K/Sn/Sb/Te system. The band gaps for the K/Pb/Sb/Te members are not well defined due to a broad tail as shown in Figure 2-15. They can be roughly estimated to be between 0.26 and 0.33

eV for KPb_5SbTe_7 and between 0.12 and 0.28 eV for $KPb_{10}SbTe_{12}$. DTA was not performed on these systems.

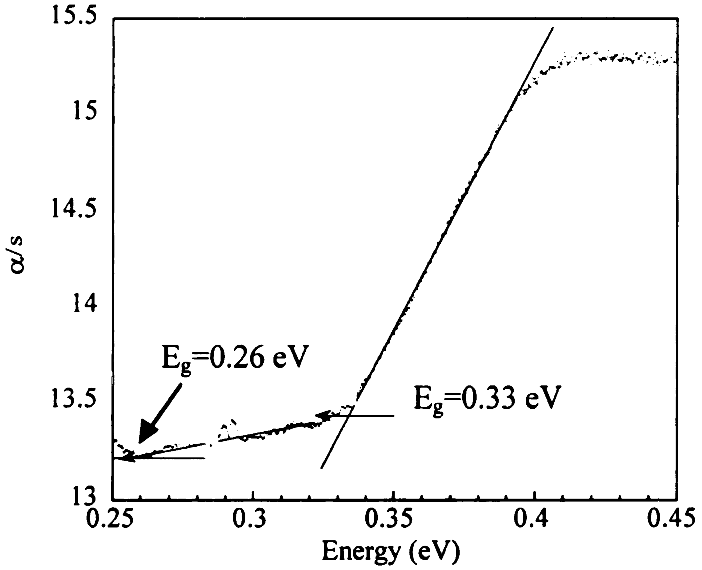

Figure 2-15: Optical absorption spectrum of KPb_5SbTe_7 showing a broad tail.

As expected the values of the energy gaps for members of the system KPb_nBiQ_{n+2} follow trends. As n increases in the K/Pb/Bi/Se and K/Pb/Bi/S systems, the energy gap decreases approaching the values of PbSe and PbS respectively. If Q is changed from Te to Se and to S the band gap increases because we substitute heavy atoms by lighter ones.

The band gap values for the different systems studied suggested that the K/Pb/Bi/Te, ~ 0.38 eV, and Ag/Pb/Bi/Te systems, ~ 0.28 eV, are the most promising for thermoelectric investigations. The values for the K/Pb/Bi/S system appear to be too high (from 0.61 to 0.87 eV) compared to the <0.5 eV that is desired. Such band gap value is one of the requirements that a material must follow in order to be a viable TE material at room temperature. If the band gap is too high, the conductivity will be too low; conversely, if the energy gap is too low, minority carriers can be created that adversely affect the Seebeck coefficient. All other systems investigated show band gap values that lie in the desirable range and we classify them as "narrow band gap semiconductors".

Transport properties

(1) K/Pb/Bi/Te system

Preliminary Seebeck coefficient measurements on pressed pellets of members of the KPb_nBiTe_{n+2} system (see Figure 2-16) showed that all the tellurium compounds were n-type, indicating that the majority carriers are electrons. The materials show narrow band gap semiconductor behavior as the absolute value of the Seebeck coefficient rises with temperature (as a metal) but possesses a high value over –100 μV/K (as a semiconductor). The Seebeck coefficient trends to 0 μV/K at 0K. These compounds possessed similar values at room temperature and no relationship was noticeable between the value of the Seebeck coefficient and the variation of the amount of lead in the samples. This indicates that we might be able to change the amount of lead in the system until an optimum value of the electrical conductivity is reached, without affecting much the Seebeck coefficient. Selected values of the Seebeck coefficient at room temperature are -130 μV/K for $KPbBiTe_3$, -110 μV/K for KPb_8BiTe_{10} and -140 μV/K for $KPb_{10}BiTe_{12}$.

$KPbBiTe_3$, KPb_8BiTe_{10} and $KPb_{10}BiTe_{12}$ were sent for further characterization. The results for $KPbBiTe_3$ (see Figure 2-17) showed a Seebeck coefficient of -47 μV/K at room temperature. Measurements on KPb_8BiTe_{10} and $KPb_{10}BiTe_{12}$ showed similar values (Figure 2-18) of -41 and -47 μV/K at 300 K respectively. In both cases, the thermopowers obtained were much lower than the ones measured with our system.

Why do these values differ so much from our measurements? The first hypothesis advanced was the following. As mentioned previously, since the products of the reactions did not have an ideal morphology for measurements (i.e. homogenous, bulk samples without physical holes), ingots were made by re-melting the compounds. It was these ingots that were shipped to Professor Uher Lab for measurements. In theory, no differences should exist in the measurement of the Seebeck coefficient between cold press pellet sample and ingot. We attributed the observed differences to the fact that during the making of the ingots, a change of the electronic composition of the material occurred either by loosing small amount of some elements or by creating new defects. These processes change the doping state and can dramatically affect the value of the Seebeck coefficient as explained in Chapter 1.

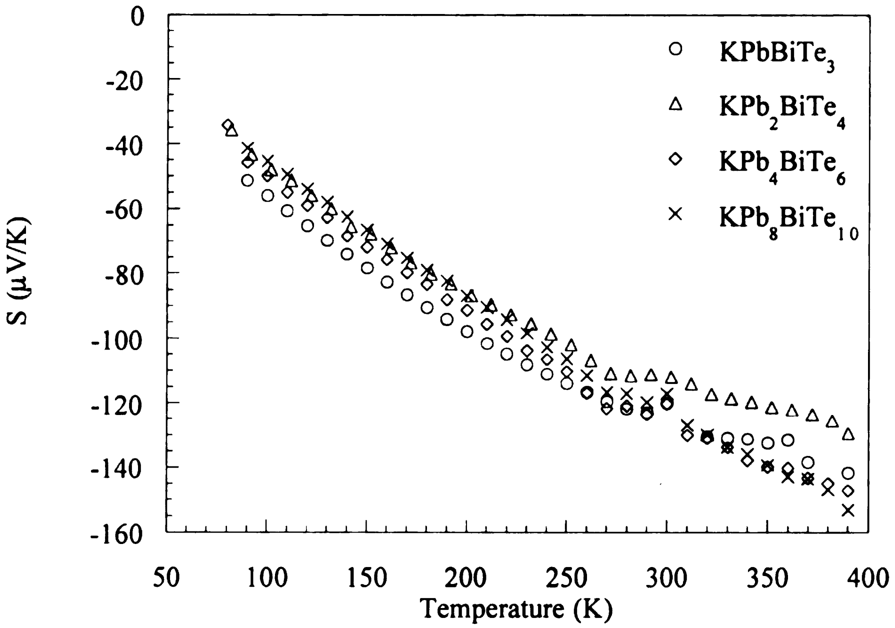

Figure 2-16: Seebeck coefficient as a function of temperature for members of the system KPb_nBiTe_{n+2} synthesized using “flame” reaction (cold pressed pellet measurement).

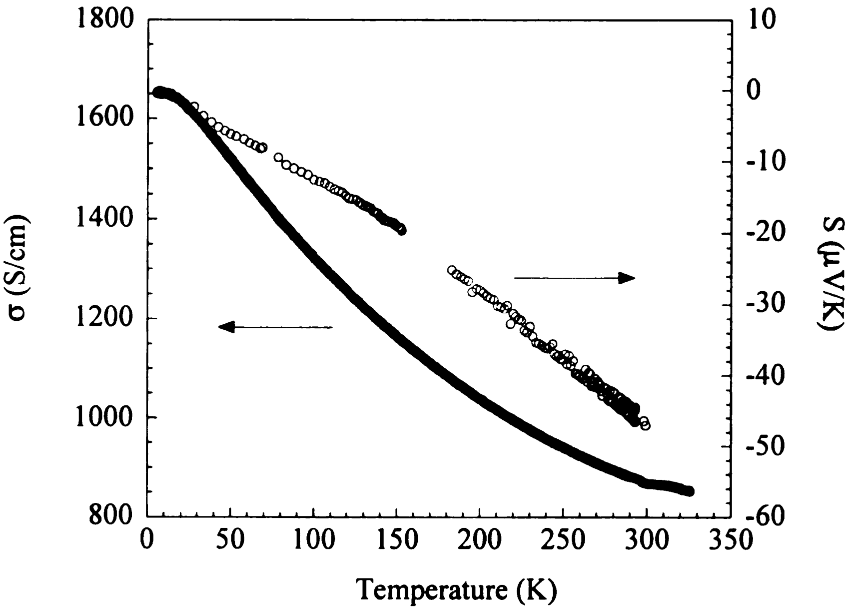

Figure 2-17: Seebeck coefficient and electrical conductivity for $KPbBiTe_3$ (ingot).

The thermal conductivity values of KPb_8BiTe_{10} and $KPb_{10}BiTe_{12}$ were measured to be ~ 2.0 W/m·K and ~ 2.2 W/m·K respectively at room temperature (see Figure 2-19). No contribution from radiative losses were noticeable in the plots. These values are very low and encouraging because they are only slightly higher than that of Bi_2Te_3. In the latter, the thermal conductivity can be decreased significantly by solid solutions experiments of $Bi_{2-x}Sb_xTe_3$ or $Bi_2Te_{3-x}Se_x$. Therefore we can expect to lower the thermal conductivity of our compounds by introducing similar disorder on the anionic and/or cationic sites through substituting for example some Bi atoms by Sb, or some Te atoms by Se atoms. Electrical conductivity measurements of ingot samples gave values of 600 S/cm and 800 S/cm for KPb_8BiTe_{10} and $KPb_{10}BiTe_{12}$ respectively at 300 K (see Figure 2-20). The value of $KPbBiTe_3$ is in the same range and equal to 900 S/cm (see Figure 2-17). The variation of the conductivity with temperature in both samples shows a metallic behavior. The conductivity values at room temperature are in the range of what is desired for thermoelectric applications and close to the value of Bi_2Te_3 (≈ 900 S/cm).

These transport properties are promising despite the low Seebeck values measured. A ZT at room temperature of 0.015 for KPb_8BiTe_{10} and 0.027 for $KPb_{10}BiTe_{12}$, can be computed using the data obtained (see Figure 2-21). The differences between the measurements on cold press pellets and ingots is at this time attributed to a change in the electronic structure of the materials when remelted.

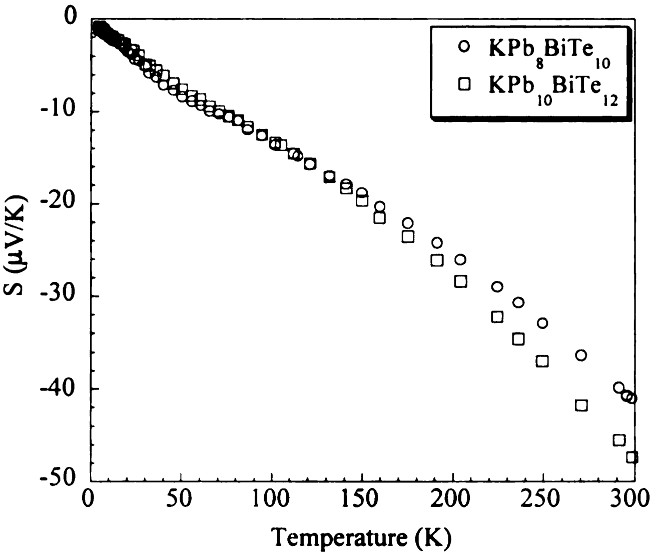

Figure 2-18: Seebeck coefficient measurement of KPb$_8$BiTe$_{10}$ and KPb$_{10}$BiTe$_{12}$ (ingots).

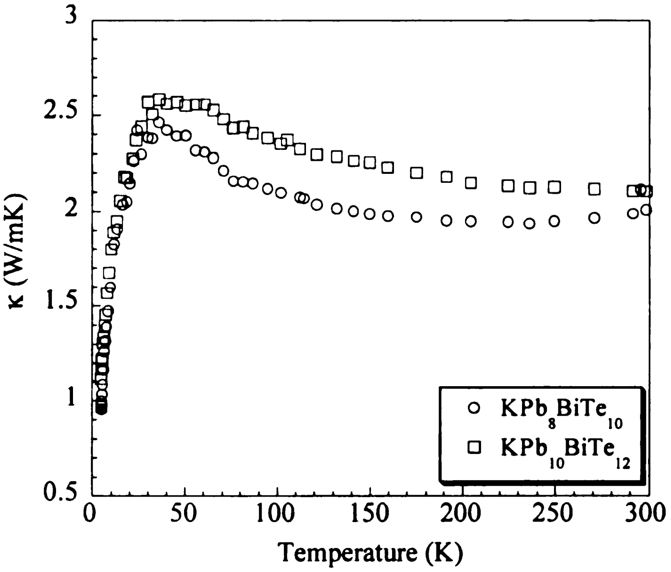

Figure 2-19: Thermal conductivity of KPb$_8$BiTe$_{10}$ and KPb$_{10}$BiTe$_{12}$ (ingots).

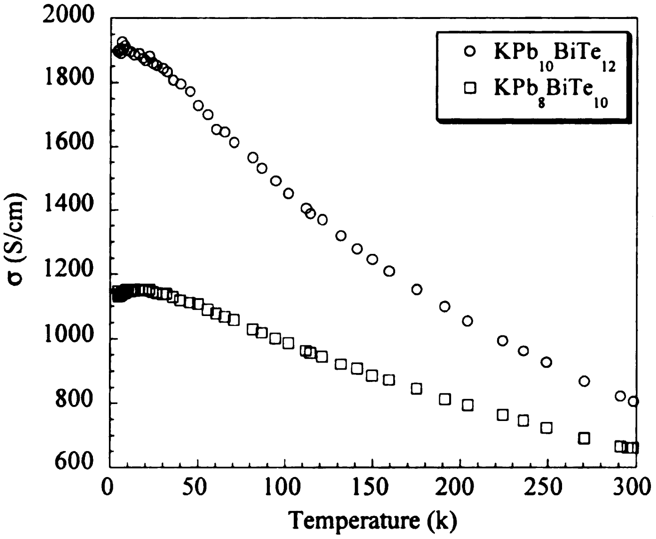

Figure 2-20: Electrical conductivity of KPb$_8$BiTe$_{10}$ and KPb$_{10}$BiTe$_{12}$ (ingots).

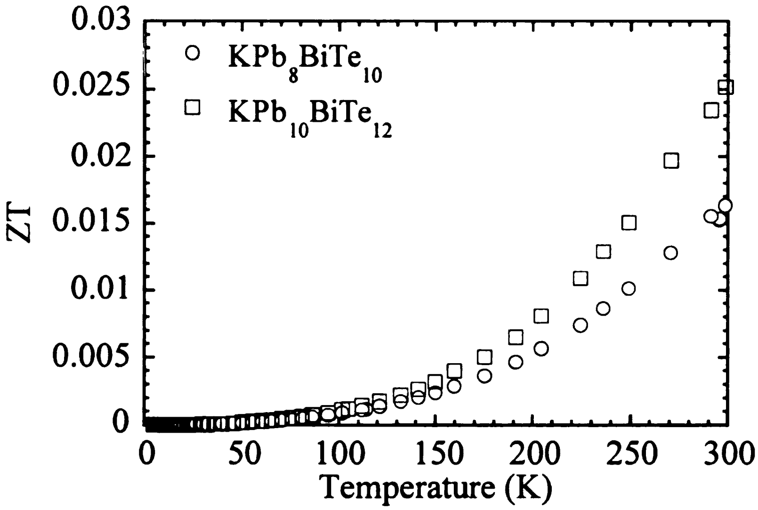

Figure 2-21: ZT versus T for KPb$_8$BiTe$_{10}$ and KPb$_{10}$BiTe$_{12}$.

Hall measurements gave the number of charge carriers (see Figure 2-22). The values at room temperature are 8.5 x10^{19} charge carrier per cm^3 for KPb_8BiTe_{10} and about 5 x10^{19} carriers per cm^3 for $KPb_{10}BiTe_{12}$. These high numbers of carriers tend to confirm that the compounds are already doped as previously indicated. They are in range of the values that are considered favorable for TE materials (see chapter I). Mobilities (see Figure 2-23) were also calculated from the number of charge carriers using Eq.2-3.

$$\sigma = N\, e\, \mu \qquad \text{Eq. 2-3}$$

They are respectively equal to 100 and 50 m^2/V·s for KPb_8BiTe_{10} and $KPb_{10}BiTe_{12}$. We are far from mobilities of 1000 cm^2/V·s that are usually found for the best TE materials. For reference[19], Bi_2Te_3 has a mobility of 1200 cm^2/V·s and PbTe a mobility of 1700 cm^2/V·s. The importance of having high mobility is evident if we consider the quality factor of a material as defined by Tuomi[20]:

$$Q_j = N_j\, \mu_j \left(\frac{m_j}{m_e} \right)^{3/2} \qquad \text{Eq. 2-4}$$

where the indices j relate to the electronic band, N_j is the degeneracy of the band. A quality factor can be attributed to each band. In turn, Q_j is proportional to the B factor (See for example Mahan)[19], from which ZT is proportional with. High mobility is therefore needed to increase the quality factor which in turn increases the efficiency of the material for TE application.

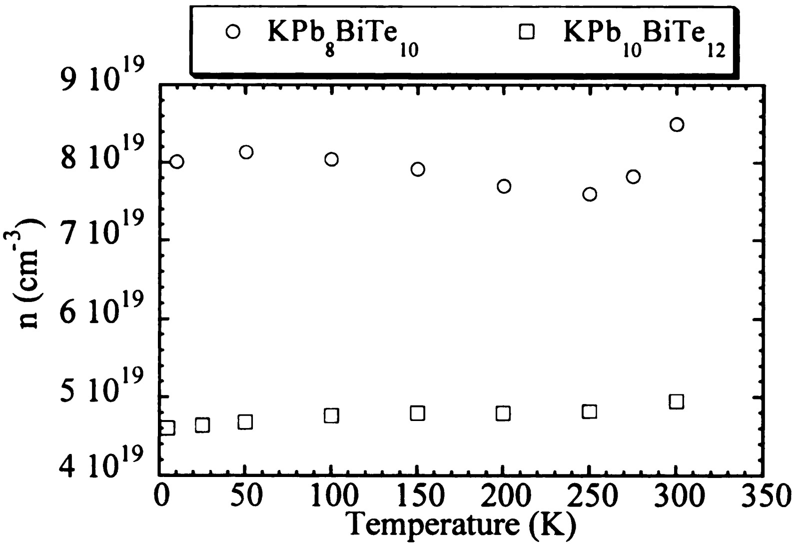

Figure 2-22: Charge carrier concentration for KPb_8BiTe_{10} and $KPb_{10}BiTe_{12}$ as a function of the temperature.

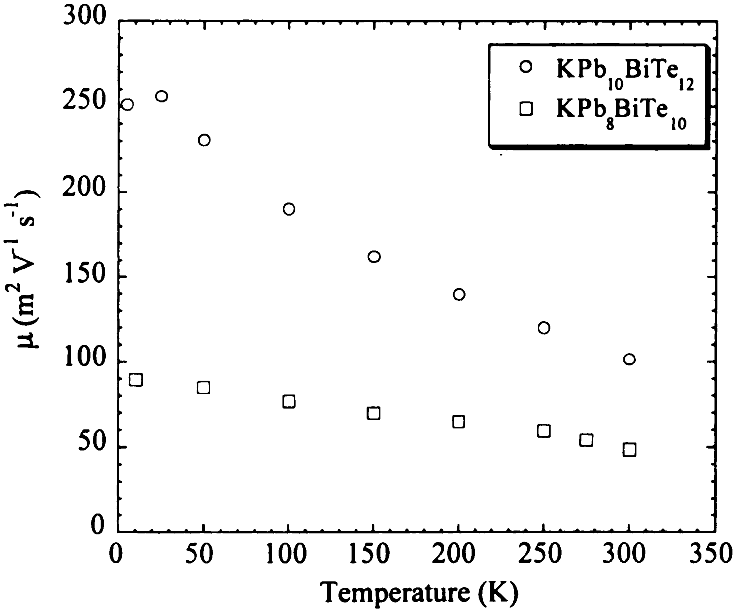

Figure 2-23: Temperature dependence of the mobility of samples of KPb_8BiTe_{10} and $KPb_{10}BiTe_{12}$.

(2) K/Pb/Bi/Se and K/Pb/Bi/S system

It was not possible to obtain reproducible Seebeck values for members of selenium system. Contacts problems at the level of the sample could be the cause of the problem. Another possibility is the set up of our to device that is set to measure compounds with medium to high electrical conductivity.

Measurements on pressed pellets of $KPb_{10}BiS_{12}$ (360 µV/K at 310 K) show high reproducible *positive* values for the Seebeck coefficient (see Figure 2-24). This impressive value has nevertheless to be taken with care because of the uncertainty on the accuracy of the measurements. Because both p-type and n-type materials are needed for their integration in thermoelectric modules, one needs to have both n- and p-type materials. Low values of electrical conductivity ranging from 1 to 3 S/cm were measured for both Selenium and Sulfur systems.

The samples were not studied further. Instead, efforts were focussed on the tellurium systems that showed more promising results.

(3) Ag/Pb/Bi/Te System

Seebeck coefficient and electrical conductivity values for the sample $AgPb_{10}BiTe_{12}$were measured (see Figure 2-25). The samples morphology was that of as-made ingots, and gave values of about –100 µV/K and 700 S/cm respectively at room temperature.

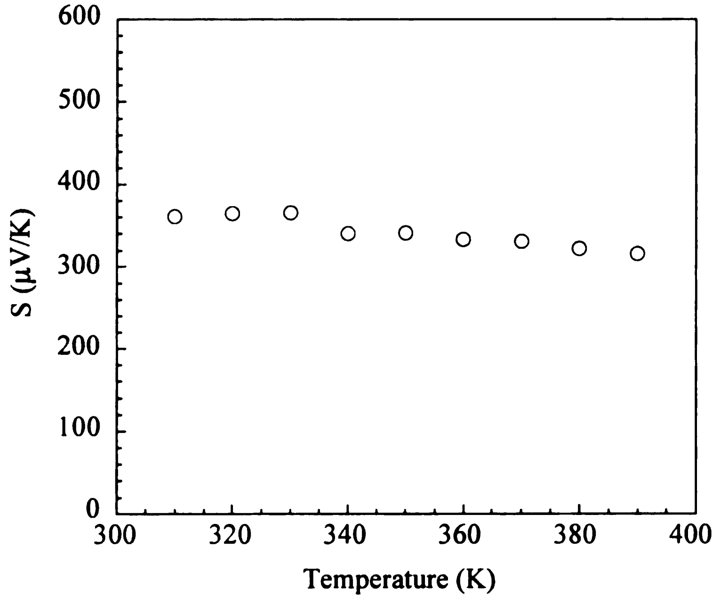

Figure 2-24: Seebeck coefficient for $KPb_{10}BiS_{12}$ (cold pressed pellet).

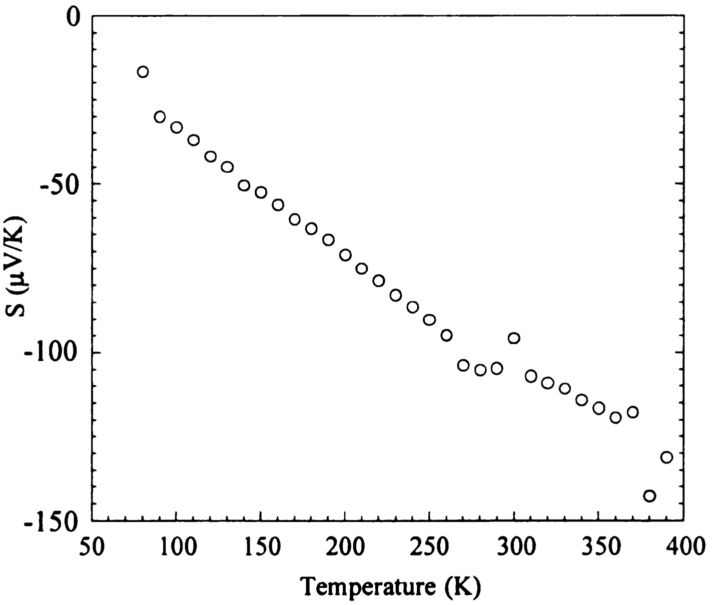

Figure 2-25: Seebeck coefficient for $AgPb_{10}BiTe_{12}$ (cold pressed pellet).

The sample was re-melted and sent for further measurements and the results show a conductivity at room temperature of 750 S/cm that agreed well with our in-house measurement (Figure 2-26). The material exhibits metallic behavior as the electrical conductivity decreases with the temperature. The Seebeck coefficient at room temperature is extrapolated to give a value of ~ -80 μV/K which also agree well with our measurements (Figure 2-27).

Lower values of Seebeck coefficient were expected for the ingot samples compared to the cold pressed ones in view of the previous differences that were noted between pressed pellet and ingots in the K/Pb/Bi/Te system. To the contrary, measurements on the Ag/Pb/Bi/Te system, seem less sensitive to the morphology of the sample. Preliminary transport properties at room temperature of other silver based systems are reported in Table 2-8.

Table 2-8. Seebeck coefficient (pressed pellets) and electrical conductivity (on ingots) for silver containing members at room temperature.

Compound	σ (S/cm)	S (μV/K)	Compound	σ (S/cm)	S(μV/K)
$AgPb_{10}SbS_{12}$	0.14	-290[2]	$Ag_2PbBi_2Te_5$	90	-50[1]
$AgPb_{10}SbTe_{12}$	760	-80[1]	$AgPb_3BiTe_5$	630	-50
			$AgPb_6BiTe_8$	1080	-85[1]

[1]: Values measured at 310 K

[2]: Strong fluctuation of S after 360 K

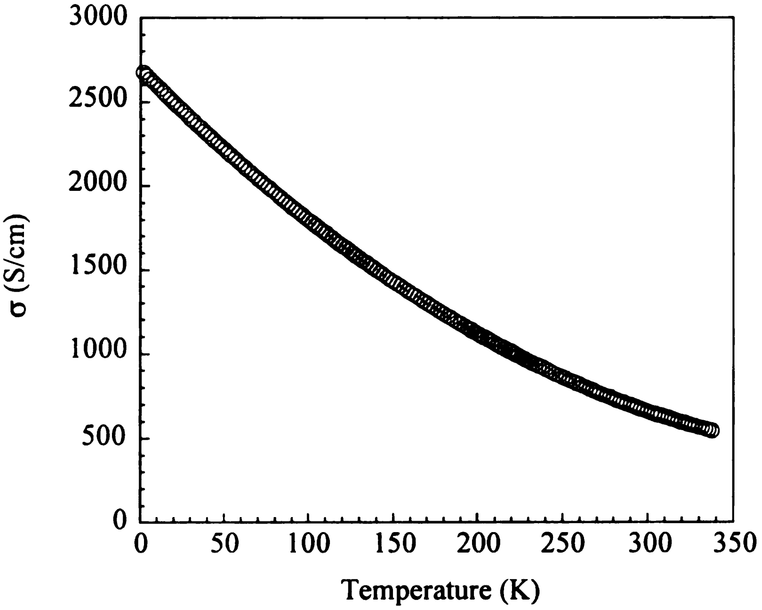

Figure 2-26: Electrical conductivity of $AgPb_{10}BiTe_{12}$ (measured on ingot).

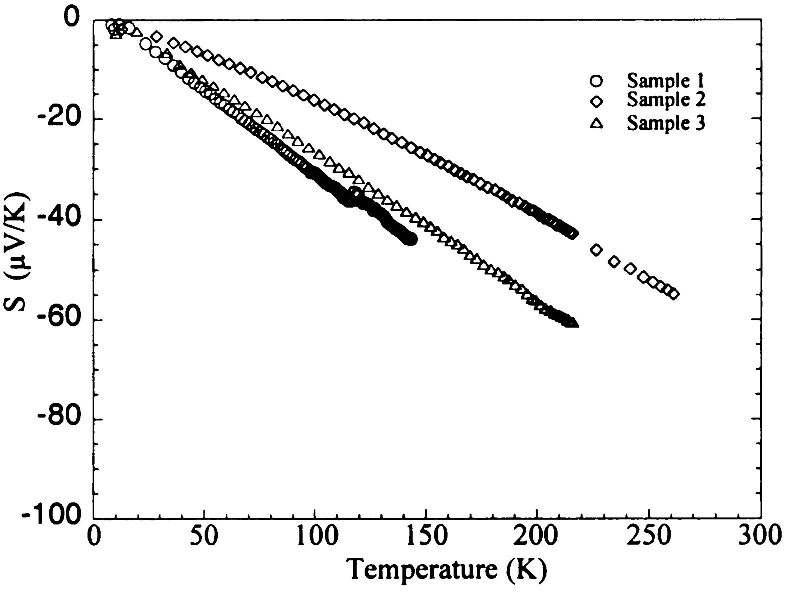

Figure 2-27: Seebeck Coefficient for $AgPb_{10}BiTe_{12}$ (measured on ingot).

As a general trend, the electrical conductivity of members of the Ag/Pb/Bi/Te system increased with the lead content. Additional work on this system is done by Dr. Sportouch that tend to confirm that this system is promising for thermoelectric application. The Ag system seems easier to work with because the stoichiometry is more easily controllable than the K/Pb/Bi/Te system due to the lack of glass attack and the good agreements between pressed pellets and ingots-made measurements.

(4) Other Related Systems

Preliminary measurements were made on systems involving Sn and/or Sb along with K and Te. Table 2-9 gives the room temperature conductivity of compounds synthesized using flame reactions. Within a system, the conductivity increases as the amount of lead or tin increases, as previously observed above in other systems. Members of the system K/Pb/Sb/Te have the lowest conductivities while the highest are found in the K/Sn/Sb/Te system.

Problems during the measurements of the Seebeck coefficient on pressed pellets appeared. High fluctuation of the measurements and high differences between the voltage at the reference and at the sample suggest that the values reported have to been taken with care. Despite these problems, the introduction of Sn in the system seems to make a p-type material. This is observed for $KSn_{10}SbTe_{12}$, and $KSn_{10}BiTe_{12}$. In these systems, the majority carriers are holes.

Table 2-9. Room temperature electrical conductivity and Seebeck coefficient for members of the K/B/M/Te system (where B is Pb or Sn and M is Bi or Sb).

Compound	σ (S/cm) (ingots)	S (μV/K) (pressed pellets)	S (μV/K) (ingots)
KPb_5SbTe_7	13	-70	-38
$KPb_{10}SbTe_{12}$	215	-25	-5
$KSnSbTe_3$	210		
KSn_5SbTe_7	2630	+44	+32
$KSn_{10}SbTe_{12}$	4250	+35[1]	+28
$KSnBiTe_3$	150		
KSn_5BiTe_7	230	+38	+10
$KSn_{10}BiTe_{12}$	990	300[2]	+32

[1]: Strong fluctuation of S

[2]: High value of the voltage measured at the sample making this measurement inaccurate.

2-4. Concluding Remarks

Several systems of the general formula $A_mB_nM_mQ_{2m+n}$ have been obtained from two types of synthesis methods: one favoring a thermodynamic synthesis (method II and III) and one favoring a kinetic approach (method I). Table 2-10 summarizes the transport and physicochemical properties of the different compounds synthesized. In view of the results discussed, it appears that the silver-based systems prepared with the flame method behave well while no method proved to be superior for the potassium/tellurium compounds. Differences in the absorption spectrum show that the flame methods tend to produce self-doping effects. The implication of this effect on the transport properties is important as the properties of pure semiconductors are dramatically changed by defects or doping impurities.

The use of the flame to prepare ingots changes the electronic structure of the compounds resulting in changes in the number of charge carriers and decrease the value of the Seebeck coefficient. Another hypothesis that can account for the differences between the samples measured at our facility and at other laboratories will be developed in the next chapter.

The bang gaps of members of the $K_mPb_nBi_mTe_{2n+m}$ system (below 0.40 eV) and their number of charge carriers are in the desirable range for TE applications. The transport properties are promising and members with high Pb content such as $KPb_{10}BiTe_{12}$ constitute good starting materials for further work. This compound possesses promising transport properties at room temperature: $S \sim -47\mu V/K$, $\sigma \sim 800 S/cm$, $\kappa \sim 2.4$ W/m·K, which give a ZT of 0.027 with some samples showing a high Seebeck coefficient of –140 μV/K. Taking the latter value into account, a respectable ZT of 0.2 is projected at room temperature.

From all the systems investigated, the K/Pb/Bi/Te and Ag/Pb/Bi/Te systems gave the best results in terms of transport properties for n-type materials. The substitution of Pb by Sn creates p-type materials with holes being the majority carriers. Both types of materials are necessary for the development of TE modules and investigation on the A/Sn/M/Q systems should be vigorously pursued.

The next step in the investigation of these cubic phases involves the decrease of the thermal conductivity by creating more disorder in the lattice using appropriate solid solutions. Such disorder can be created, as already mentioned, by substitution of appropriate elements on the anionic or cationic positions by other elements belonging to the same group of the periodic table. An increase of the thermopower is also necessary and could be achieved by such doping experiments as well.

Table 2-10. Physical and Transport properties for members of different systems.

Compounds	Cell Par. (A)	E_g (eV)	S_{RT} (μV/K)	σ_{RT} (S/cm)	κ_{RT} (W/m·K)	ZT_{RT}
$KPbBiTe_3$			-47	910		
KPb_8BiTe_{10}	6.459	0.38	-41	600	2.0	0.015
$KPb_{10}BiTe_{12}$	6.471	0.38	-47	800	2.2	0.027
KPb_nBiSe_{n+2}	6.217 / 6.136	0.675 / 0.46				
KPb_nBiS_{n+2}	5.998 / 5.935	0.87 / 0.61	360			
$AgPb_{10}BiTe_{12}$	6.4212	0.28	-110	750		

References

1. G.D. Guseinov, E.M. Godzhaev, Kh.Ya. Khalilov, F.M. Seidov, A.M. Pashaev, *Inorg. Mater.*, 8, 9, **1972,** 1377-1381
2. S.K. Plachkova, I.V. Odin, A.A. Sher, A.V. Novoselova, *Inorg. Mater.*, 16, 7, **1980**, 823-825
3. J.H. Wernick, *Am. Mineral.*, 45, **1960**, 591-598
4. L.H. Brixner, *Am. Mineral.*, 50, **1965**, 259-260
5. S.N. Hoda, L.L.Y. Chang, *Am. Mineral.*, 60, **1975**, 621-633
6. S. Sportouch, M. Bastea, P. Brazis, J. Ireland, C.R. Kannewurf, C. Uher, M.G. Kanatzidis, *Mat. Res. Soc. Symp. Proc.*, 545, MRS, **1999**, 123
7. I. Borissova, St. Decheva, St. Dimitrova, P. Moraliisky, Godishnik Na Sofuskiya Universitet, Fizicheski Fakultet, 65, **1972**, 167-176
8. E.A. Shrabek, D.S. Drimmer, "Properties of the General TAGS System", in CRC Handbook of Thermoelectricity, Ed. by D.M. Rowe, **1994,** 267
9. M. Evain, J.M. Barbet, P. Deniard, R. Brec, Powder Diffraction Meeting, Toulouse, France, **1990**
10. M. Evain, U-Fit:"A Cell Parameter Refinement Program", Institut des Materiaux de Nantes, France, **1992**
11. C. Uher, J. Yang, S. Hu, *Phys. Rev. B*, 59, 13, **1999**, 8615-8621
12. T.J. McCarthy, S.-P. Ngeyi, J.-H. Liao, D.C. DeGroot, T. Hogan, C.R. Kannewurf, M.G. Kanatzidis, *Chem. Mater.*, 5, 3, **1993**, 331-340
13. T. Hogan, N. Ghelani, S. Loo, S. Sportouch, S.-J. Kim, D.-Y. Chung, M.G. Kanatzidis, ICT Meeting, Baltimore, **1999**, In Press.
14. T.B. Zhukova, A.I. Zaslavskii, *Krystallografiya*, 16, 5, **1971**, 918-922
15. G. Gattow, J. Zemann, *Z. Anorg. Allg. Chem.*, 279, **1955**, 324-327
16. Y. Noda, S. Ohba, S. Sota, Y. Saito, Acta Crystallogr. B, 39B, **1983**, 312-317
17. L. Vegard, *Z. Phys.*, 5, **1921**, 17
18. O. Glemser, M. Filcek, *Z. Anorg. Allg. Chem.*, 279, 1955, 321-323
19. G.D. Mahan, *Solid State Phys.*, 51, **1998,** 81
20. D. Tuomi, *J. Elechtrochem. Soc.*, 131, **1984**, 2319

Chapter 3

Decreasing the Thermal Conductivity of $KPb_{10}BiTe_{12}$ by Mass Fluctuation via Solid Solution Experiments

3-1. Introduction

Optimization of the transport properties of TE materials involves the decrease of the thermal conductivity to a value close to 1 W/m·K[1]. Reduction of the lattice thermal conductivity can be obtained by different scattering mechanism due to electron-phonon in heavily doped compounds, electron charge transfer in mixed valence systems, or mass fluctuation. The latter can be achieved via solid solution experiments (also referred to as alloying). For example, the thermal conductivity of Bi_2Te_3[2] can be successfully reduced from 1.7-1.9 to 1.5-1.6 W/m·K (depending on the number of charge carriers) when alloyed with Sb_2Te_3.

Results from exploratory synthesis and preliminary measurements showed that high-lead content members of the KPb_nBiTe_{n+2} system possess one of the most promising transport properties among all systems investigated in this Thesis. These compounds are members of the general family of quartenary chalcogenides $A_mB_nM_mQ_{2m+n}$ (where A is Ag or K, B is Pb or Sn, M is Bi or Sb and Q is Te, Se, or S), and crytallize with the NaCl cubic structure type.

Among all the compositions investigated, $KPb_{10}BiTe_{12}$ appears to be the most appropriate candidate for further work. This choice was driven by the conclusion that the Seebeck coefficient was relatively high and not (or little) a sensitive function of the value of n, in contrast of the electrical conductivity that increases with n. From a practical point of view, members with high values of n proved to be more easily synthesized using the "flame reaction" (Method II and III in Chapter 2) because of their low content in potassium, and less glass attack.

Promising transport properties were observed for $KPb_{10}BiTe_{12}$ and reported in Chapter 2. The Seebeck coefficient at room temperature is equal to -47 μV/K on ingot and -140 μV/K on cold pressed pellet; the electrical conductivity is close to 800 S/cm, and the thermal conductivity reaches ~2.2 W/m·K.

Statistical disorder is already present in the K/Pb/Bi/Te system. Atoms of K, Pb, and Bi occupy the same positions in the cationic sub-lattice of the crystal (the Na^+ position in the NaCl structure), while the tellurium atoms seat on the anionic sub-lattice (Cl^- positions). Additional disorder is possible on these sites by replacing some Pb atoms by Sn or Bi atoms by Sb. Furthermore, the anionic positions occupied by Te can also be disordered by introduction of selenium and/or sulfur atoms. The systems K/Pb/Bi/Te, K/Sn/Bi/Te, and K/Pb/Sb/Te, as well as the selenium analogues, are members of the same general family studied in this Thesis. Having the same chemical bonding (ionic-covalent) and being isomorphous to the cubic NaCl type lattice, solid solutions between them should be possible. Substitution of potassium atoms by Cs, Rb or Ag should also be feasible but this was not investigated in this work. By carrying out such substitutions, the thermal conductivity of $KPb_{10}BiTe_{12}$ is expected to drop to a value closer to the one of optimized $Bi_2Te_{3-x}Se_x$ alloys or perhaps even lower.

3-2. Experimental Section

Reagents

All reagents were elements. As mentioned in the previous chapter, high purity K, Pb, Bi, Te, Se, S, Sn and Sb were used.

Synthesis

Method II described in Chapter 2 was used for the synthesis of all compounds described in this chapter. For example, $KPb_{10}BiTe_6Se_6$ was prepared by mixing under nitrogen atmosphere, 0.052 g (1.33 mmole) of K, 2.762 g (13.3 mmole) of Pb, 0.2786 g (1.33 mmole) of Bi, with 0.6316 g (8 mmole) of Se and 1.021 g (8 mmole) of Te. The mixture was loaded into a 13-mm carbon coated silica tube. The tube was sealed under vacuum ($< 10^{-4}$ Torr) and heated for 1 hour at 500 °C (pre-reaction). The tube was opened and the material was transferred into a new 13-mm silica tube (without carbon coating in order to be able to see the melt during the next step). The tube was then sealed under vacuum at the same residual atmosphere and heated with a high temperature torch flame. Members of solid solutions other than $KPb_{10}BiTe_{12-x}Se_x$ were heated to 150 °C for 1 hour instead of the 500 °C used in the pre-reaction step.

Physical and Transport Measurements.

See previous chapter.

3-3. Result and Discussion

Synthesis and Crystallographic Data

(1) The solid solutions $KPb_{10}BiTe_{12-x}S_x$

Unfortunately, solid solutions in this system could not de prepared due to phase separation. Stoichiometries having values of x equal to 1, 3, 6, 9 corresponding respectively to the formulae $KPb_{10}BiTe_{11}S$, $KPb_{10}BiTe_9S_3$, $KPb_{10}BiTe_6S_6$, and $KPb_{10}BiTe_3S_9$ were tried. In each case, the X-ray diffraction powder pattern of the products show a mixing of two phases (see Figure 3-1a) corresponding to members of the KPb_nBiTe_{n+2} and KPb_nBiS_{n+2} systems. As the amount of tellurium was increased in the system, the intensity of the peaks corresponding to the tellurium phase increased as the phase became dominant. Annealing of the samples for 1 day at 750 C did not result in a single phase (see Figure 3-1b). Phase separation is a consequence of the large ionic size difference between tellurium and sulfur atoms that do not favor good stacking in the NaCl structure type. Such effects are well known for solid solutions of ZnTe-ZnS[3], where the solid solutions exists only up to 8 mole percents of ZnTe in ZnS and up to 5 mole percents of ZnS in ZnTe. In our case, we only investigated solid solutions having from 9

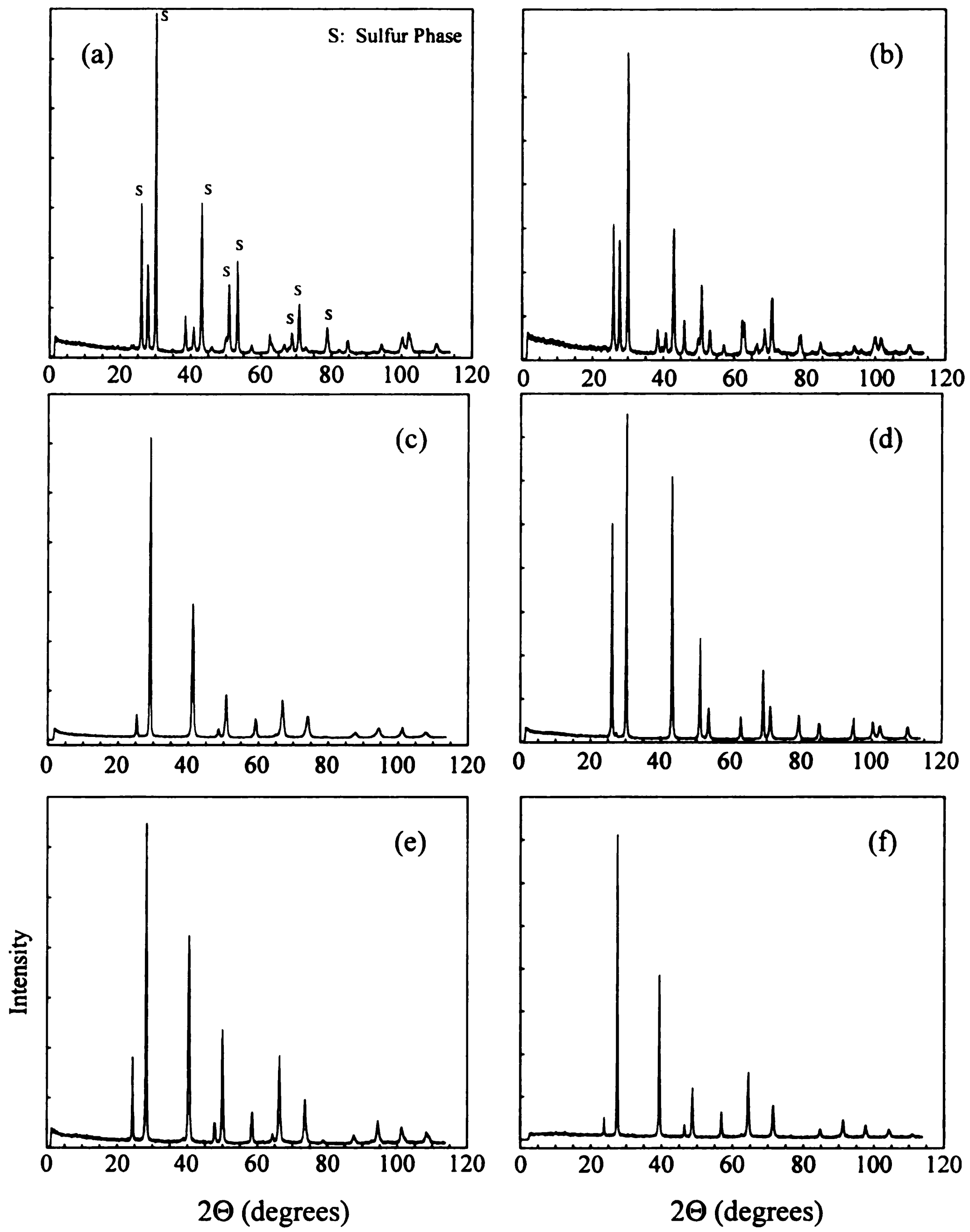

Figure 3-1: X-ray diffraction powder patterns of (a) $KPb_{10}BiTe_3S_9$, (b) $KPb_{10}BiTe_3S_9$ after annealing, (c) $KPb_{10}BiTe_9Se_3$, (d) $KPb_{10}BiSe_3S_9$, (e) $KPb_{10}Bi_{0.5}Sb_{0.5}Te_6Se_6$, and (f) $KPb_{10}BiTe_{12}$ (shown for comparison).

to 91 mole percents of $KPb_{10}BiTe_{12}$ in $KPb_{10}BiS_{12}$, therefore solid solution outside this range might be possible.

(2) The solid solutions $KPb_{10}BiTe_{12-x}Se_x$

In contrast to the previous system, the Te/Se one formed solid solutions readily. The compounds $KPb_{10}BiTe_{11}Se$, $KPb_{10}BiTe_9Se_3$, $KPb_{10}BiTe_6Se_6$, $KPb_{10}BiTe_3Se_9$, and $KPb_{10}BiTe_1Se_{11}$ corresponding respectively to values of x equal to 1, 3, 6, 9, and 11 were synthesized in two identical batches (a) and (b). Small quantities of products in batch (a) were made (between 1 and 1.2 g), while the objective of batch (b) was to obtain enough sample (between 2.5 and 5 g) for measurements. Every sample of each batch shows pure powder pattern corresponding to a single NaCl type phase (see Figure 3-1c).

The cell parameters were calculated and follow, as expected, a linear dependence on composition, i.e. Vegard's Law[4] (see Table 3-1 and Figure 3-2). Surprisingly, when selenium and tellurium are mixed in solid solution, the system behaved well under the conditions of Method II, while the end-members show inconsistency in the values of the cell parameters under the same experimental conditions. The differences in the values of the cell parameters that appeared between the compounds of batch (a) and (b) is attributed to a lack of homogeneity in batch (b) due to the larger quantity synthesized.

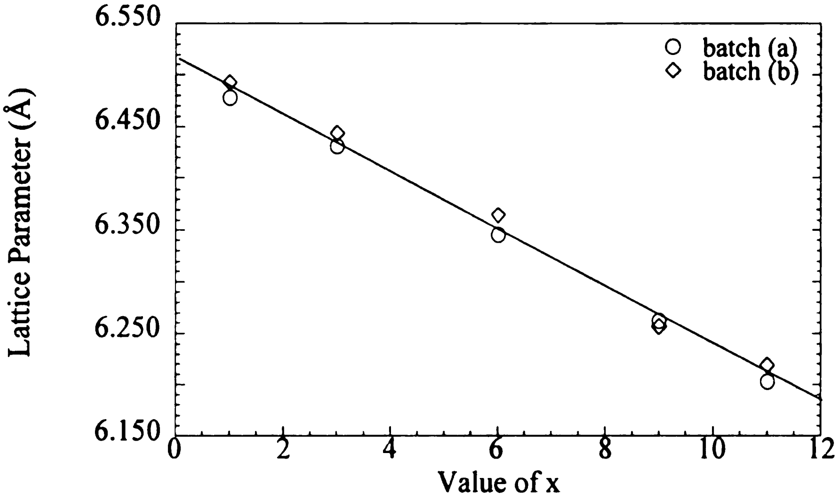

Figure 3-2: Cell parameter variation for the solid solutions $KPb_{10}BiTe_{12-x}Se_x$.

Table 3-1. Cell parameters for solid solutions of $KPb_{10}BiTe_{12-x}Se_x$.

Compound	Cell Parameter (Å)	Cell Parameter (Å)
	batch (a)	batch (b)
$Pb_{10}BiTeSe_{11}$	6.203 (2)	6.219 (1)
$KPb_{10}BiTe_3Se_9$	6.262 (3)	6.257 (2)
$KPb_{10}BiTe_6Se_6$	6.346 (2)	6.365 (2)
$KPb_{10}BiTe_9Se_3$	6.431 (2)	6.444 (2)
$KPb_{10}BiTe_{11}Se$	6.478 (1)	6.493 (2)

(3) The solid solutions $KPb_{10}BiSe_{12-x}S_x$

In accordance with the reasonable size differences between sulfur and selenium atoms, solid solutions of these two systems gave a pure single phase. Values of x equal to 1, 3, 6, 9, and 11 corresponding respectively to the compounds $KPb_{10}BiSe_{11}S$, $KPb_{10}BiSe_9S_3$, $KPb_{10}BiSe_6S_6$, $KPb_{10}BiSe_3S_9$, and $KPb_{10}BiSeS_{11}$ were prepared. All samples show pure cubic phases in perfect agreement with the NaCl structure type (see Figure 3-1d). The cell parameters were calculated and reported in Table 3-2. The lattice parameter decreases with x, as small atoms (S) substitute larger ones (Se). The system deviates from Vegard's law as shown on Figure 3-2. Instead, the observed lattice parameters follow a parabolic dependence on compositions of type:

$$a = x_1a_1 + x_2a_2 + \Delta a.$$

Urusov[5] studied different deviations from Vegard's law using geometric models. In the case of the NaCl structure, he concluded that secondary and higher shift orders are responsible for parabolic deviations. These shifts are created by atomic displacements that can be expressed as $\delta_i = A\left(\frac{u}{R^2}\right)$ where *i* is the order of the shift, A is a constant depending of *i*, $u = \frac{1}{2}\Delta R$, and *R* is the interatomic distance. We can expect such effect to be present in the system studied because of the high disorder on both anionic and cationic sites. Such distortions in the structure due to atomic displacements seem to be responsible for the deviation from Vegard's law observed.

Table 3-2: Cell parameters for solid solutions of $KPb_{10}BiSe_{12-x}S_x$.

Compound	Cell Parameter (Å)	Compound	Cell Parameter (Å)
$KPb_{10}BiSeS_{11}$	5.931 (2)	$KPb_{10}BiSe_9S_3$	6.079 (2)
$KPb_{10}BiSe_3S_9$	5.977 (2)	$KPb_{10}BiSe_{11}S$	6.097 (2)
$KPb_{10}BiSe_6S_6$	6.029 (2)		

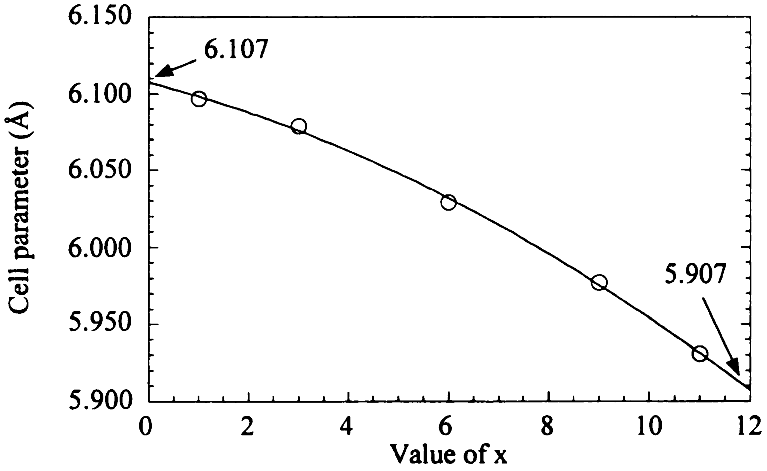

Figure 3-3: Cell parameter variation for the solid solutions $KPb_{10}BiSe_{12-x}S_x$.

(4) Solid solutions of the type $KPb_{10}Bi_{1-x}Sb_xTe_6Se_6$

Members of the solid solutions $KPb_{10}Bi_{1-x}Sb_xTe_6Se_6$ (where x = 0.25, 0.5, and 0.75) were synthesized. X-ray powder patterns show pure cubic NaCl phase for all samples (see Figure 3-1f). The cell parameters were calculated as previously mentioned and are reported in Table 3-3. From these data, we can see that the cell parameters deviate slightly from Vegard's law similarly to the $KPb_{10}BiSe_{12-x}S_x$ solid solutions (see Figure 3-4). The value calculated for $KPb_{10}BiTe_6Se_6$ in the previous chapter has been used for the case x = 0, which corresponds to the same stoichiometry. By extrapolation, the cell parameter of $KPb_{10}SbTe_6Se_6$ can be estimated to be close to 6.258 (2) Å.

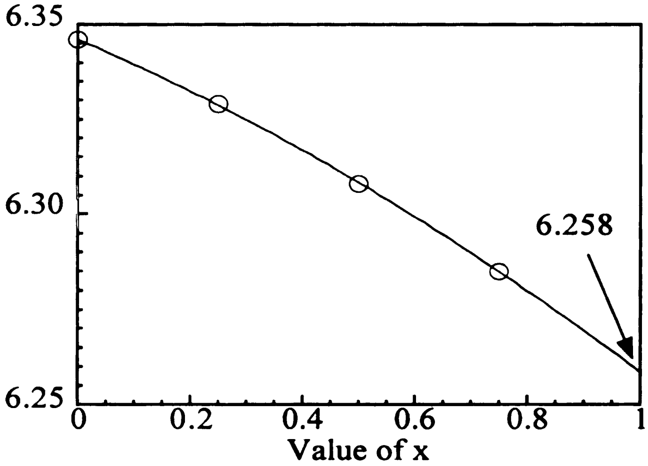

Figure 3-4: Cell parameter variation for the solid solutions $KPb_{10}Bi_{1-x}SbTe_6Se_6$.

Physical Properties

Thermal Analysis

Differential thermal analysis of solid solutions $KPb_{10}BiTe_{12-x}Se_x$ did not show any melting peaks in accordance with the lack of similar peaks for the two end-member systems KPb_nBiTe_{n+2} and KPb_nBiSe_{n+2}. Similarly, the compounds $KPb_{10}Bi_{1-x}Sb_xTe_6Se_6$ did not show any clear endothermic peaks either (see Figure 3-5).

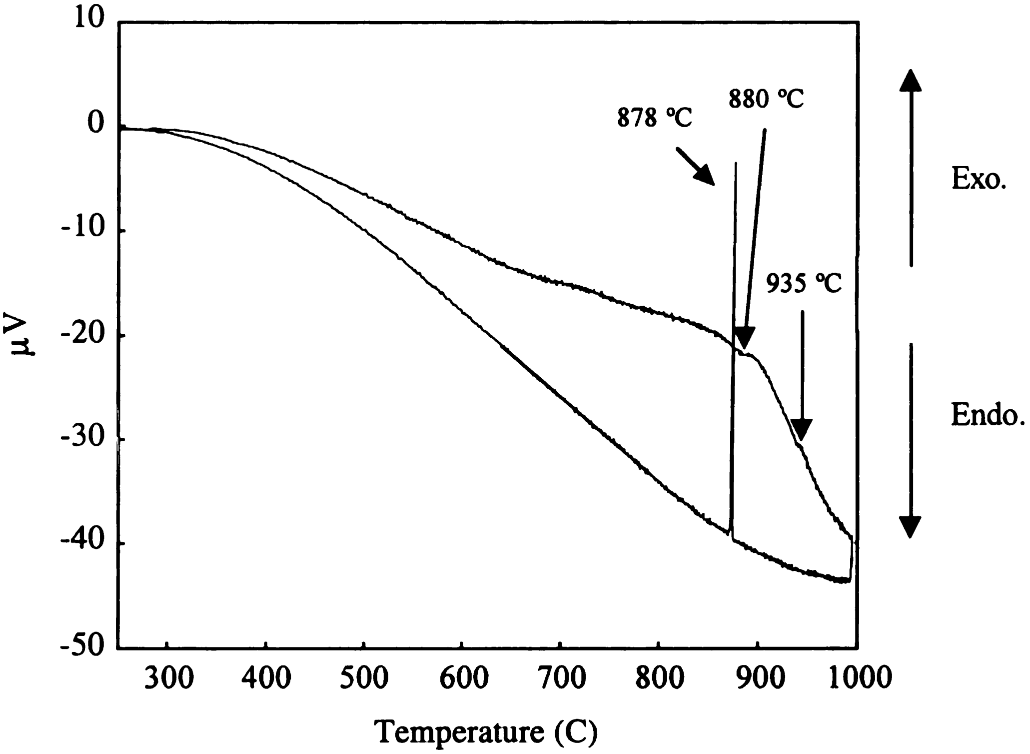

Figure 3-5: DTA of $KPb_{10}Bi_{0.25}Sb_{0.75}Se_6S_6$ showing the recrystallisation and melting temperatures.

Nevertheless, sharp exothermic peaks corresponding to recrystallisation temperatures (T_{cryst}) were observed and reported in Table 3-3. This suggests that melting indeed occurs below 1000 °C but the corresponding endothermic peak is masked by the broad background which begins to increase endothermically above 880 °C. Such increase could be due to the initiation of reactive glass attack by the material. Such glass attack was observed on the DTA tubes indicating that these differences are most certainly due to a loss of K and Se that reacted with silica. Small exothermic peaks can be seen around 940 °C and can be attributed to the melt of the material. This does not constitute the melting point of the material but instead it must be seen as the melting point of a Te-rich composition due to the change in the stoichiometry that occurred during glass attack. These values are nevertheless indicative of the range of melting temperatures for the solid solutions investigated. The lattice parameters calculated from X-ray powder diffraction after the DTA experiment show an increase in their values to a value close to the one of PbTe 6.462 Å, supporting the above discussion.

Energy Gap

Due to self-doping effects created by the rapid cooling of the material during synthesis ("flame" reaction), no band gaps were observed on diffuse reflectance spectra for members of the solid solutions $KPb_{10}BiTe_{12-x}Se_x$ as well as for $KPb_{10}BiSeS_{11}$, $KPb_{10}BiSe_3S_9$, and $KPb_{10}BiSe_6S_6$. Energy gaps were nevertheless observed for $KPb_{10}BiSe_9S_3$ and $KPb_{10}BiSe_{11}S$ and calculated to be 0.51 and 0.45 eV respectively. These values have to be considered as upper limits and do not constitute the true band gaps that must lie below. Therefore it is difficult to compare them and to conclude that $KPb_{10}BiSe_9S_3$ possesses a higher band gap than $KPb_{10}BiSe_{11}S$. In fact, we expect the opposite since the system KPb_nBiS_{n+2} was observed to have higher energy gaps than KPb_nBiSe_{n+2}.

Table 3-3. Cell parameters, energy gaps, recrystallization and melting temperatures (T_{cryst} and T_m), for members of the system $KPb_{10}Bi_{1-x}Sb_xTe_6Se_6$.

Value of x	Cell Parameter (Å) (before DTA)	E_g (eV)	T_{cryst} (°C)	T_m (°C)	Cell Parameter (Å) (after DTA)
0.25	6.329 (3)	0.35	890	939	6.476 (4)
0.5	6.308 (2)	0.34	898	935	6.454 (2)
0.75	6.285 (2)	0.32	878	935	6.452 (1)

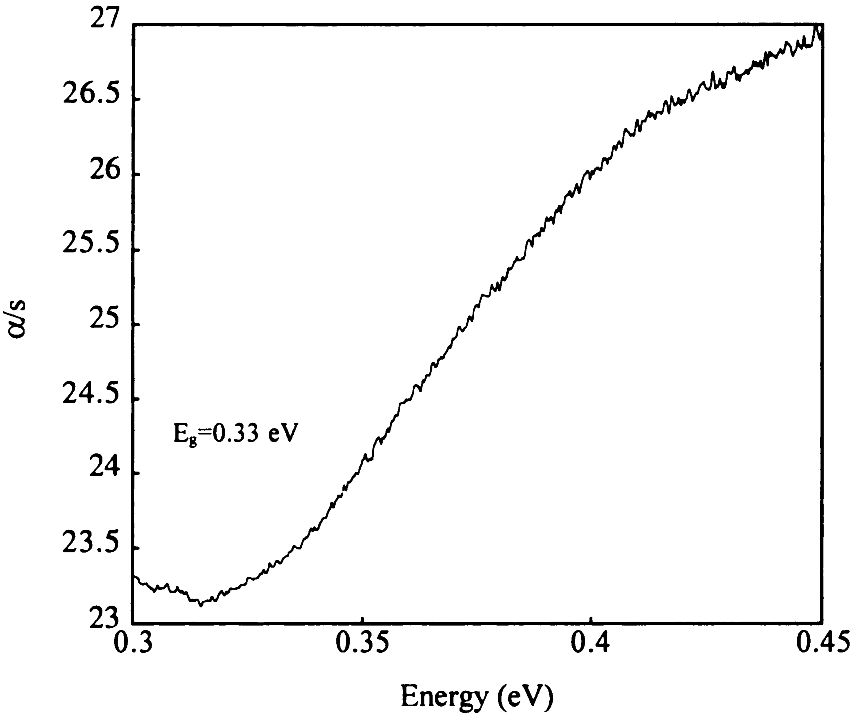

Figure 3-6: Optical absorption spectrum of $KPb_{10}Bi_{0.5}Sb_{0.5}Se_6S_6$ showing a band gap.

Energy gaps were observed for solid solutions $KPb_{10}Bi_{1-x}Sb_xTe_6Se_6$ (see Table 3-3 and Figure 3-6). Substitution of Bi by Sb decreases the band gap as expected, because lighter atoms replace heavier ones. Although no band gap was observed for $KPb_{10}BiTe_6Se_6$, we can estimate it to be slightly above 0.35 eV considering the values obtained for the solid solutions $KPb_{10}Bi_{1-x}Sb_xTe_6Se_6$.

Transport Properties

(1) The solid solutions $KPb_{10}BiTe_{12-x}Se_x$

Transport properties for different members of this system are summarized in Table 3-4. Room temperature electrical conductivity show an increase with increasing Te content in the samples of batch (a), but no trend was observed in batch (b). By substituting selenium for tellurium atoms, we increase the band gap and therefore should decrease the electrical conductivity. This explains the trend observed as more Se atoms are introduced in the system. Surface effects and non-homogeneity might be responsible for the constant values of the electrical conductivity measured for samples of batch (b).

Seebeck coefficient measurements on the samples of batch (a) show strong fluctuation in the values of S at temperature between 450 K and 500 K. This reproducible feature is shown in Figure 3-7 that represents the third Seebeck measurement cycle of the compound. Such fluctuation is believed to be due to a dilatation of the pressed pellet with increase in temperature that could produce cracks. As the temperature decreases, the pellet contracts, restoring the original contacts. This hypothesis is supported by the observation of a transversal line (possibly the crack line) on the some sample surface after measurements.

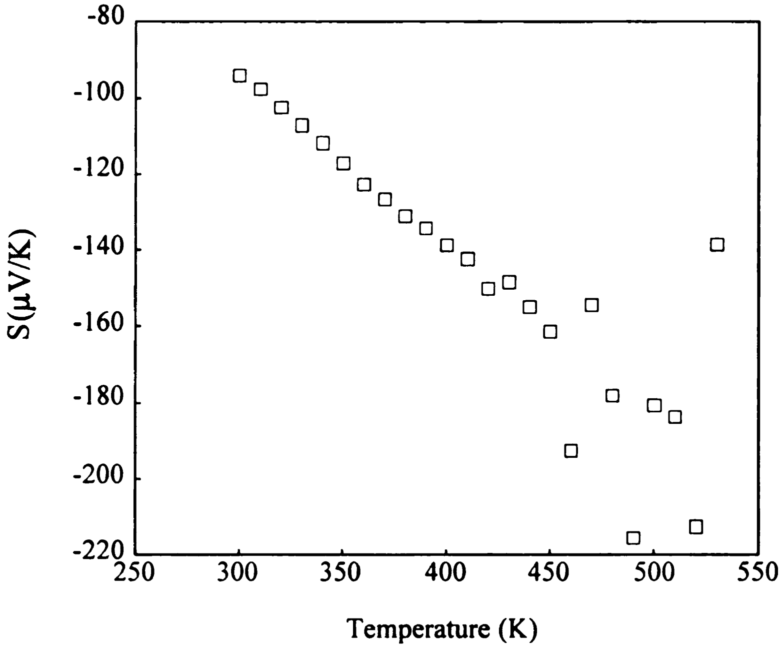

Figure 3-7: Seebeck coefficient for $KPb_{10}BiTe_{11}Se$ (batch a) measured on cold pressed pellet.

Because of the good values obtained from the sample $KPb_{10}BiTe_{11}Se$ of batch (b), i.e. S = -162 μV/K and σ = 570 S/cm, the material was sent for additional measurement. The thermal conductivity, after correction due to the radiative losses (see Figure 3-8), is about 1.78 W/m·K at room temperature. The linear variation of the radiative part as a function of T^3 validates the correction made (see Figure 3-9) as explained in Chapter 1. As expected, by mixing Te and Se atoms in the Cl^- site we decreased the long range ordering and we were able to decrease the thermal conductivity by about 15 % in the case of $KPb_{10}BiTe_{11}Se$.

Table 3-4. Room temperature Seebeck coefficient (on pressed pellet) and electrical conductivity (on ingot) for solid solutions $KPb_{10}BiTe_{12-x}Se_x$.

Compound	S_{RT} (μV/K) batch (a)	S_{RT} (μV/K) batch (b)	σ_{RT}(S/cm) batch (a)	σ_{RT} (S/cm) batch (b)
$KPb_{10}BiTeSe_{11}$	-97	-97	270	640
$KPb_{10}BiTe_3Se_9$	-95	-115	340	570
$KPb_{10}BiTe_6Se_6$	-150	-156	407	780
$KPb_{10}BiTe_9Se_3$	-102	---	646	470
$KPb_{10}BiTe_{11}Se$	-94	-162	782	570

The Seebeck coefficient was measured to be equal to -60 μV/K at room temperature (see Figure 3-10) and is in the range of other previous samples measured outside our lab. Its negative sign indicates that the charge carriers responsible for electrical conductivity are electrons. This value is lower than what we recorded on pressed pellet (-162 μV/K). In Chapter 2, we attributed the differences in the Seebeck measurements between cold pressed pellets and ingots, to a change in the electronic structure of the materials taking place perhaps near the grain boundaries. Nevertheless, $KPb_{10}BiTe_{11}Se$ was sent as obtained from synthesis, thus the previous explanation does not hold anymore.

Electrical conductivity at room temperature was measured to be about 460 S/cm (see Figure 3-10), which is close to what we measured (570 S/cm) but lower than the value recorded for $KPb_{10}BiTe_{12}$ for the reason mentioned previously. In accordance with all the samples studied so far, the temperature dependence is typical of a metallic behavior.

As mentioned, no band gaps were observed in the diffuse reflectance I.R. spectrum, but the plot of the Seebeck measurement showed a minimum that can be used to calculate it as explained in Chapter 1 (see Figure 3-11). Using Eq. 1-14, the band gap at 415 K can be estimated to be equal to 0.11 eV. During the study of the K/Pb/Bi/Te system, we estimated the energy gap of $KPb_{10}BiTe_{12}$ to be around 0.38 eV. Due to self-doping this value is an upper limit and the calculated band gap from Seebeck measurements on $KPb_{10}BiTe_{11}Se$ indicates that the real band gap of $KPb_{10}BiTe_{12}$ should lie between 0.11 and 0.38 eV.

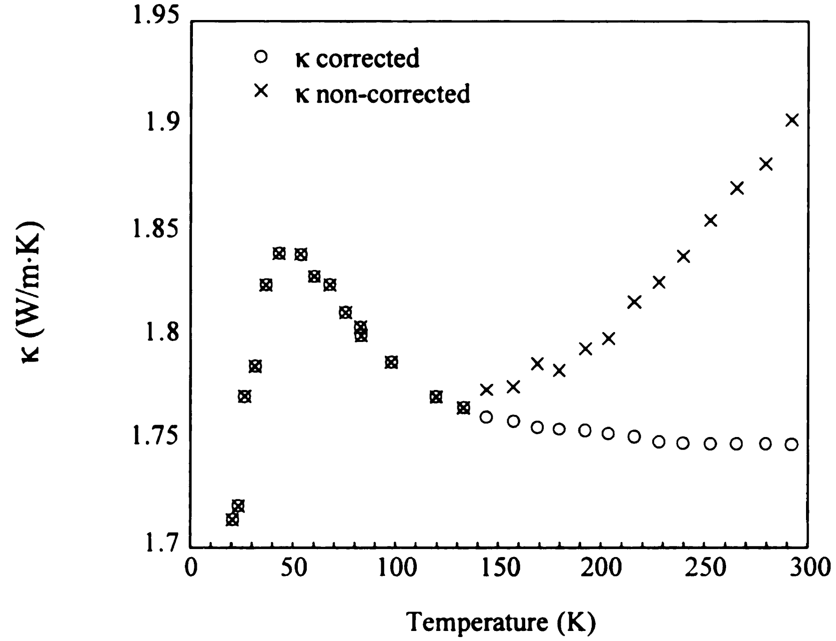

Figure 3-8: Thermal conductivity of $KPb_{10}BiTe_{11}Se$ before and after correction.

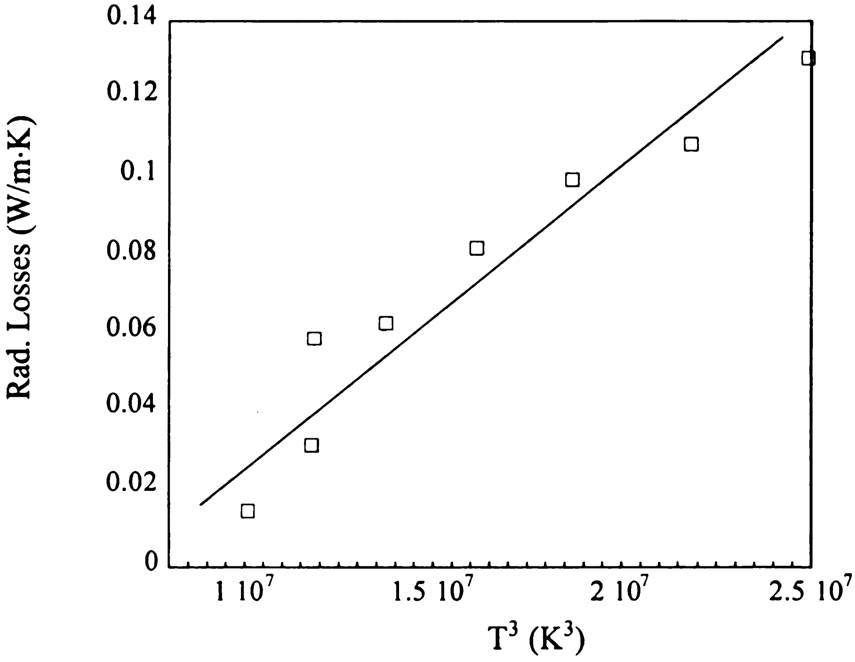

Figure 3-9: Radiative losses as a function of T^3.

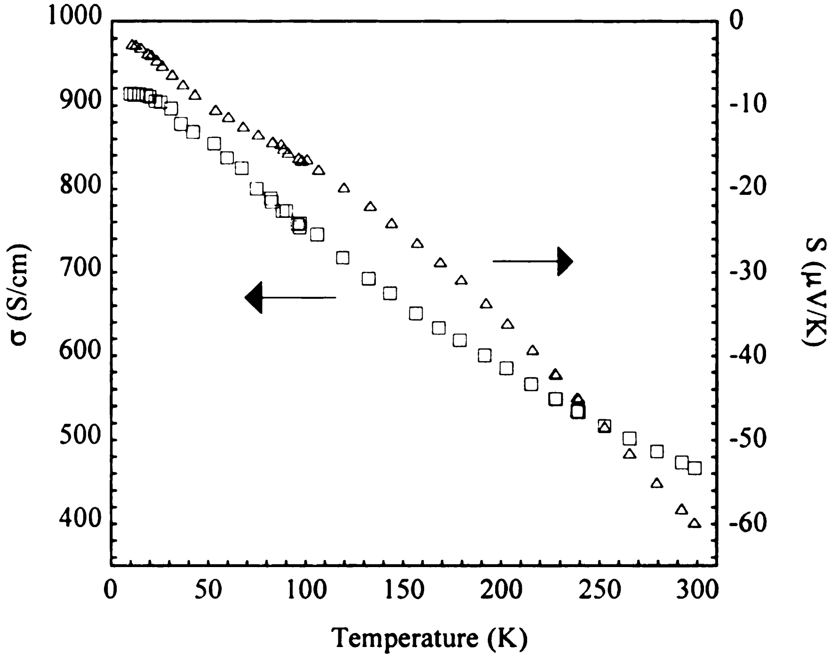

Figure 3-10: Seebeck coefficient and electrical conductivity for $KPb_{10}BiTe_{11}Se$.

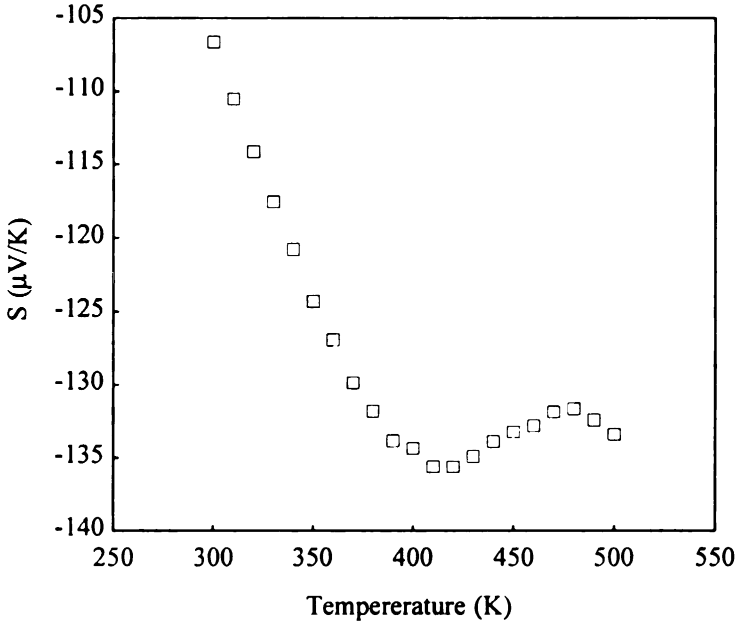

Figure 3-11: Seebeck coefficient showing a minimum for $KPb_{10}BiTe_{11}Se$.

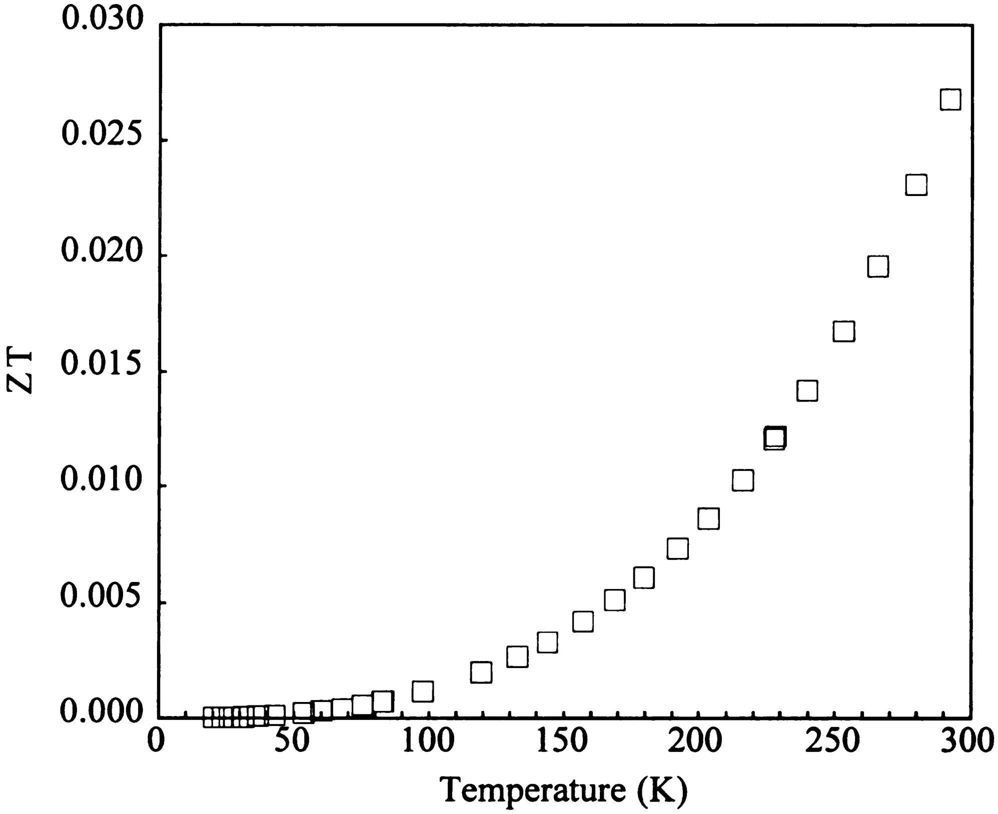

Figure 3-12: Figure of merit ZT for a sample of $KPb_{10}BiTe_{11}Se$.

The measured transport properties on $KPb_{10}BiTe_{11}Se$ gave a figure of merit ZT equal to 0.026 at room temperature (see Figure 3-12), which is similar to ZT calculated for $KPb_{10}BiTe_{12}$ at the same temperature. Even though, we succeeded in decreasing the thermal conductivity of $KPb_{10}BiTe_{12}$ by introduction of disorder in the anionic sites, lower value of the electrical conductivity compensated the gain obtained in the figure of merit. Introduction of appropriate doping agents should raise this value to a higher level.

(2) The solid solutions $KPb_{10}BiSe_{12-x}S_x$

Surprisingly, no problems were encountered during measurements of the Seebeck coefficient on cold pressed pellets for solid solutions $KPb_{10}BiSe_{12-x}S_x$ (see Figure 3-13) in contrast of measurements on the individual $K_mPb_nBi_mSe_{2m+n}$ and $K_mPb_nBi_mS_{2m+n}$ systems.

The variations of the Seebeck coefficients and the electrical conductivities as a function of the temperature agree: an increase of S results in a decrease of σ (see Table 3-5). This is observed for all the TE materials. Electrical conductivity values are lower than for the ones measured for solid solutions of $KPb_{10}BiTe_{12-x}Se_x$. Generally, alloying of a system such as K/Pb/Bi/Te with one having higher band gaps such as K/Pb/Bi/Se, raised the transition energy and therefore decreases the electrical conductivity. In contrast, when more Se substituted S atoms in the solid solutions $KPb_{10}BiSe_{12-x}S_x$, σ increased. No samples were sent for additional measurement because of the low electrical conductivities (below 500 S/cm) compared to members obtained in other families.

Table 3-5. Room temperature Seebeck coefficient (on pressed pellet) and electrical conductivity (on ingot) for solid solutions $KPb_{10}BiSe_{12-x}S_x$.

Compound	σ_{RT} (S/cm)	S_{RT} (μV/K)
$KPb_{10}BiSeS_{11}$	765	-98
$KPb_{10}BiSe_3S_9$	370	- 42 (at 310 K)
$KPb_{10}BiSe_6S_6$	210	-107
$KPb_{10}BiSe_9S_3$	115	-214 (at 310 K)
$KPb_{10}BiSe_{11}S$	135	-198

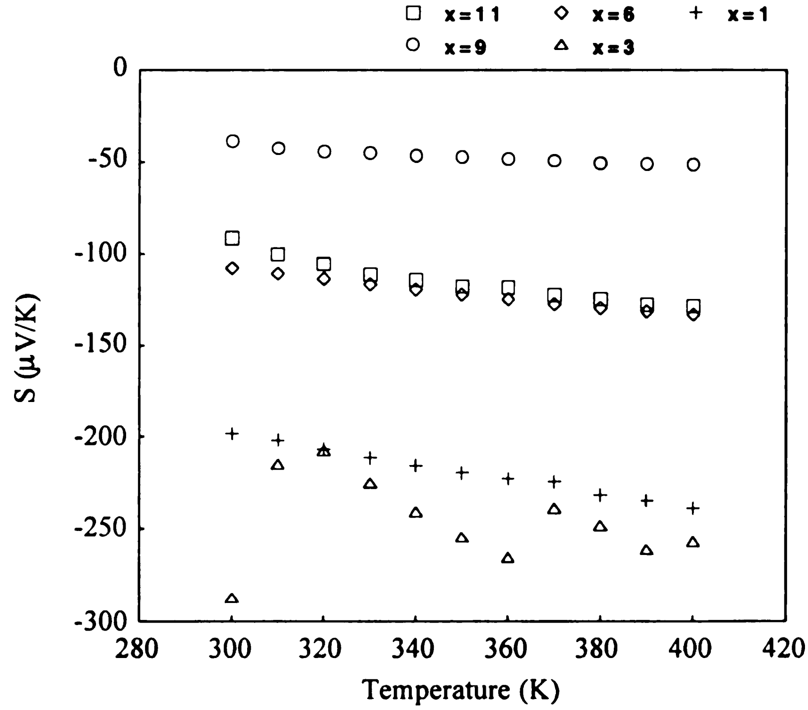

Figure 3-13: Seebeck coefficient of the solid solution $KPb_{10}BiSe_{12-x}S_x$ (cold pressed pellets).

(3) Other solid solutions of $KPb_{10}Bi_{1-x}Sb_xTe_6Se_6$

In addition to solid solutions on the anionic positions, further disorder is possible in $KPb_{10}BiTe_6Se_6$ by replacing some bismuth atoms by antimony. Promising results emerged from preliminary measurements (see Table 3-6).

Table 3-6. Room temperature Seebeck coefficient (on pressed pellet) and electrical conductivity (on ingot) for solid solutions $KPb_{10}Bi_{1-x}Sb_xTe_6Se_6$.

Value of x	σ_{RT} (S/cm)	S_{RT} (μV/K)
0.25	990	-152
0.5	595	-200
0.75	380	-280

The values of the Seebeck coefficient are negative and increased significantly with x, to reach a maximum for x=0.75. Surprisingly, the electrical conductivity of $KPb_{10}Bi_{0.75}Sb_{0.25}Te_6Se_6$ is in the same range than for $KPb_{10}BiTe_{12}$ contrary to what was observed for the solid solutions of $KPb_{10}BiTe_{1-x}Se_x$. Nevertheless, this is in accordance with the decrease of the energy gap observed (from 0.38 eV for $KPb_{10}BiTe_{1-x}Se_x$ to 0.35 eV for $KPb_{10}Bi_{0.75}Sb_{0.25}Te_6Se_6$). Energy band calculations would be useful to show the effect of substituting Sb for Bi on the energy band diagram. Transport properties results obtained from samples sent were encouraging, disappointing, and intriguing.

Encouraging, because the thermal conductivities show a decrease as the amount of antimony increases in the system to a value approximately equal to 1.1 W/m·K at room temperature for the sample $KPb_{10}Bi_{0.25}Sb_{0.75}Te_6Se_6$ (see Figure 3-14). This value is lower than the thermal conductivity of Bi_2Te_3 (1.5 W/m·K) at room temperature. The family of compounds investigated in this work, proved to have a thermal conductivity that can be decreased easily by introduction of additional disorder in the lattice. Due to the freedom in the composition and stoichiometry, several solid solutions were made and more can be prepared until a low limit in κ is reached.

Nevertheless the results were also disappointing and intriguing because the electrical conductivities at room temperature were measured to be about half of our measurements (see Figure 3-15). Electrical conductivities were re-measured on our equipment after received back the samples, and agreed measurements made outside our laboratory. The difference between the two sets of measurements that we made in our laboratory resides in the fact that the first set (that gave the best values) was made on ingots from synthesis, uncut, while the second set of measurements were made on ingots cut from the center of the bulk materials. Because of the technique employed for conductivity measurement (four-probe touching technique), the samples measured must have a flat surface as well as being physically homogenous.

Differences in the measurements are most certainly due to surface homogeneity problems of the uncut ingots, the smaller ingots cut with a diamond saw having a more homogenous and “clean’ surface. Another plausible explanation is the possibility of having a gradient of concentrations in the material created during the synthesis. It is known than during single crystal growth of Bi_2Te_3, different part (top, middle, and bottom) of the crystal show different transport properties. In our case, it is suspected that the flame reaction employed creates a gradient of concentration not only following the transversal axes (as commonly seen in single crystal growth) but also from the center of the ingot to the outer part.

Finally, the most interesting measurements were those of the Seebeck coefficient. The values are equals to –100, -95, and –120 μV/K for the compounds with $x = 0.25$, 0.5 and 0.75 respectively (see Figure 3-16). These values are much lower (of about 50%) from what we measured on pressed pellet samples taken from the top part of the uncut ingot (see Figure 3-17). Two possibilities were considered to explain these differences:

1- The carrier concentration is not the same in all parts of the ingot as advanced previously. Therefore, the samples that we use to make the measurement (top part of the ingot) and those sent for further measurements (core of the ingot) do not contain the same charge carrier concentrations.

2- In theory, the Seebeck coefficient should not be different if measured on powder or on ingot. Nevertheless, is it possible that in the case of these compounds, the physical state (press pellet or ingot) of the sample can affect the value of the measurements? Additional investigations are needed to better understand and perhaps take advantage of this effect.

In order to check these hypotheses, pieces of ingots measured outside our laboratory were cut and re-measured. The ingots were then ground, cold pressed into pellets, and measured a third time. Figure 2-18 shows the results. The pressed pellet samples show an increase of the Seebeck coefficient of about 50 to 65 % compared to the ingots. We do not have any explanation for this differences but it is interesting to note that p-type Bi_2Te_3 used in industry is under the form of a pellet while the n-type is under the form of an ingot.

From Seebeck measurements, we conclude that differences of charge carrier concentration exist in different parts of the sample. Nevertheless, this can not account by itself for the change in the values when measurements are made on ingot and pressed pellet of the same sample. Further work needs to be done to explain this effect.

Compared to $KPb_{10}BiTe_{12}$, the figure of merit for the best of these materials $KPb_{10}Bi_{0.5}Sb_{0.5}Te_6Se_6$ (see Figure 2-19) tripled due to a low value of the thermal conductivity and an increase in the Seebeck coefficient. If we can double the Seebeck coefficient by making sintered press pellet without loosing too much conductivity, the ZT could increase significantly. Such experiment were carried on in Chapter 4.

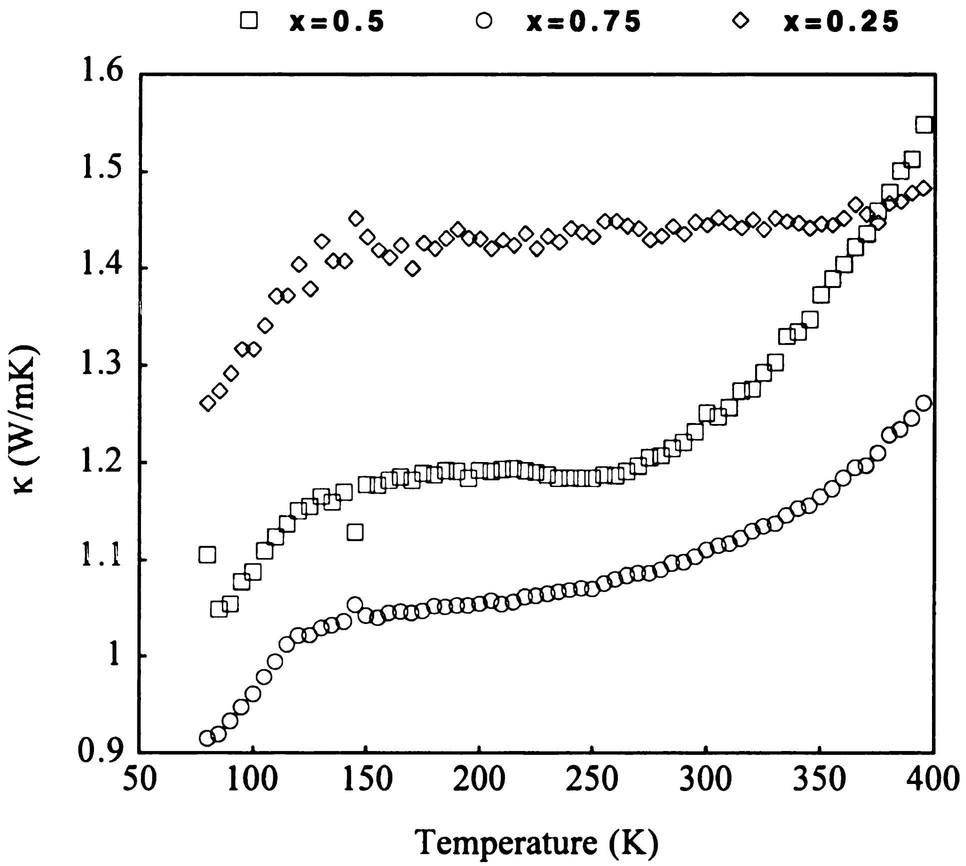

Figure 3-14a: Thermal conductivity for the solid solutions $KPb_{10}Bi_{1-x}Sb_xTe_6Se_6$ (on ingots and before correction).

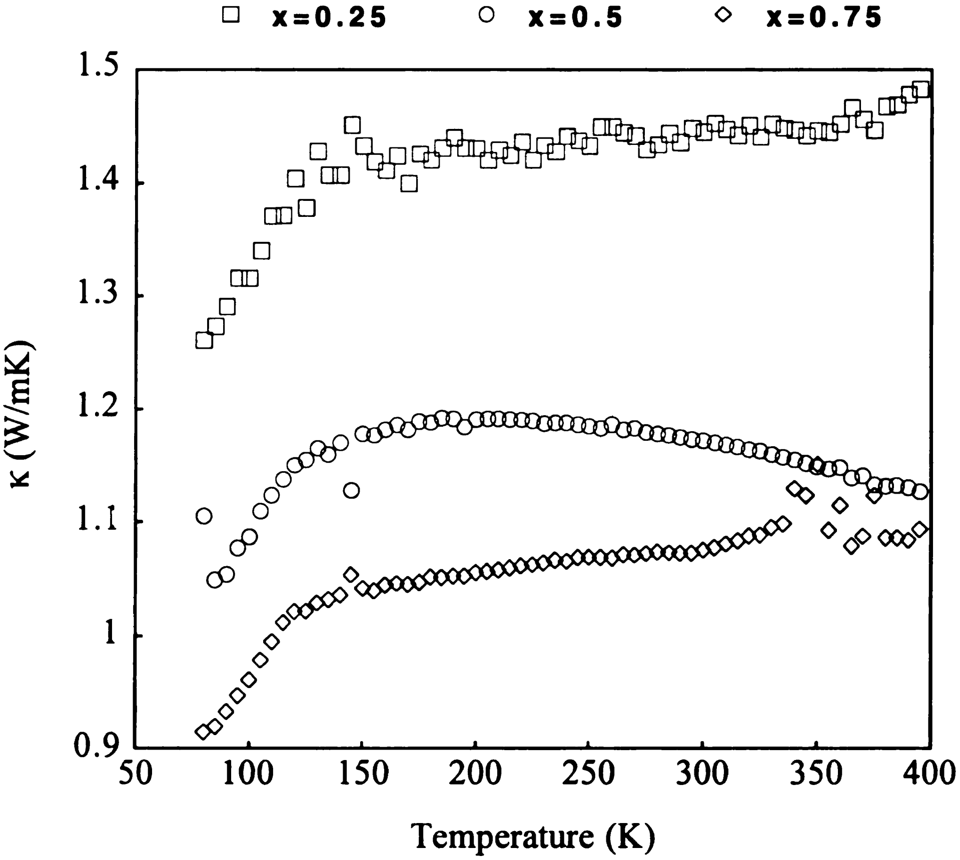

Figure 3-14b: Thermal conductivity for the solid solutions $KPb_{10}Bi_{1-x}Sb_xTe_6Se_6$ (on ingots and after correction).

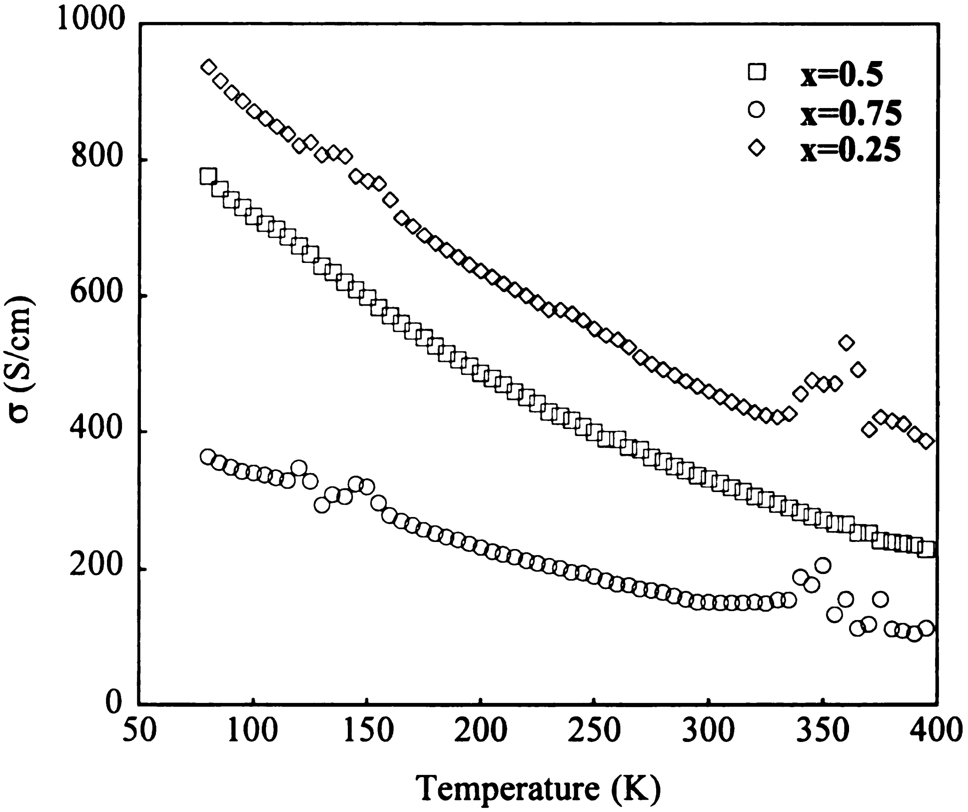

Figure 3-15: Electrical conductivity for the solid solutions $KPb_{10}Bi_{1-x}Sb_xTe_6Se_6$ (ingots).

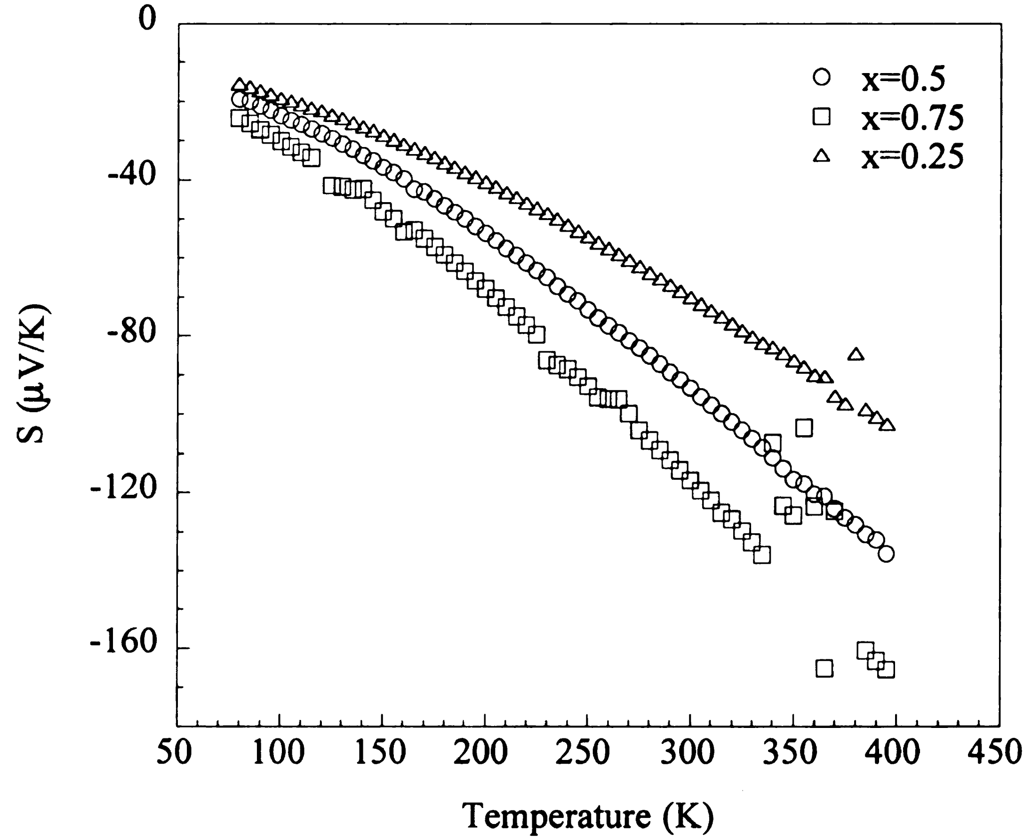

Figure 3-16: Seebeck coefficient for the solid solutions $KPb_{10}Bi_{1-x}Sb_xTe_6Se_6$ (ingots).

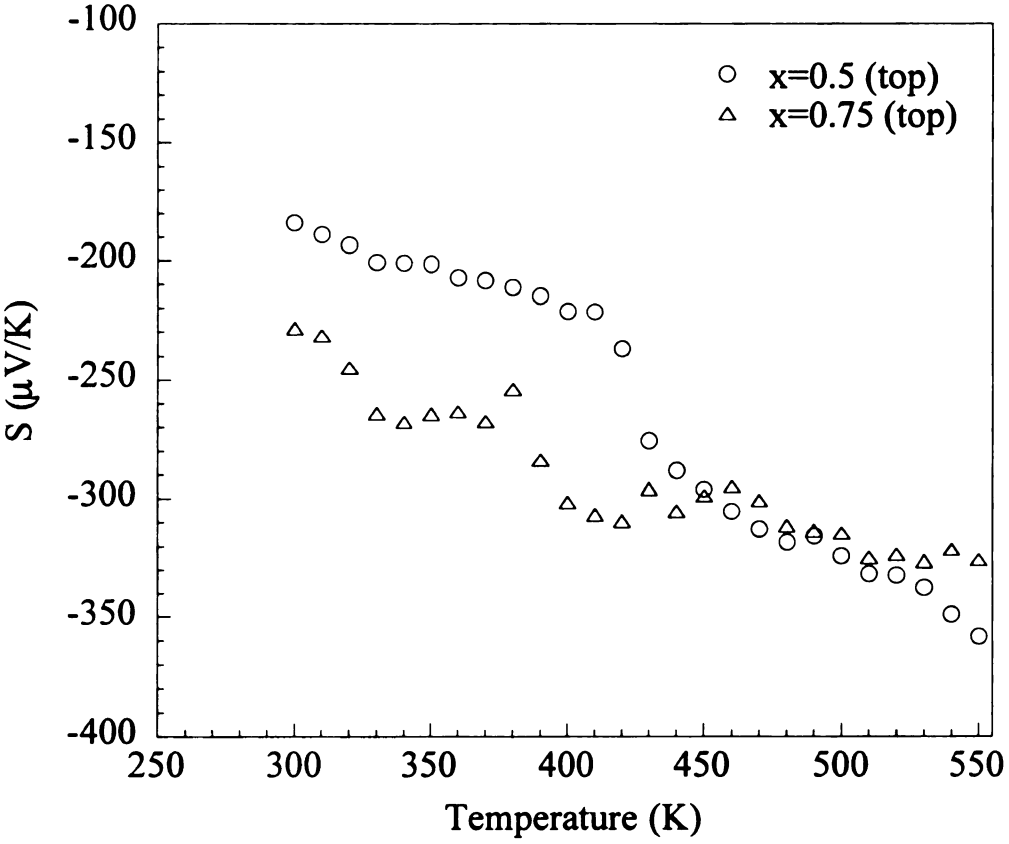

Figure 3-17: Seebeck coefficient for the solid solutions $KPb_{10}Bi_{1-x}Sb_xTe_6Se_6$ (pellets).

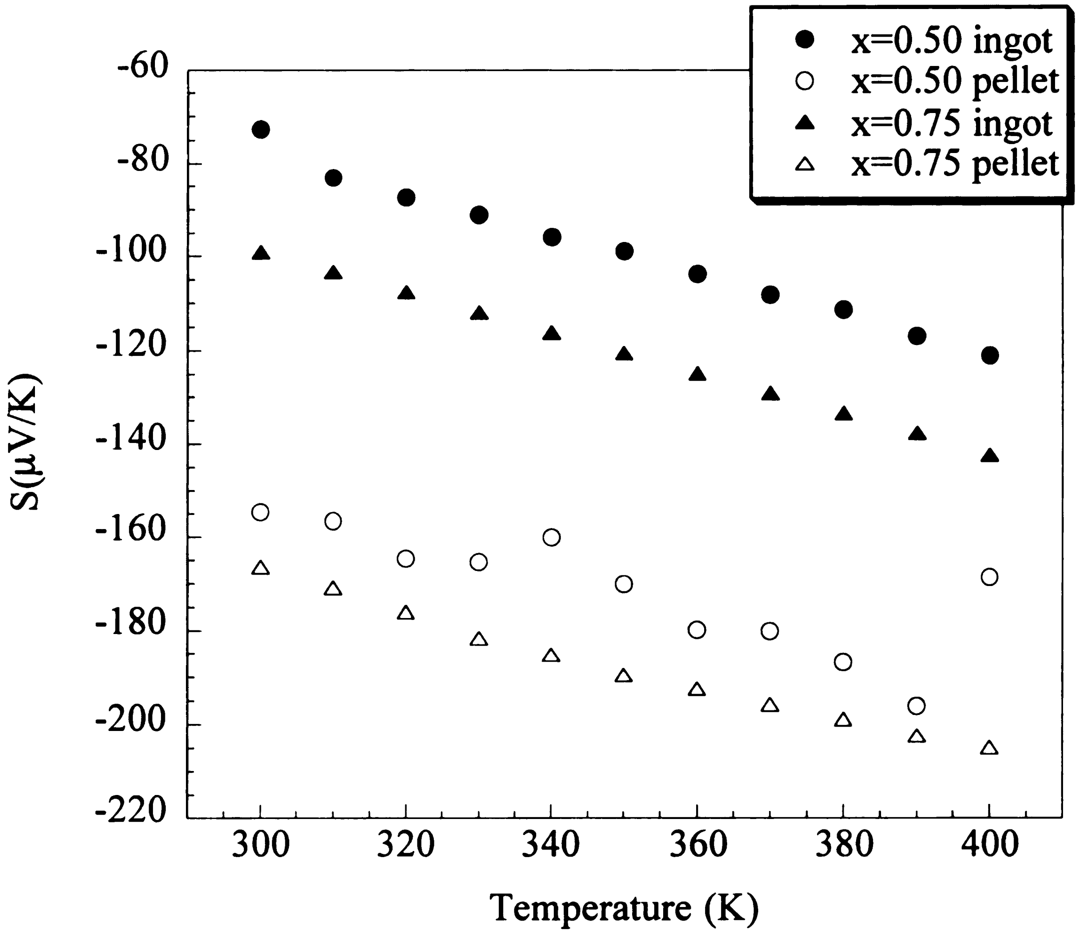

Figure 3-18: Seebeck coefficient for the solid solutions $KPb_{10}Bi_{1-x}Sb_xTe_6Se_6$ (ingots and pressed pellets).

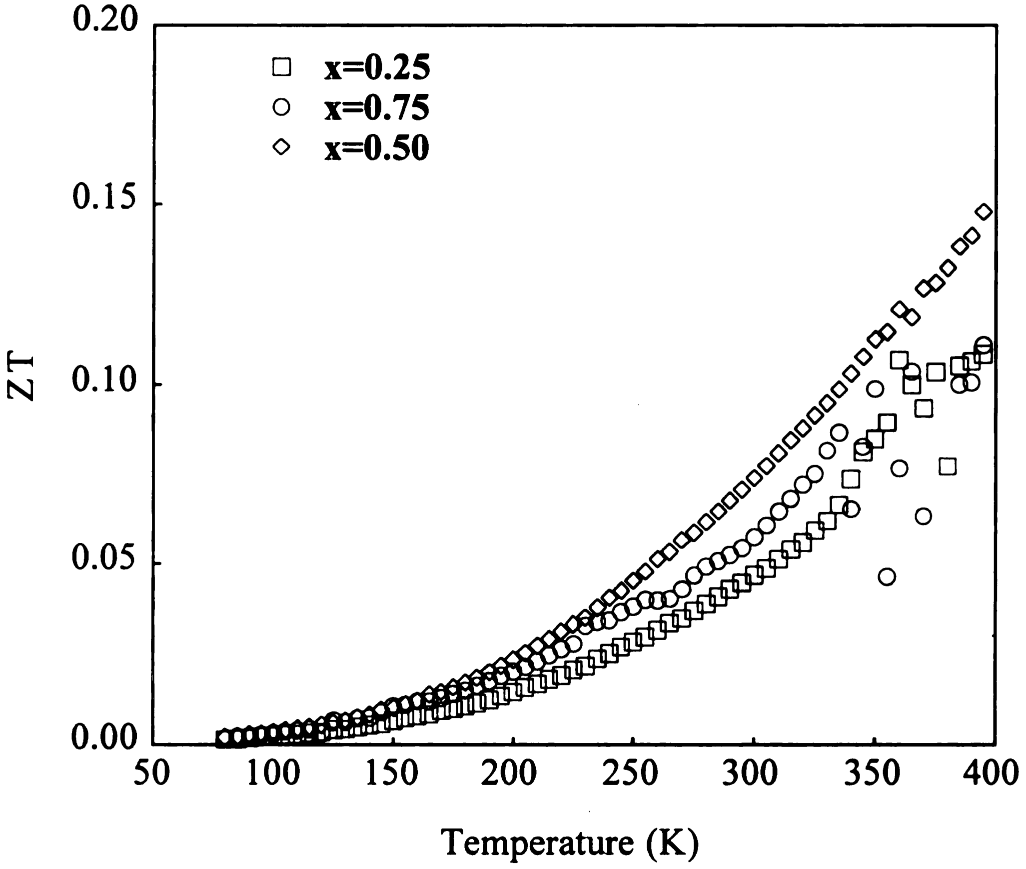

Figure 3-19: Figure of merit ZT for the solid solutions $KPb_{10}Bi_{1-x}Sb_xTe_6Se_6$.

3-4. Concluding Remarks

It has been shown in this chapter that reducing the thermal conductivity of members of the family of compounds $A_mB_nM_mQ_{2m+n}$ is possible by introducing further disorder in the structure on the anionic and on the cationic positions. A reduction of 50% of the thermal conductivity was obtained for the compound of formula $KPb_{10}BiTe_{12}$ by alloying with $KPb_{10}BiSe_{12}$ and by substitution of some atoms of Bi by atoms of Sb. It has also been discovered that the physical state of the material, i.e. ingot or cold pressed pellet, affects the value of the Seebeck coefficient. In addition to this effect, a gradient of temperature during synthesis is most certainly responsible for a change in the charge carrier concentration along the ingots synthesized during flame reactions. It is important to note that if we succeed in having an electrical conductivity of about 400 S/cm on pressed pellet, the ZT at room temperature would be extremely promising (0.50) due to the high values of Seebeck coefficient and to the low thermal conductivity. In this case, we would expect to have even lower thermal conductivity on pressed pellets (not measured) than on ingots due to an increase in the grain boundary, increasing further the figure of merit.

Having successfully decreased the thermal conductivity, we will examine in the next chapter the effect of introduction of doping agents on the best materials obtained so far, i.e. $KPb_{10}BiTe_6Se_6$ and $KPb_{10}Bi_{0.5}Sb_{0.5}Te_6Se_6$. We expect to be able to raise the Seebeck coefficient without affecting to a great extend the electrical conductivity.

References

1. G.D. Mahan, *Solid State Phys.*, 51, **1998,** 81
2. H. Sherrer, S. Sherrer, "Bismuth Telluride, Antimony Telluride, and Their Solid Solution", in CRC Handbook of Thermoelectrics, Ed. by D.M. Rowe, **1994**, 211-237
3. S. Larach, R.E. Shrader, C.F. Stocker, *Phys. Rev.*, 108, 3, **1957**, 587
4. L. Vegard, *Z. Phys.*, 5, **1921**, 17
5. V.S. Urusov, *Zhurnal Strukturnoi Khimii*, 33, 1, **1992**, 80

Chapter 4

Effect of Doping Agents on the Transport Properties of $KPb_{10}BiTe_6Se_6$ and $KPb_{10}Bi_{0.5}Sb_{0.5}Te_6Se_6$

4-1. Introduction

In the previous chapter, the thermal conductivity κ of $KPb_{10}BiTe_{12}$ was decreased significantly by introduction of additional disorder in the structure via different solid solutions on both anionic and cationic sites. Atomic substitutions of half of the Te atoms by Se and half of the atoms of Bi by Sb lowered the value of κ of about 50%. The observed value, close to 1 W/m·K, satisfies one of the criteria that a good TE material should follow[1]. Unfortunately, the electrical conductivity decreased also by a factor of two, compensating the gain obtained from mass fluctuation. The alloying of K/Pb/Bi/Te system with the system K/Pb/Bi/Se increased the energy gap to a value lying between the energy gaps of the two end-members; this, in turn, had for consequence to decrease the electrical conductivity.

To enhance the Seebeck coefficient and/or the electrical conductivity of thermoelectric materials, small amounts (usually <1 atomic %) of impurities are introduced into the compounds. In order for this addition to be fully efficient, the starting materials must be as pure as possible. As we mentioned in the previous chapter, in view of the diffuse reflectance spectra, most of the compounds we are investigating seem to be already self-doped during flame reactions. Consequently, it is expected that doping experiments might not be totally efficient, but we hope to see a trend in the transport properties as a function of the amount and type of dopant added. The thermal conductivity measured for $KPb_{10}Bi_{0.5}Sb_{0.5}Te_6Se_6$, being mainly dominated by the lattice contribution (κ_l=0.93 W/m·K and κ_e=0.24 W/m·K at room temperature), introduction of additional carriers should not affect it greatly.

The choice of a doping agent is theoretically straightforward as described in Chapter 1, nevertheless in practice it is more difficult to have the desired atomic sites substituted. This implies that several agents must be tried. In this work, we chose two different approaches to dope the compounds. In the first one, no specific sites were chosen to be doped and instead, chemical dopants were added to the system in excess. In the second approach, substitutions on selected atom were made.

The Seebeck coefficient can be written as a function of the Fermi level ξ as[2]:

$$\mathrm{S} = \frac{k_B}{e}(5/2 + s - \xi) \qquad \text{Eq. 4-1}$$

With k_B being the Boltzmann's constant and s the scattering parameter. In turn, the charge carrier concentration is related to the Fermi level ξ as shown in Eq. 4-2.

$$\mathrm{n} = 2(2\pi m^* k_B T / h^2)^{3/2} \exp\xi = A\exp\xi \qquad \text{Eq. 4-2}$$

Where m* is the effective mass. Introducing the natural logarithm, the Fermi level is proportional to ln (n) and therefore S is proportional to -ln (n), i.e. 1/ln (n). n is the charge carrier concentration. Since the electrical conductivity can be written as $\sigma = ne\mu$ (μ is the mobility and e is the charge of the majority carriers), S is therefore proportional to 1/ln (σ). Because of this, if the electrical conductivity increases, the Seebeck coefficient should decrease. Therefore, an optimum range of carrier concentration has to be found that will optimize simultaneously S and σ.

4-2. Experimental Section

Reagents

All the reagents were taken under their elemental forms. As mentioned in Chapter I, high purity K, Pb, Bi, Sb, Sn, Te, and Se were used

Synthesis

The same procedure as the one described in Chapter 3 was followed for the synthesis of all the doped samples. All elements were mixed in 13-mm carbon coated quartz tubes. For example, $KPb_{10}BiTe_6Se_6$ was doped with 0.05% Sn by mixing under nitrogen atmosphere 0.052 g (1.3 mmole) of K, 2.762 g (13.3 mmole) of Pb, 0.277 g (1.3 mmole) of Bi with 1.020 g (8 mmole) of Te, 0.630 g (8 mmole) of Se and 0.0024 g (0.02 mmole) of Sn. The mixture was loaded into a 13-mm carbon coated quartz tube, sealed under nitrogen atmosphere at a residual pressure inferior of 10^{-4} Torr. The tube was then heated in a furnace at 150 C for one hour. After opening the tube, the materials were loaded into a new 13-mm non-carbon coated quartz tube (in order to see the melt during the next step) and melted using a high torch flame.

An alternative preparation would be to synthesize large amount of material (e.g. $KPb_{10}BiTe_6Se_6$) and to use it at starting material. Unfortunately, it is not possible to synthesize very large amount of material using the flame reaction because of the exothermic process that occurs. About 4 to 5 grams constitute the charge limit of the tubes that we tried in order to avoid explosion. Therefore, the material to dope was synthesized with the dopant already introduced in the mixture.

$KPb_{10}BiTe_6Se_6$ was doped by Ag, Sb, and Sn by adding weight percentage of each element as excess to the system. On the other hand, $KPb_{10}Bi_{0.5}Sb_{0.5}Te_6Se_6$ was doped by both excess and substitution of atomic percentage of Bi by Sn.

4-3. Results and Discussion

Synthesis and X-ray Powder Diffraction Data

X-ray powder diffraction patterns of doped $KPb_{10}BiTe_6Se_6$ show pure cubic single phase in accordance with a NaCl structure type (see Figure 4-1a). The cell parameters were calculated from these experimental data and are reported in Table 4-1.

Weight percentages of doping agents were added to $KPb_{10}BiTe_6Se_6$. The choice of using weight percentages has been found to be inappropriate because, as shown in Table 4-2, the corresponding mole percentages exceed for values superior to 0.05 %the limit of what is considered as doping. The addition of impurities (Ag, Sb, or Sn) can then be more accurately seen as solid solutions experiments. For such cases, it is impossible to know the composition of the compounds formed. For example, in the case of 1.0 weight % of Ag mixed with $KPb_{10}BiTe_6Se_6$, Ag can substitute potassium atoms giving compounds with stoichiometries ranging from $KPb_{10}BiTe_6Se_6$ (if no Ag substitute K) to $K_{0.7}Ag_{0.3}Pb_{10}BiTe_6Se_6$. In view of these data, large differences in the values of the cell

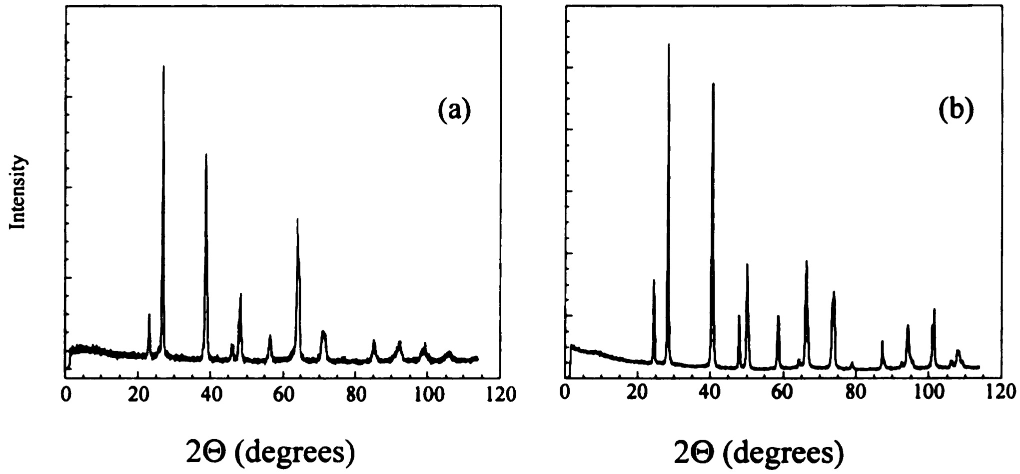

Figure 4-1: X-ray diffraction powder patterns of (a) $KPb_{10}BiTe_6Se_6$ doped with 0.1 weight % of Sn and (b) $KPb_{10}Bi_{0.5}Sb_{0.5}Te_6Se_6$ doped with 0.23 atomic % of Sn substituted for Bi.

parameters were observed between to the cell parameter of $KPb_{10}BiTe_6Se_6$ (6.340 Å) calculated in chapter 2 and those of the doped compounds.

Table 4-1. Cell parameters for doped $KPb_{10}BiTe_6Se_6$ with different agents.

Mole % dopant	Cell Parameter (A)	Mole % dopant	Cell Parameter (A)
0.62 % Ag	6.276 (2)	0.57 % Sn	6.292 (1)
1.67 % Ag	6.281 (2)	1.52 % Sn	6.296 (3)
16.52 % Ag	6.280 (2)	2.97 % Sn	6.302 (2)
33.04 % Ag	6.281 (1)	15.01 % Sn	6.303 (2)
0.57 % Sb	6.305 (2)	30.03 % Sn	6.302 (2)
1.52 % Sb	6.399 (4)[1]		
14.97 % Sb	6.398 (4)[1]		
29.95 % Sb	6.304 (5)		

[1] Very high values suggesting evaporative loss of materials during flame reaction

Progressive substitution of Ag for K cannot account for those differences, because no trends are noted in the variation of the cell parameter with the amount of Ag introduced. Instead, silver atoms seem to substitute potassium until a level is reached and then be incorporated in interstitial sites keeping the cell parameter constant (1)

---

(1) A realignment of the X-ray beam of our CPS 120 INEL diffractometer that occurred between record of the powder pattern of $KPb_{10}BiTe_6Se_6$ and those of doped samples could be responsible for a shift in the calculation of cell parameters. In order to check this hypothesis, the X-ray diffraction powder pattern of $KPb_{10}BiTe_6Se_6$ was re-taken and the cell parameter re-calculate. A new value of 6.302 (2) Å showed that the re-alignment of the beam is responsible for the considerable shift noted.

Table 4-2. Correspondence between weight and atomic percentages of concentration for different doping agents of $KPb_{10}BiTe_6Se_6$.

Dopant	Weight %	Atomic %	Dopant	Weight %	Atomic %
Ag	0.02	0.62	Sn	0.02	0.6
	0.05	1.67		0.05	1.55
	0.5	16.52		0.1	3
	1.0	33.04		0.5	15
Sb	0.02	0.57		1.0	30
	0.05	1.52			
	0.5	14.97			
	1.0	29.95			

Table 4-3. Cell parameters for Sn doped $KPb_{10}Bi_{0.5}Sb_{0.5}Te_6Se_6$.

% Sn in excess	Cell Parameter (A)	% Sn substitution	Cell Parameter (A)
0.05	6.297 (2)	0.05	6.300 (2)
0.15	6.288 (2)	0.15	6.296 (2)
0.23	6.289 (2)	0.23	6.309 (1)
0.53	6.287 (2)	0.47	6.302 (1)

The lattice parameters of Table 4-3 were calculated from X-ray powder diffraction patterns showing pure cubic phases for all doped samples of $KPb_{10}Bi_{0.5}Sb_{0.5}Te_6Se_6$ (see Figure 4-1b). The cell parameter of $KPb_{10}Bi_{0.5}Sb_{0.5}Te_6Se_6$ was calculated in Chapter 3 to be 6.308 Å. The difference noted from the data of Table 4-3 is not significant enough to be conclusive on the substitution effect of Sn.

Energy gap

The values of the band gaps for doped $KPb_{10}BiTe_6Se_6$ samples calculated from diffuse reflectance spectroscopy are reported in Table 4-4. All the spectra observed show similar features (see Figure 4-2a) characteristic of self-doped materials. As mentioned previously, this is probably due to many defects due to the “flame” reaction. No band gaps were observed for the compounds doped by Sn.

To the contrary of the previous case, compounds of $KPb_{10}Bi_{0.5}Sb_{0.5}Te_6Se_6$ doped with Sn, show clear band gaps. In view of the diffuse reflectance spectrum, the energy gaps are most certainly indirect and show a broad tail the real value of E_g (see Table 4.5 and Figure 4-2b). Those features are due to the energy levels created by the impurities added. The shape of the spectrum indicates that they are probably shallow donor levels close to the conduction edge. This indicates that the compounds are effectively doped as expected.

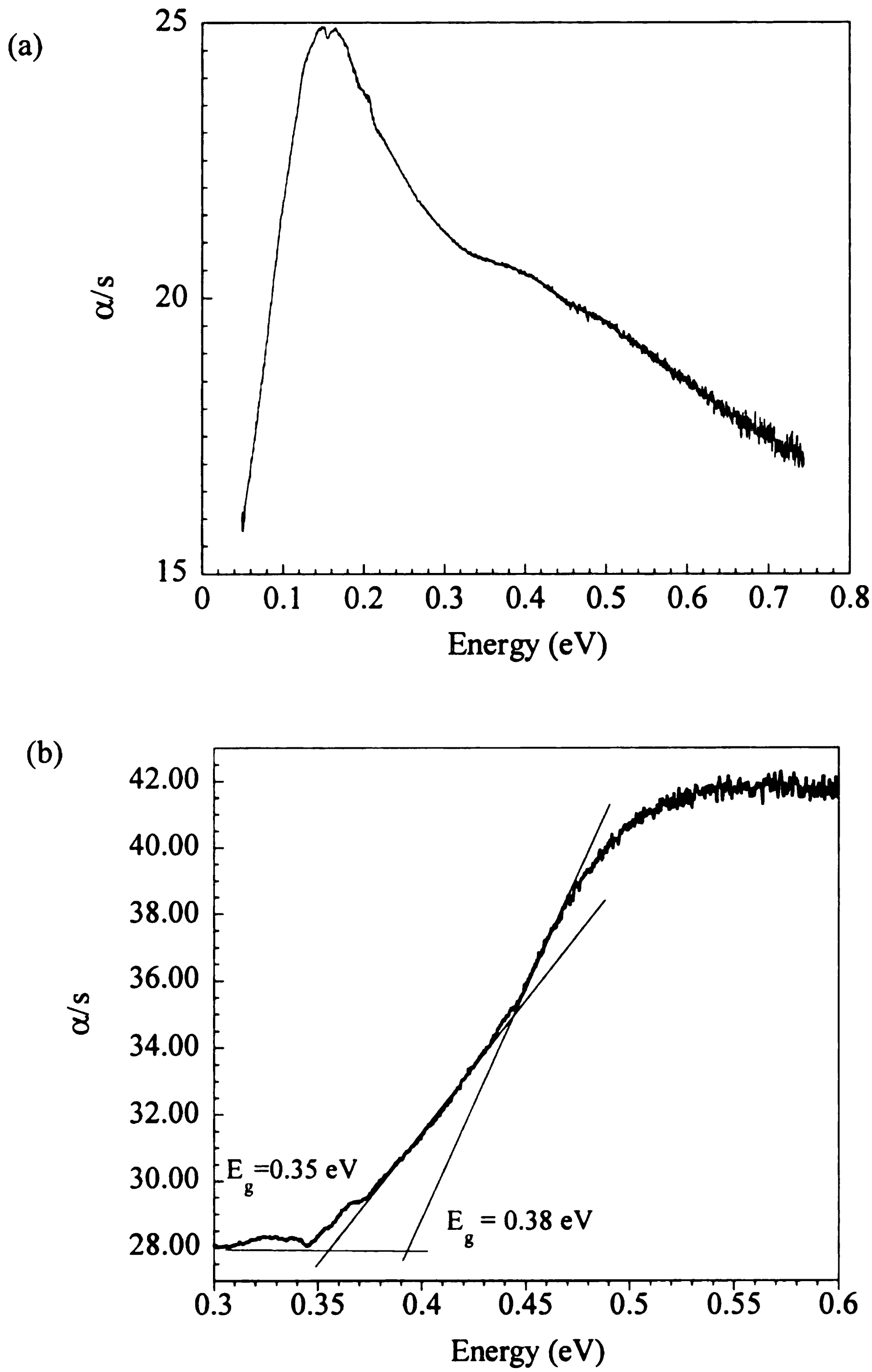

Figure 4-2: Optical absorption spectra of (a) $KPb_{10}BiTe_6Se_6$ doped with 0.1 weight % Sn and (b) $KPb_{10}Bi_{0.5}Sb_{0.5}Te_6Se_6$ doped with 0.05 % Sn and showing a broad tail.

Table 4-4. Energy gaps for $KPb_{10}BiTe_6Se_6$ doped with Ag and Sb.

% Ag	E_g (eV)	% Sb	E_g (eV)
0.02	no band gap	0.02	0.37
0.05	no band gap	0.05	0.36
0.10	0.33	0.10	0.33
0.50	0.35	0.50	no band gap

Table 4-5. Energy gaps for $KPb_{10}Bi_{0.5}Sb_{0.5}Te_6Se_6$ doped with Sn.

% Sn in excess	E_g (eV)	% Sn substitution	E_g (eV)
0.05	0.35-0.38	0.05	0.35-0.41
0.15	0.35-0.40	0.15	0.35-0.39
0.23	0.40-0.42	0.23	0.40
0.53	0.36	0.47	0.35-0.41

Transport Properties

(a) Doped $KPb_{10}BiTe_6Se_6$

Among the three different doping agents tried on $KPb_{10}BiTe_6Se_6$, Sn presented the most promising results (see Table 4-6). The electrical conductivity at room temperature was slightly lower than for the Sb and Ag doped compounds but the Seebeck coefficient measured on cold pressed pellets show much higher values (see Figure 4-3). No trend was visible in the variation of the Seebeck coefficient as a function of the amount of dopant. This was expected due to the uncertainty on the compounds formed.

Because of the probable increase of the disorder in the lattice, we expect low thermal conductivity caused by the formation of solid solutions. An ingot of $KPb_{10}BiTe_6Se_6$ doped with 0.1 weight percentage (corresponding to a doping level of 3 atomic % of Sn) was sent for additional measurements.

The results show a negative Seebeck coefficient of -120 μV/K (see Figure 4-4) at room temperature, indicating that the majority charge carriers responsible for the electrical conductivity are electrons. This value is lower than the -160 measured in our system as expected. In accordance with the observation made in Chapter 3, the morphology of the samples affects the measurement of the Seebeck coefficient.

A large radiative loss contribution can be seen on the thermal conductivity plot starting at a low temperature of 100 K. After correction, the thermal conductivity due only to the electrical and lattice contribution was calculated to be equal to about 0.79 W/m·K (see Figure 4-5). The plot of the residual part versus T^3 (Figure 4-6) shows a linear relationship, which validates the correction made according to the T^3 dependence of the radiative losses, mentioned in Chapter 1. The thermal conductivity obtained after correction is extremely low (below the required value for TE materials). Because we added large amount of Sn (3 atomic %), it is reasonable to think that some atoms of Sn substituted lead atoms making an additional solid solution $KPb_{10-y}Sn_yBiTe_6Se_6$ that decreased κ.

Unfortunately, the electrical conductivity σ has a value at room temperature of 150 S/cm, which is much lower than what we measured on our instrument (880 S/cm). Differences between measurement techniques used in our lab and by our collaborators cannot account for such differences. Acceptable differences between such techniques lay

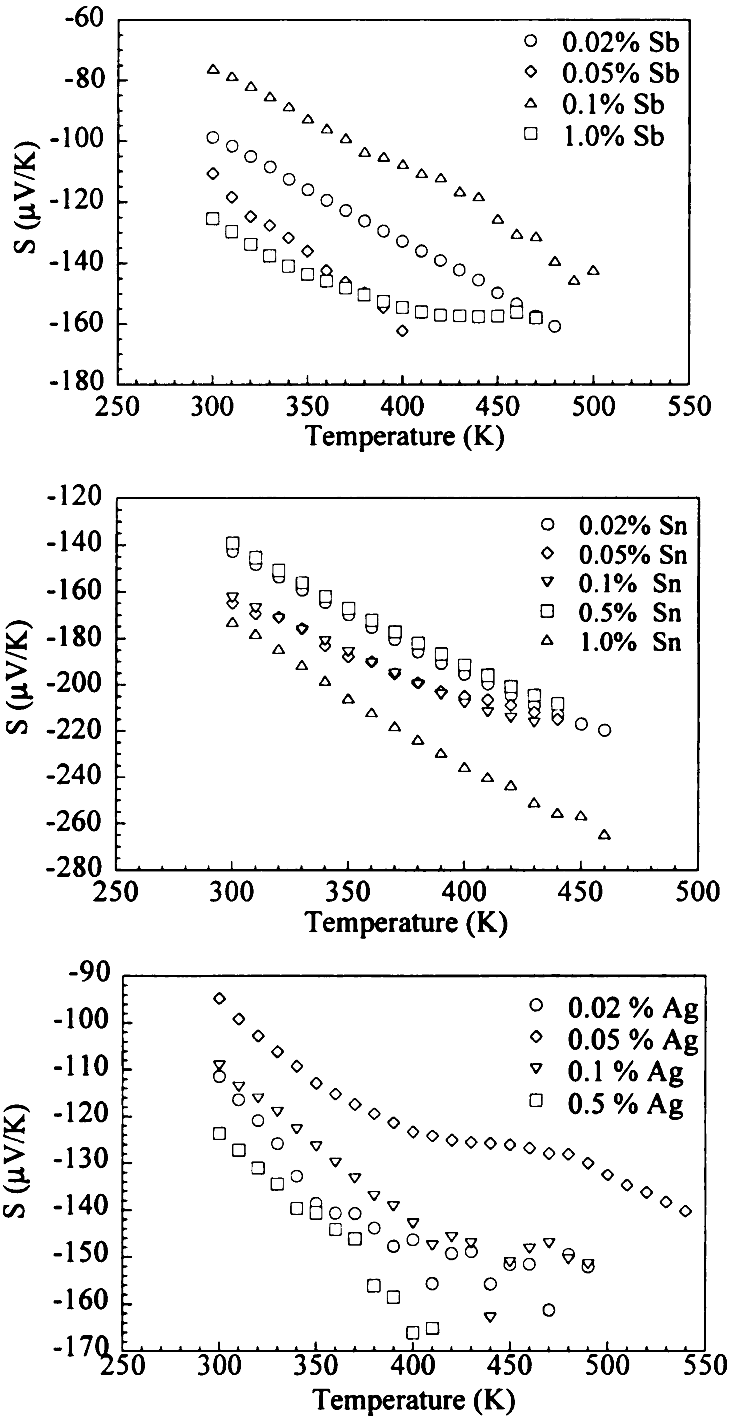

Figure 4-3: Seebeck coefficient (on cold pressed pellets) for $KPb_{10}BiTe_6Se_6$ doped with different doping agents. (The percentages shown are weight percents).

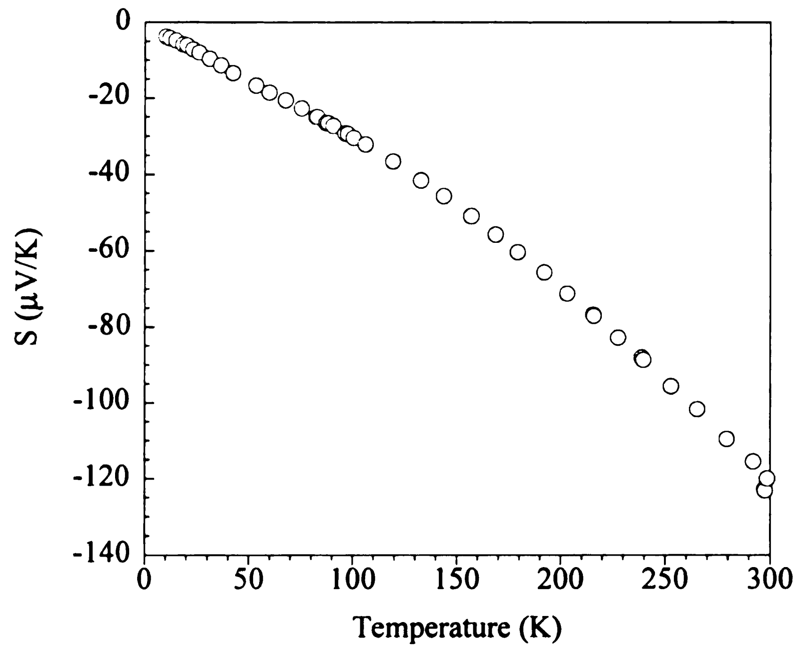

Figure 4-4: Seebeck coefficient of $KPb_{10}BiTe_6Se_6$ doped with 0.1 weight % of Sn (ingot).

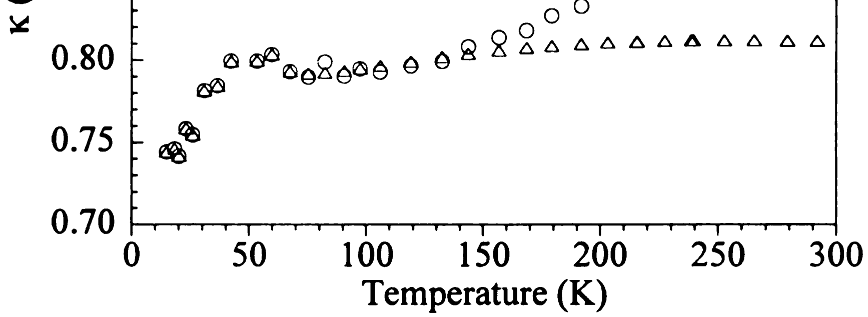

Figure 4-5: Thermal conductivity of $KPb_{10}BiTe_6Se_6$ doped with 0.1 weight % of Sn (ingot).

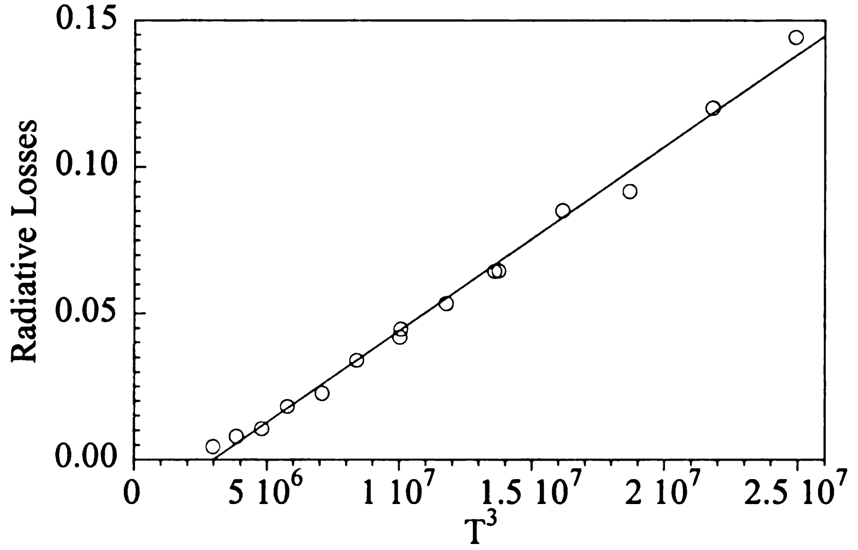

Figure 4-6: Radiative losses versus T^3 for thermal conductivity of $KPb_{10}BiTe_6Se_6$ doped with 0.1 weight % Sn (ingot).

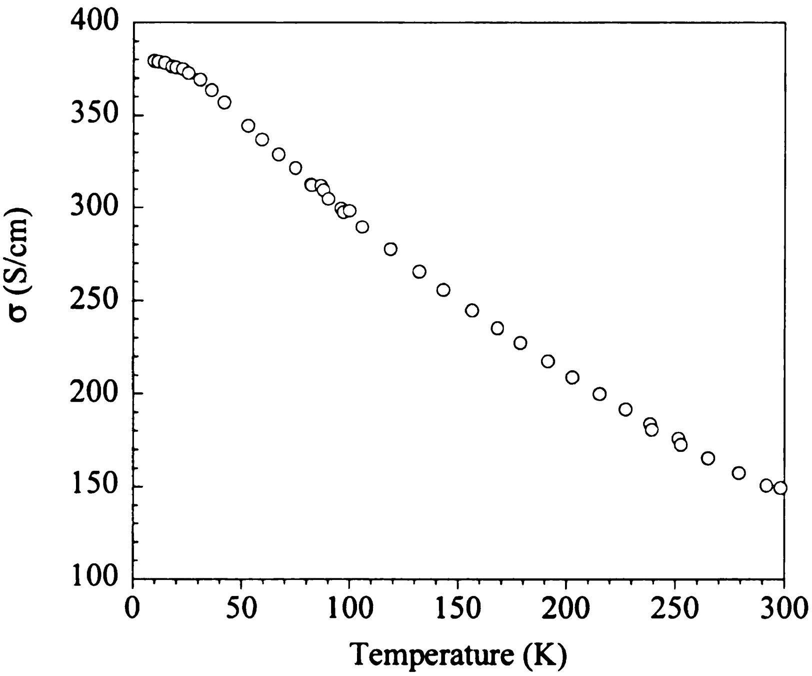

Figure 4-7: Electrical conductivity of $KPb_{10}BiTe_6Se_6$ doped with 0.1 weight % of Sn (ingot).

around 100%, instead of the 400% noted for this measurement. It has been observed that oxidation of the surface of the materials appeared for the potassium members of the family studied in this Thesis. Etching with diluted HCl restores the integrity of the surface. This degradation effect along with is probably responsible for the differences noted. A decrease of the number of charge carrier could be the cause of the metallic dependence of σ shown in Figure 4-7. Such decrease could be attributed to bounding of the charge carriers (electron) with holes, and defects.

From the data obtained, we calculate a room temperature value of ZT of 0.081. This is an improvement from the previous measurements due to a decrease of the thermal conductivity and an increase of the Seebeck coefficient. The low electrical conductivity is responsible for keeping the figure of merit from further increase. By proper treatment of the surface of the material before measurement, we should obtain higher value of σ. If the conductivity were keep at 880 S/cm, we would obtain a ZT at room temperature of 0.47.

(b) Doping of $KPb_{10}Bi_{0.5}Sb_{0.5}Te_6Se_6$

From the previous discussion on doped samples of $KPb_{10}BiTe_6Se_6$, introduction of Sn in $KPb_{10}Bi_{0.5}Sb_{0.5}Te_6Se_6$ was realized. Atomic percents lower than 1% were used in order to avoid solid solutions.

Sn was added in excess with the hope that the Seebeck coefficient will increase as observed for $KPb_{10}BiTe_6Se_6$. Atoms of Sn were also substituted for Bi in order to introduce additional charge carriers and increase the electrical conductivity.

Table 4-6. Transport properties for $KPb_{10}BiTe_6Se_6$ doped with Ag, Sb, Sn measured at our lab (σ measured on ingots and S on cold pressed pellets).

Dopant	%	σ_{RT} (S/cm)	S_{RT} (μV/K)	S_{MAX} (μV/K)	T_{MAX} (K)
Ag	0.02	800	-110	-147	390
	0.05	1190	-95	-140	520
	0.1	875	-110	-147	410
	0.5	930	-120	-162	470
Sb	0.02	792	-100	-160	480
	0.05	1120	-110	-162	400
	0.1	1240	-85	-145	490
	0.5	1025	-125	-157	440
Sn	0.02	700	-140	-220	460
	0.05	740	-160	-210	450
	0.1	880	-160	-220	430
	0.5	600	-140	-210	440
	1.0	600	-180	-270	460

Excess of Sn

As expected, a tremendous increase in the Seebeck coefficient was observed on preliminary measurements of cold pressed pellets of doped compounds. Unfortunately, measurements on ingots show a decrease by a factor to 3 to 4 from the previous values (see Figure 4-8). A trend is visible as the Seebeck coefficient increases slightly with the amount of Sn introduced. It is difficult to account for a trend in the values of the electrical conductivity.

The room temperature electrical conductivity measurements do not show any clear trend. Similar measurements on cold pressed pellets show low values as expected due to grain boundary effects (see Table 4-7).

Table 4-7. Electrical conductivity of $KPb_{10}Bi_{0.5}Sb_{0.5}Te_6Se_6$ doped with various amount of Sn (measured on cold pressed pellets and on ingots).

Concentration dopant	σ (S/cm) on ingot	σ (S/cm) on pressed pellets
0.05 %	500	3.5
0.15 %	480	10
0.53 %	310	2.5

After annealing under nitrogen atmosphere of the material doped with 0.15% Sn, for 5 days at 500 °C, the electrical conductivity increased to 64 S/cm. The corresponding Seebeck coefficient was measured to be –263 μV/K. Further annealing for 1 day at 650 °C, raised σ to 350 S/cm but decrease S to –80 μV/K (see Table 4-8).

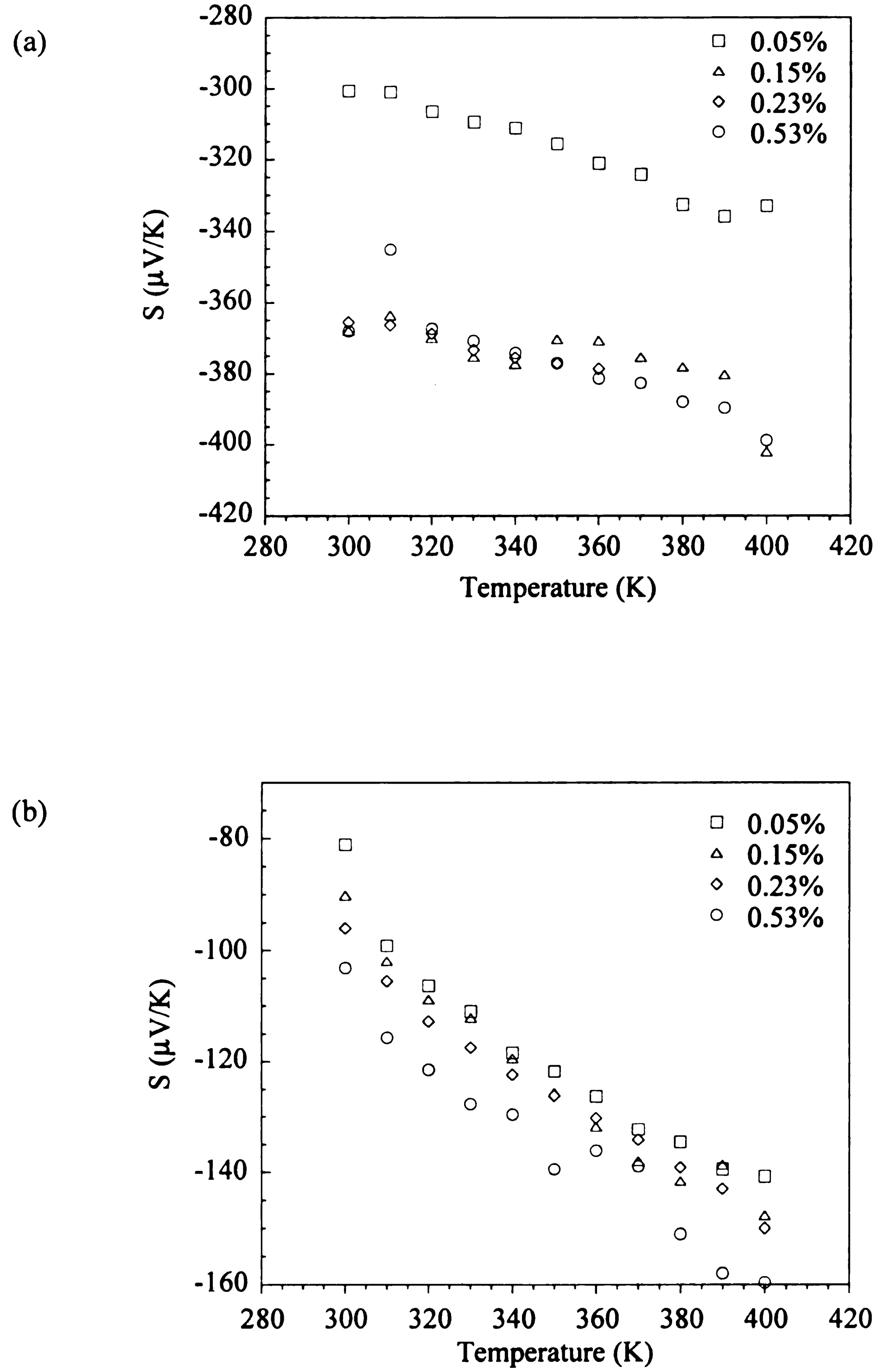

Figure 4-8: Seebeck coefficient of $KPb_{10}Bi_{0.5}Sb_{0.5}Te_6Se_6$ doped by excess of various amount of Sn on Bi sites (a) measured on cold pressed pellets and (b) on ingots.

Table 4-8. Effect of annealing on the transport properties of pressed pellets of $KPb_{10}Bi_{0.5}Sb_{0.5}Te_6Se_6$ doped with 0.15 % Sn.

Conditions	σ_{RT}(S/cm)	S_{RT} (μV/K)	$S^2\sigma$ (mW/m·K)	ZT (prediction)[a]
Initial	10	-367	0.13	0.039
After first annealing	64	-263	0.44	0.13
After second annealing	350	-80	0.22	0.068

[a]: ZT predictions were made using κ of ~1 W/m·K

The power factor $S^2\sigma$, reach a maximum of 0.44 mW/m·K after the first annealing. If we use a value of 1 W/m·K for the thermal conductivity, a predicted ZT at room temperature is equal to 0.13. These experiments are in agreement with the observation made by Fano[3] on sintered pressed pellets of PbTe. He concluded that donor levels are introduced in lead telluride pressed pellets during the powdering process. This created a cross over of inverse carrier sign since PbTe was p-doped. Similar explanation can be adopted to explain the differences that we observed between Seebeck measurements on cold pressed and ingot samples. Our materials being n-type, powdering introduces acceptor levels (defects) that recombine the charge carriers and increase the Seebeck coefficient. Annealing of the pellet restore the initial properties observed on ingot by eliminating the donor levels.

Substitution of Sn for Bi

The measured values for σ and S are similar to the one obtained in the previous case (see Table 4-9). The materials are n-type as expected indicating that the charge carriers are electrons. No increase in the electrical conductivity is observed suggesting Sn did not substitute the Bi atoms.

Table 4-9. Seebeck coefficient and electrical conductivity at room temperature for $KPb_{10}Bi_{0.5}Sb_{0.5}Te_6Se_6$ doped with various amount of Sn.

Concentration Sn	S_{RT} (μV/K) pellet	S_{RT} (μV/K) ingot	σ_{RT} (ingot)
0.05 % excess	-300	-80	500
0.15 % excess	-367	-90	480
0.23 % excess	-365	-96	500
0.53 % excess	-370	-103	310
0.05 % substitution	-175	-93	370
0.15 % substitution	-300	-106	300
0.23 % substitution	-345 (at 320 K)	-90	500
0.47 % substitution	-342 (at 320 K)	-70	297

4-4. Concluding Remarks

Doping experiments on $KPb_{10}BiTe_6Se_6$ and $KPb_{10}Bi_{0.5}Sb_{0.5}Te_6Se_6$ show that excess of Sn increased considerably the Seebeck coefficient measured on cold pressed pellets. Nevertheless, these values are much lower when measured on ingots. In view of the conclusion made by Fano and considering the annealing experiments, the difference noted between pressed pellet and ingot Seebeck measurements is most certainly due to the introduction of acceptor levels during the grinding process. These levels are attributed to defects created by the pulverizing the materials. Such defects could be surface traps and may be eliminated by annealing the pressed pellets, restoring the original Seebeck coefficient measured on ingots and increasing the electrical conductivity.

It was not possible to raise σ for the solid solutions $KPb_{10}Bi_{0.5}Sb_{0.5}Te_6Se_6$ by substitution of Sn for atoms of Bi. Such substitution did not seem to take place and the results of Seebeck and electrical conductivity measurements are similar to those obtained when excess of Sn was introduced in the system.

As excess amount of Sn is increased in the system, the values of the Seebeck coefficient increase. No maximum in the Seebeck coefficient was reached suggesting that even larger amount of tin should be introduced until a maximum is reached. The increase in the Seebeck coefficient does not correspond with a pronounced decrease of σ. This is encouraging for further increase of the power factor $S^2\sigma$.

Annealing for 5 days at 500 °C of pressed pellets of $KPb_{10}Bi_{0.5}Sb_{0.5}Te_6Se_6$ doped with 0.15 % Sn gave a predicted ZT of 0.13 (if we assume a thermal conductivity of 1 W/m·K). Further studies are necessary to take full advantages of the powdering effect.

Finally, it is important to point that the materials should be synthesized first and then doping agents should be added. This probably would result in more clear trends and more accurate data. Unfortunately, this was not possible using the flame method. Ingot growth using the Bridgeman method could resolve this problem.

References

1 G.D. Mahan, *Solid State Physics*, 51, 81, **1998**, 111

2 C.M. Bhandari, D.M. Rowe, “Optimization of Carrier Concentration”, in CRC Handbook of Thermoelectrics, Ed. by D.M. Rowe, **1994**, 43

3 V. Fano, “Lead Telluride and Its Alloys”, in CRC Handbook of Thermoelectrics, Ed. by D.M. Rowe, **1994**, 257

Conclusion

The investigation of the family of cubic chalcogenides compounds of general formula $A_mB_nM_mQ_{2m+n}$ show that the system K/Pb/Bi/Te possess the most promising transport properties among all the other systems studied. In this system, no clear dependence of the Seebeck coefficient (S) on the value of n was observed, to the contrary of the electrical conductivity (σ) that increased with n. This observation lead to a further study of the member $KPb_{10}BiTe_{12}$.

It has been observed that the thermal conductivity of this compound (2.2 W/m·K) can be successfully decreased by introduction of disorder in both anionic and cationic sublattices. The lowest value of κ was measured for $KPb_{10}Bi_{0.5}Sb_{0.5}Te_6Se_6$ doped with 0.1 weight % of Sn. This very good value of about ~0.78 W/m·K is most probably due to substitution of some Pb atoms by Sn (0.1 weight % correspond to 3 atomic % of dopant).

Tin seems to play a decisive role in the enhancement of the Seebeck coefficient. The values were observed to be extremely high for cold pressed pellets of doped samples: from -140 to –180 μV/K for addition of Sn in excess to $KPb_{10}BiTe_6Se_6$ and from –300 to –380 μV/K for addition to $KPb_{10}Bi_{0.5}Sb_{0.5}Te_6Se_6$. Measurements on ingots gave unfortunately lower values: from –80 to –105 μV/K for $KPb_{10}Bi_{0.5}Sb_{0.5}Te_6Se_6$ and about –120 μV/K for $KPb_{10}BiTe_6Se_6$ doped with 0.1% Sn. Nevertheless, these values are the highest measured in this work. In contrast, of Sn, addition of Sb and Ag do not seem to affect the values of the Seebeck coefficients.

Addition of antimony increased the electrical conductivities to values slightly above 1000 S/cm without affecting largely the Seebeck coefficients. Further work should investigate the role of Sb as a chemical agent to increase σ. The effect on the power factor $S^2\sigma$ of introduction of both Sb and Sn in the system must also be study in more details.

A synthetic method must be found in order to synthesis large amount of material that can be used for doping experiments. This would suppress the uncertainty on the composition of the materials obtained because of the mixing of the dopants to the elements before synthesis.

The differences noted between measurements of the Seebeck coefficient on cold pressed pellets and ingots are attributed to the introduction of defects in the structure during the powdering process. The defects create acceptor levels that "kill" the electrons which are the main charge carriers as shown by the negative sign of the Seebeck coefficients. This had for consequence to decrease the charge carrier concentration n. As it has been demonstrate in Chapter 4, because the Seebeck coefficient is proportional to 1/Ln (n), S is therefore increased. Annealing experiments proved that these defects can be eliminated. The Seebeck coefficients were then restored, after several annealing processes, to values close to the ones observed on ingots. Accordingly, the electrical conductivity values increased as the grain boundary effects are decreased.

An optimum power factor was reached after annealing for 5 days at 500 °C. Using a conservative value of 1 W/m·K for the thermal conductivity κ, a ZT of 0.13 at room temperature was calculated for $KPb_{10}Bi_{0.5}Sb_{0.5}Te_6Se_6$ doped with 0.15 atomic % of Sn and annealed as described above. Additional experiments need to be done using shorter annealing time (24 h instead of 5 days). A higher power factor could be obtained which would be accompaigned by a lower value of κ due to the shorter annealing time.

The differences in electrical conductivity between measurements made at our laboratory and by our collaborators can be attributed to three factors:

1. A difference of charge carrier concentrations exists in different part of the ingots due to the use of the "flame" reaction.
2. A surface effect takes place for most of the samples investigated. Such degradation of the surface can nevertheless be repaired by etching in diluted HCl.
3. An error due to the difference between the techniques employed for measurement of σ with our collaborators can account for values decreased by a factor of 2.

The narrow band gap compounds studied in this Thesis constitute promising thermoelectric materials. Further improvement of the materials pass by the resolution of the problems evoked above. Investigation of the silver system Ag/Pb/Bi/Te might be an alternative to the use of potassium that is responsible to glass attack and that limit the amount of material that we were able to synthesis.

It is obvious that a lot of work need to be done to improvement the n-type material $KPb_{10}BiTe_{12}$ and to develop a p-type analogue, necessary to the creation of industrial modules.